Miguel Ignez Jorge de Ramirez Cordeiro
Licenciado em Ciências de Engenharia Civil

Efficiency Assessment of Seismic Retrofitting Using Buckling Restrained Braces

Dissertação para obtenção do Grau de Mestre
em Engenharia Civil - Perfil Estruturas

Orientador: Professor Doutor Corneliu Cismaşiu,
Professor Associado, FCT/UNL

Júri:

Presidente: Professor Doutor João C. G. Rocha Almeida
Arguente: Professor Doutor Filipe Pimentel Amarante dos Santos
Vogal: Professor Doutor Corneliu Cismaşiu

FACULDADE DE CIÊNCIAS E TECNOLOGIA
UNIVERSIDADE NOVA DE LISBOA

2017

Efficiency Assessment of Seismic Retrofitting Using Buckling Restrained Braces

“Copyright” Miguel Ignez Jorge de Ramirez Cordeiro, FCT/UNL e UNL

A Faculdade de Ciências e Tecnologia e a Universidade Nova de Lisboa têm o direito, perpétuo e sem limites geográficos, de arquivar e publicar esta dissertação através de exemplares impressos reproduzidos em papel ou de forma digital, ou por qualquer outro meio conhecido ou que venha a ser inventado, e de a divulgar através de repositórios científicos e de admitir a sua cópia e distribuição com objetivos educacionais ou de investigação, não comerciais, desde que seja dado crédito ao autor e editor.

Acknowledgements

First and foremost, I would like to thank Dr. Corneliu Cismaşiu for his guidance, knowledge and specially his patience. When things didn't go as expected Dr. Corneliu's understanding and trust were key, and for that I am grateful.

Second, I would like to thank Faculdade de Ciências e Tecnologia da Universidade Nova de Lisboa for providing full access to the Civil Engineering Departement's Computer lab, without which it was impossible to conclude this dissertation. A word of acknowledgement to Dr. Corneliu, again, for speeding up the access process and trusting me with the faculty's precious equipment.

A special thanks to my FCT friends and colleagues, specially Jorge Cruz, Delcio Macaia, Nuno João Monteiro, Hugo Rebelo, Bernardo Albergaria and César Campos, for the support, uncountable discussions, unlimited work breaks and good times. To you all my very sincere thank you and wish you nothing but good fortune for the future to come.

To my childhood and long time friends, I leave you the greatest of acknowledgements, you're friendship and support means the world to me. I hope we can continue to cherish it for countless years to come. Life has its ups and downs and it hasn't always been easy. Specially to Gaio, Gonçalo, Inês, Joana, Jorge and Tomé you've been there through them all, you make the ups higher and the downs shallower. Wish you nothing but the best and will be there whenever you need me.

Last but not least, my most sincere and biggest thank you to my family, for their unconditional love and support. Everything I am today its because of you, of what you've provided and the belief you've deposit in me. My special sign of gratitude to my parents, for being the perfect parents for an imperfect child. Hope you're proud.

Abstract

The main purpose of the present dissertation is to study the efficiency of buckling restrained braces (BRB) when used as seismic dampers in reinforced concrete frame structures.

The study was conducted on the RC frame structure reported by Sarno and Manfredi. Their experimental campaign results, available for the structure with and without BRBs, were used to calibrate a numerical model implemented in the FE program *SeismoStruct*.

A probabilistic approach was used next to assess the efficiency of the BRBs. Following the provisions of the Probabilistic Model Code of the Joint Committe of Structural Safety, several key parameters in the FE model were assumed to have a probabilistic distribution. Random generation of their values allowed to create 50 numerical models of the structure.

Subsequent non-linear incremental dynamic analysis preformed on these structures without any type of bracing, provided with BRB and traditional bracing, yielded fragility curves that can be used to estimate the damage reduction in the controlled structures and assess efficiency of the BRBs when used as seismic retrofitting.

Buckling restrained braces have shown to be capable of reducing the damage caused by strong ground motions due to seismic actions.

Keywords:

Non-linear dynamic analysis, Finite Elements, Buckling Restrained Braces, Fragility.

Resumo

O principal objetivo da presente dissertação é o estudo da eficácia dos contraventamentos de encurvadura impedida (BRB) como amortecedores sísmicos em estruturas de betão armado.

O estudo foi conduzido na estrutura porticada de betão armado apresentada no estudo experimental de Di Sarno e Manfredi. Os resultados da sua campanha experimental, disponíveis para a estrutura com e sem BRBs, foram usados como base para a calibração de um modelo numérico implementado no software de elementos finitos *SeismoStruct*.

Foi adotada uma abordagem probabilística para aferir a eficácia dos BRBs. Seguindo as provisões do *Probabilistic Model Code da Joint Committe of Structural Safety*, alguns parâmetros chave do modelo de EF considerou-se terem uma distribuição probabilística. Através da geração aleatória dos seus valores 50 modelos numéricos da estrutura foram criados.

Subsequentemente, através de análises dinâmicas incrementais (IDA) realizadas nessas estruturas, sem qualquer contraventamento e com BRBs, foram desenvolvidas curvas de fragilidade que possibilitam uma estimativa da redução de dano nas estruturas controladas e uma avaliação da eficácia dos BRBs quando utilizados como reforço sísmico.

Os BRBs mostraram serem capazes de reduzir o dano causado por fortes ações sísmicas neste tipo de estruturas.

Palavras chave:

Análise dinâmica não-linear, Elementos Finitos, Contraventamentos de encurvadura empedida, Fragilidade.

Resumo alargado

Introdução

Os sismos são conhecidos por causar graves problemas à sociedade, especialmente em regiões com alta sismicidade. São dos fenómenos naturais mais perigosos, não só pelo elevado número de perdas humanas e patrimoniais, mas também devido à sua elevada imprevisibilidade.

Um acontecimento sísmico de grande importância para Portugal ocorreu em Novembro de 1755. Lisboa foi abalada por um sismo de 8.5 na escala de magnitude de momento, despoletando vários incêndios e um tsunami. O ano de 1755 foi um grande marco, uma vez que na reconstrução da cidade foram utilizados sistemas de mitigação das ações horizontais. Foram utilizadas estruturas porticadas de madeira capazes de resistir às cargas verticais, mas flexíveis o suficiente para não sofrerem danos significativos quando sujeitas a ações sísmicas.

Desde então, a engenharia tem vindo a evoluir e novos códigos e regulamentações de projeto foram aparecendo assim como soluções de reforço estrutural. No entanto, nem todos os edifícios existentes foram construídos segundo as exigências atuais, sendo que muitos destes edifícios antigos possuem fraca resistência lateral. Estas estruturas não possuem o espaçamento adequado dos estribos nas vigas, pilares e nós estruturais, resultando numa fraca resistência ao corte destes elementos. Baixa percentagem de armadura longitudinal, betões de baixa resistência e varões de aço lisos são encontrados em muitos desses edifícios.

Para atenuar estas deficiências uma técnica de reforço bastante utilizada consiste na utilização de contraventamentos para conferir à estrutura resistência horizontal adicional. O mais comum, consiste na utilização de perfis metálicos dispostos num determinado padrão por forma a dar ao edifício alguma resistência lateral. Este tipo de reforço funciona até um certo ponto, uma vez que a encurvadura destes perfis esbeltos reduz significativamente a capacidade que estes têm de absorver esforços.

Uma técnica alternativa utilizada correntemente são os contraventamentos com a sua encurvadura impedida. O principio base destes dispositivos é de impedir a ocorrência da encurvadura e, dessa forma, permitir que os perfis continuem a absorver esforços. Na Figura 1 é apresentada uma ilustração de um contraventamento de encurvadura impedida (BRB) e os seus principais componentes.

Como foi mencionado anteriormente, os sismos causam grandes perdas quer ao

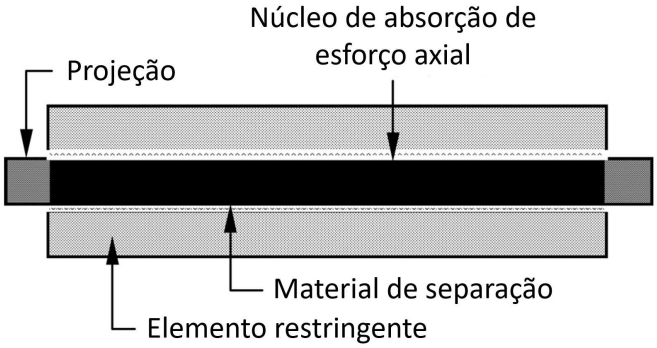

Figura 1: Composição típica de um BRB [1]

nível de vidas humanas, quer ao nível de património edificado, traduzindo-se em grandes perdas socioeconómicas. Assim sendo, o estudo e investigação, não só de novas técnicas de projeto, mas também técnicas de reforço sísmico são de grande importância em Engenharia Civil. Na presente dissertação é investigada, através de um estudo de vulnerabilidade e fragilidade, a eficiência do uso de BRBs como reforço sísmico.

Contraventamentos de Encurvadura Impedida

Contraventamentos convencionais são utilizados correntemente em Engenharia Civil para resistir a ações horizontais, no entanto devido à sua esbelteza estes ao sofrerem encurvadura perdem a capacidade de suster essas solicitações, e exibem ciclos histeréticos fechados, Figura 2.

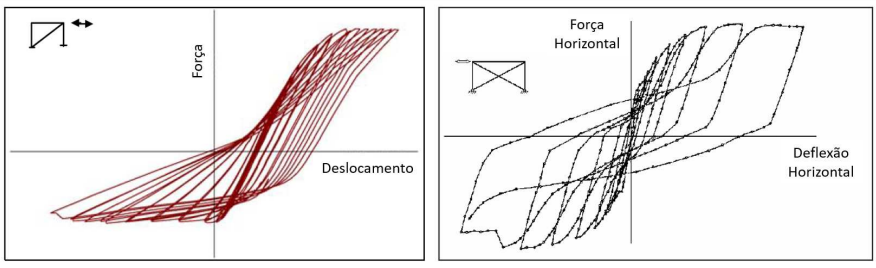

Figura 2: Comportamento típico dos contraventamentos convencionais (adaptado de [2]).

Muitas configurações de BRBs têm sido propostas, mas geralmente seguem o mesmo princípio e possuem os mesmos componentes: um núcleo de aço, responsável por absorver as cargas axiais; um elemento restringente, responsável por impedir a ocorrência de encurvadura; um sistema de separação entre os dois anteriores componentes, por forma a garantir que o núcleo pode deslizar livremente dentro do elemento restringente e para permitir a sua expansão

transversal no caso de cedência à compressão; e por fim, um segmento de transição reforçado, responsável por fazer a ligação à estrutura e por garantir que a cedência ocorre no núcleo restringido e não nos segmentos de ligação. Na Figura 3 podemos observar algumas das configurações propostas até hoje.

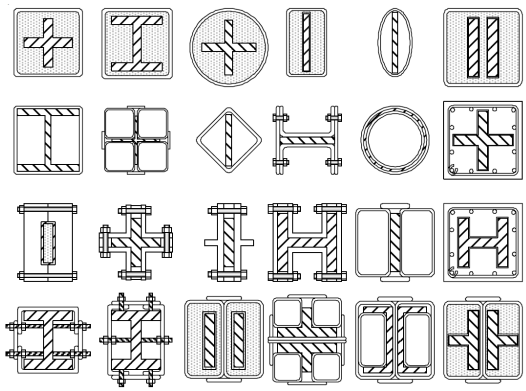

Figura 3: Configurações da secção transversal dos BRBs. [3]

Ao restringir a ocorrência da encurvadura, o contraventamento passa a exibir comportamentos semelhantes à compressão e tração, demonstrando um comportamento histerético melhorado, com ciclos de carga e descarga mais abertos, Figura 4.

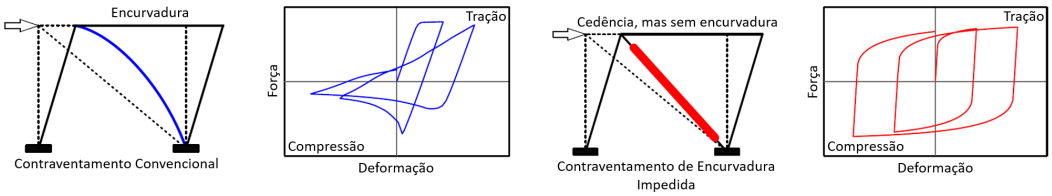

Figura 4: Comparação do comportamento de contraventamentos convencionais e dos BRBs. [4]

Para obter este comportamento o sistema de separação entre o núcleo e o membro restringente é de extrema importância, pois garante que o núcleo desliza livremente e permite a expansão do núcleo em caso de cedência à compressão. Muitos materiais, como silicone, telas de vinil, diferentes tipos de espumas, entre outros, foram testados como sistema de separação, assim como o recurso a espaçamentos de espessura variada.

As ligações destes dispositivos também foram alvo de vários trabalhos de investigação: ligações aparafusadas, ligações pin, diferentes placas *gusset*, entre outros.

Atualmente, na Europa, o dimensionamento de BRBs não está presente nos regulamentos [5], no entanto, existem regulamentos que permitem o uso destes dispositivos fornecendo recomendações de teste, performance e manutenção, como em [6] e [7].

Os BRBs têm demonstrado um bom comportamento histerético e uma boa

capacidade de absorver energia. Em 2000 a Nippon Steel & Sumitomo publicou um relatório técnico [8] onde 11 BRBs com diferentes características foram ensaiados em 5 ensaios experimentais. Os resultados demonstraram que os dispositivos podiam aguentar cerca de 200 ciclos de carga e uma extensão de $\pm$0.75% correspondendo a um ângulo de *drift* de 1/100, antes da rutura. Os autores concluíram que os ensaios clarificaram as propriedades de fadiga dos dispositivos, assim como o suficiente comportamento histerético para serem aplicados como amortecedor sismico.

Nos dias de hoje existem edifícios a tirar partido deste tipo de dispositivos. A Nittele Tower no Japão, sede da Nippon Television [9], é um exemplo da utilização prática destes dispositivos, assim como o edifício federal Wallace F. Bennett em Salt Lake City, nos Estados Unidos da América, no qual se recorreu ao uso de BRBs, não só como uso estrutural, mas também arquitetónico.

Caso de Estudo

Na presente dissertação, o trabalho experimental desenvolvido por L. Di Sarno e Manfredi [10] serviu de base para a calibração dos modelos numéricos e consequente validação.

Modelos Experimentais

Foram ensaiadas duas estruturas porticadas de betão armado idênticas, à escala real. As estruturas contêm dois pórticos de 2,55m numa direção e um único pórtico de 4,40m na outra direção ortogonal. Contêm dois pisos com alturas de 3,5m e 3,44m para o primeiro e segundo piso respetivamente. As lajes dos pisos têm uma espessura de 25cm para o primeiro e 20cm para o segundo piso. As plantas e cortes transversais das estruturas são apresentados na Figura 5. Por sua vez, na Figura 6 estão representadas as secções transversais das vigas e pilares das estruturas, juntamente com a armadura longitudinal e transversal. As fundações são compostas por um ensoleiramento geral de 6m por 7m, e uma espessura de 50cm.

As estruturas foram deliberadamente dimensionadas com deficiências estruturais, sem estarem em concordância com os códigos vigentes. Os materiais de construção, tanto o betão como as armaduras, possuem baixas resistências quando comparadas com o exigido pelos regulamentos.

O betão possui uma resistencia média à compressão de f_{cm} =19,4MPa, calculada através de ensaios realizados em 21 provetes cubicos retirados de vigas, pilares e vigas, e apresenta um módulo de elasticidade de E_{cm} =26672MPa. Através de ensaios realizados em varoes de aço, aferiram-se os valores médios apresentados na Tabela 1.

A estrutura foi dimensionada tendo em conta apenas as cargas verticais, de acordo com [11]. A laje de 25cm do primeiro piso inclui as cargas permanentes, recobrimento e paredes divisórias, perfazendo um total de 8,13kN/m^2. O mesmo princípio foi aplicado à laje de cobertura, perfazendo um total de 5,43kN/m^2. A massa sísmica total da estrutura é de 33,61 toneladas, divididas em 18,66 e 14,95 toneladas no primeiro e segundo piso, respetivamente.

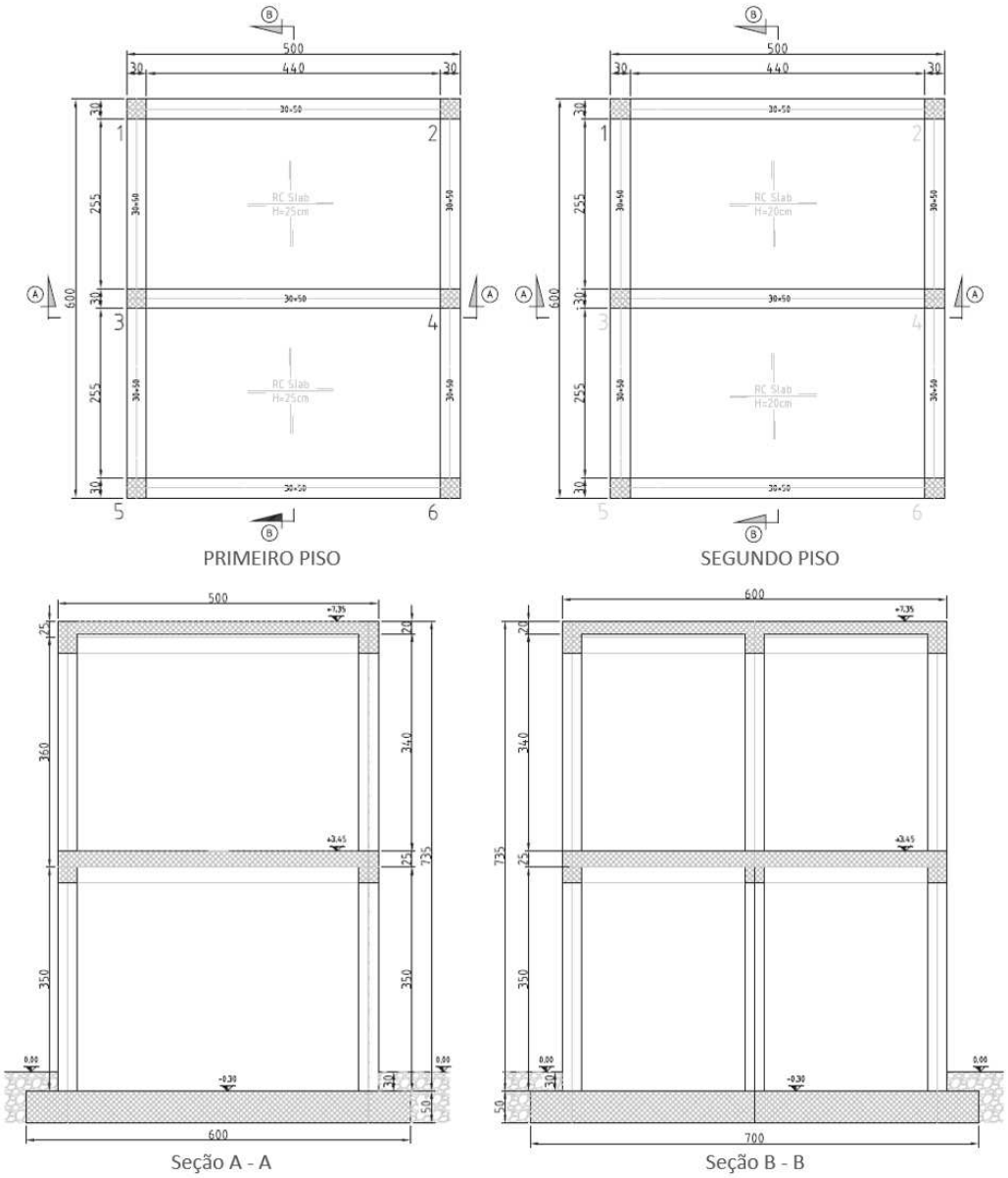

Figura 5: Plantas e cortes transversais das estruturas de teste [10]

Sistema de Reforço

Dois tipos de BRBs foram utilizados na estrutura, um no piso térreo e outro no primeiro piso. Os dispositivos foram aplicados em série conjuntamente com um tubo de aço estrutural com 101,6mm de diâmetro exterior e uma espessura de 6,3mm. O aço do tubo estrutural é de classe S275, com um tensão de cedência de 275MPa. Os BRBs foram dimensionados de acordo com [12]; assumindo um deslocamento entre pisos de 0,3% e uma deformada lateral em forma de triângulo invertido. Na Tabela 2 estão apresentados os valores dos parâmetros mecânicos dos BRBs, obtidos por meio de testes.

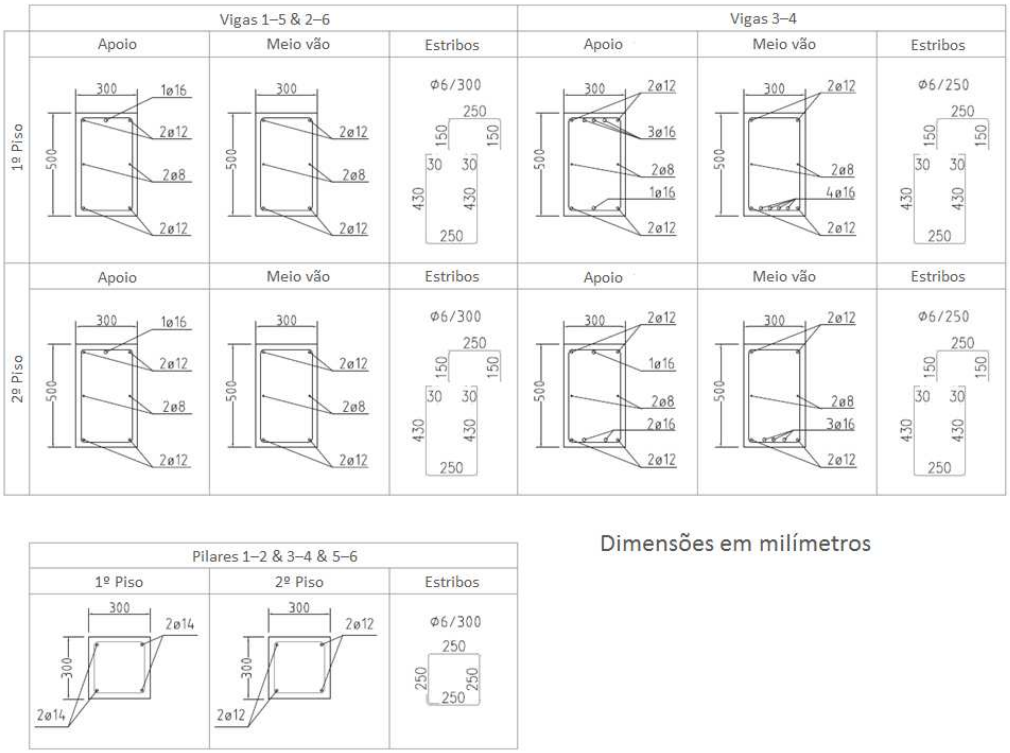

Figura 6: Representação das secções transversais das vigas e pilares das estruturas de teste [10].

Tabela 1: Propriedades mecânicas das armaduras [10]

	Tensão de cedência (Limite inferior)	**Tensão de cedência (Limite superior)**	**Tensão de rutura**	**Rácio tensão última/tensão de cedência**		
				Limite inferior	**Limite superior**	**Extensão última**
	[MPa]	[MPa]	[MPa]	[-]	[-]	[%]
Média	334.1	348.1	444.0	1.33	1.28	41
DP*	14.4	10.8	36.62	0.07	0.09	5
COV (%)	4.3	3.1	8.25	5.55	7.21	13

*Desvio padrão

Os tubos estruturais foram dimensionados por forma a não prejudicarem o funcionamento dos BRBs, com uma força última superior à dos dissipadores.

Campanha Experimental

As estruturas foram testadas dinamicamente para identificar as suas propriedades modais e foi testada a sua resistência lateral, aplicando um deslocamento até à

Tabela 2: Parâmetros mecânicos dos BRBs do primeiro e segundo piso

	Comprimento [m]	Força de cedência [kN]	Força máxima [kN]	Rigidez axial elástica [kN/mm]
Piso térreo	0.91	75	90	70
Primeiro piso	1.10	40	50	40

rutura (Pushover). As frequências modais da estrutura foram estimadas através da análise do ruído ambiente e de vibrações impostas, com recurso a martelo de impacto. Por forma a recolher os dados do ensaio, as estruturas foram devidamente instrumentadas, com acelerómetros, extensómetros, transdutores e medidores laser, Figura 7. Na presente dissertação, quando referidos os eixos ortogonais X e Y estes referem-se aos representados na Figura 7.

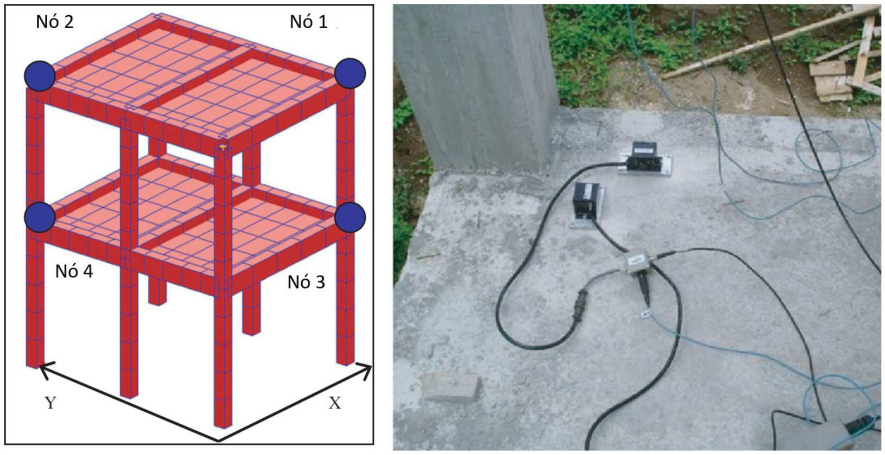

Figura 7: Posicionamento dos acelerómetros durante a campanha experimental [10].

Resultados Experimentais

Resposta Modal

Na Tabela 3 estão apresentados os valores das frequências de vibração para a estrutura simples e reforçada.

Resposta Lateral Monotónica

Foi executado um teste pushover estático e posteriormente foram obtidas as curvas de capacidade para cada uma das estruturas, simples e reforçada. Na Figura 8 está representada a curva de capacidade da estrutura simples.

A curva de capacidade correspondente à estrutura reforçada é apresentada na Figura 9.

Tabela 3: Frequências de vibração, em hertz, estimadas experimentalmente para a estrutura simples e reforçada [10]

		Modos de vibração					
Input	**Estrutura**	**1º Lateral X**	**2º Lateral Y**	**3º Torção**	**4º Lateral X**	**5º Lateral Y**	**6º Torção**
Ruído ambiente	Simples	3.15	3.30	4.75	8.80	9.31	13.10
	Reforçada	3.15	3.30	n.a.	8.85	9.36	n.a.
Impacto martelo	Simples	3.15	3.40	4.75	9.13	9.24	13.08
	Reforçada	3.15	3.30	4.84	8.76	9.25	12.94

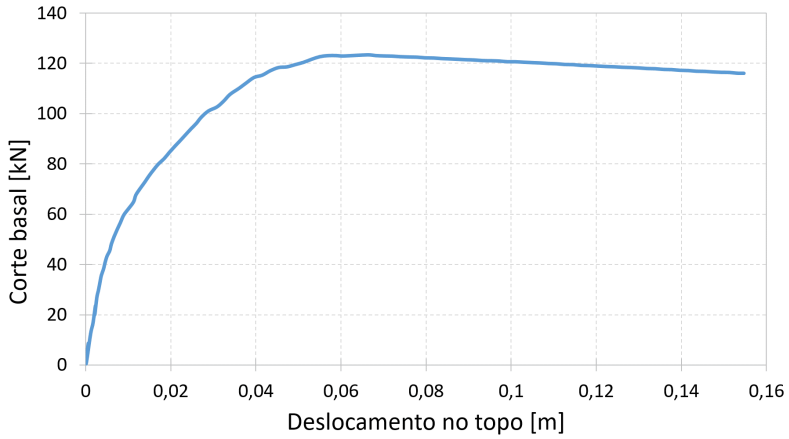

Figura 8: Curva de capacidade da estrutura simples (adaptado de [10])

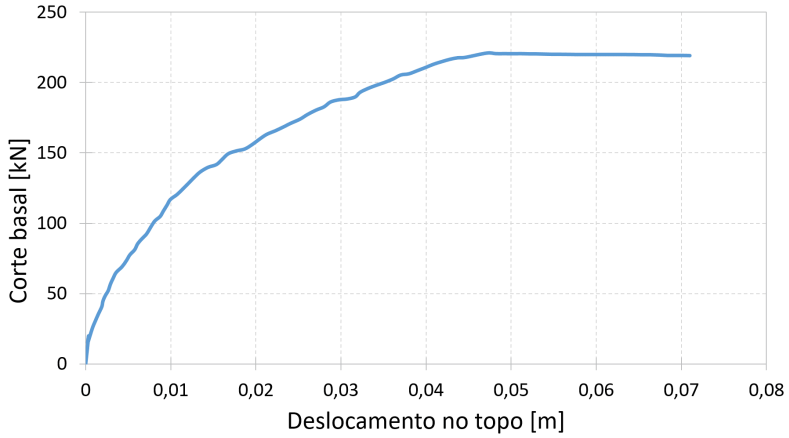

Figura 9: Curva de capacidade da estrutura reforçada (adaptado de [10])

Desenvolvimento e Calibração do Modelo Numérico

Com base nos resultados apresentados anteriormente foram desenvolvidos e calibrados dois modelos numéricos da estrutura de teste: um modelo da estrutura sem qualquer tipo de reforço, daqui em diante denominada "'Estrutura Simples"',

e outro modelo da estrutura reforçada com os BRBs, daqui em diante denominada "'Estrutura BRB"'. Foi criado um modelo adicional da estrutura de teste, desta vez reforçada com contraventamentos tradicionais, denominada "'Estrutura CBF"'. Os modelos numéricos foram desenvolvidos no programa de elementos finitos *SeismoStruct*, com base nos desenhos de projeto (Figuras 5 e 6) e os materiais definidos anteriormente.

Estrutura Simples

Inicialmente, todos os materiais foram corretamente definidos e introduzidos no *SeismoStruct*, tendo sido utilizada uma relação não linear e uniaxial de confinamento constante para modelar as relações constitutivas do betão.

As relações constitutivas do aço utilizado nas armaduras foram moduladas recorrendo a uma simples relação tensão-extensão proposta por Menegotto e Pinto [13] com regras de endurecimento isotrópico sugeridas por Filipou et al. [14].

Com os materiais devidamente definidos, as secções transversais e distribuição das armaduras foram implementadas no programa *SeismoStruct*, de acordo com o estipulado na Figura 6.

Foram definidos os tipos de elementos numéricos para representar cada um dos elementos estruturais. Um elemento de *frame* 3D *force-based* inelástico foi adotado para as vigas e colunas, permitindo considerar a não linearidade geométrica e dos materiais. Para a configuração destes elementos têm de ser selecionados uma secção transversal, o número de secções de integração e o número de fibras. Nas vigas, 200 fibras individuais e 7 secções de integração foram selecionadas. Por sua vez, os pilares foram subdivididos em 300 fibras longitudinais e foram adotadas 7 secções de integração.

Para a modelação das lajes, foi considerada uma combinação de elementos de *frame* elásticos, juntamente com restrições do tipo diafragma rígido, como demonstrado na Figura 10.

Os elementos de *frame* elásticos adicionados ao modelo numérico possuem as mesmas características da respetiva laje: rigidez axial, rigidez de flexão nas duas direções e ainda rigidez de torção.

Adicionalmente, elementos de massa pontual foram adicionados para considerar o peso próprio e as cargas de projeto. Uma vez que a estrutura é simétrica, foram definidos apenas dois elementos de massa pontual dispostos de acordo com o ilustrado na Figura 10.

Finalmente, para simular o ensoleiramento geral todos os pilares foram considerados encastrados.

Após a definição do modelo numérico, a campanha experimental foi recriada numericamente para calibrar e validar o modelo.

Resposta Modal

Inicialmente, procedeu-se a uma análise modal e os valores das frequências de vibrações foram obtidas. Na Tabela 4 é apresentada uma comparação entre os resultados numéricos e os experimentais.

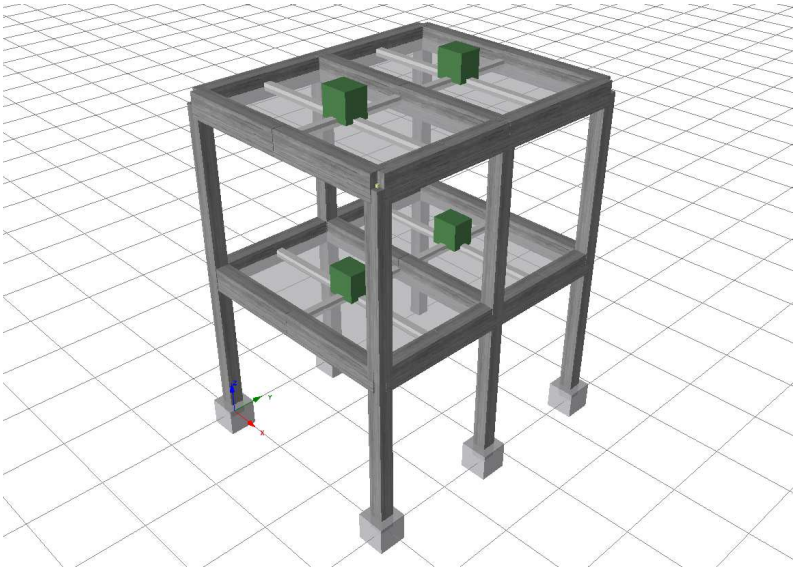

Figura 10: Solução adotada para a modelação das lajes

Tabela 4: Frequências de vibração: Estrutura Real vs. Modelo Numérico

Modo	Estrutura Real [Hz]	Modelo Numérico [Hz]	Erro [%]
1	3.15	3.157	0.233
2	3.30	3.261	1.183
3	4.75	4.695	1.151
4	8.80	8.280	5.913
5	9.31	8.383	9.952
6	13.10	12.046	8.045

Para os três primeiros modos de vibração existe uma grande proximidade dos valores das frequências, com o erro relativo para estes abaixo dos 2%. Nos três restantes modos verificou-se uma maior disparidade, mas sempre com erros abaixo dos 10%, o que foi considerado aceitável.

Pushover Estático

Foi recriada a análise pushover estática na direção longitudinal (Y), resultando desta análise a curva de capacidade numérica da estrutura. Na Figura 11 é apresentada uma comparação entre as curvas de capacidade da estrutura real e do modelo numérico. As curvas apresentam um traçado idêntico, sendo o maior erro relativo de aproximadamente 5%.

Foi também realizada uma análise pushover na direção transversal (X) e obteve-se a respetiva curva de capacidade. Na Figura 12 apresenta-se uma comparação das curvas de capacidade em ambas as direções.

Com a realização de ambas as análises podemos concluir que o modelo numérico da Estrutura Simples simula a realidade de forma fidedigna e, como tal, o modelo

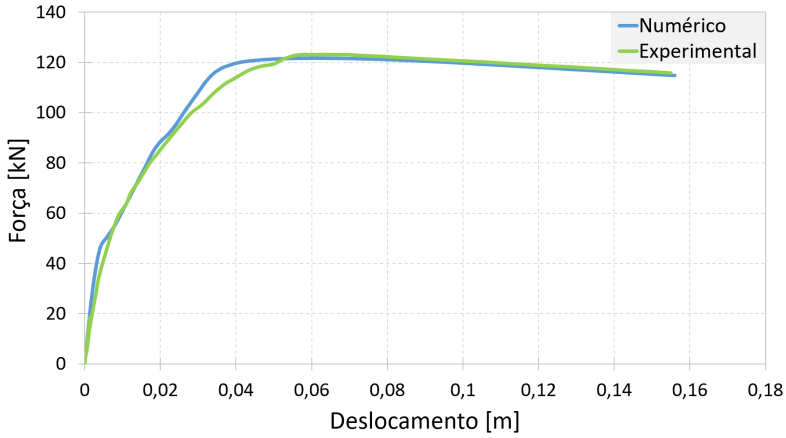

Figura 11: Comparação entre as curvas de capacidade da estrutura real e do modelo numérico

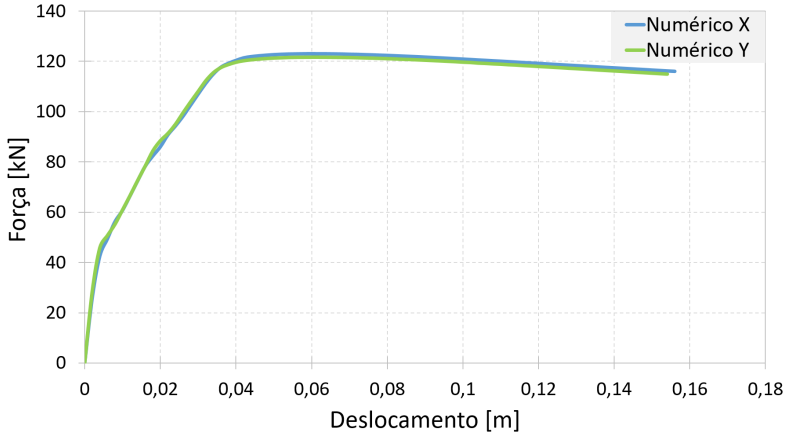

Figura 12: Comparação das curvas de capacidade numéricas em ambas as direções ortogonais

foi considerado calibrado e validado.

Estrutura BRB

Para proceder à validação da Estrutura BRB é de extrema importância que o sitema de reforço, seja corretamente calibrado e validado.

Calibração dos BRBs

Para tal, três modelos numéricos foram desenvolvidos: modelo do BRB isolado, modelo do conjunto BRB com o tubo estrutural e um modelo de um só elemento equivalente ao conjunto anterior. Para cada modelo foi realizado um teste de compressão e de tração numéricos.

Através de ensaios aos componentes, desenvolvidos por Di Sarno e Manfredi [10], foram obtidos os paramêtros mecênicos dos BRBs, que estão apresentados na Tabela 2. Desses ensaios resultou que os BRBs admitem deslocamentos axiais

de ±20mm.

Modelo Numérico do BRB Isolado

Para a modelação dos BRBs foi considerada uma secção circular com diamêtro de 0.1016m, juntamente com a relação constitutiva Dodd-Restrepo para o aço, assim como um elemento de treliça presente no *SeismoStruct*.

Nas Figuras 13 e 14 são apresentadas as curvas força-deslocamento dos ensaios numéricos de tração e compressão, respetivamente. Pode ser observado que estão em conformidade com os dados da Tabela 2.

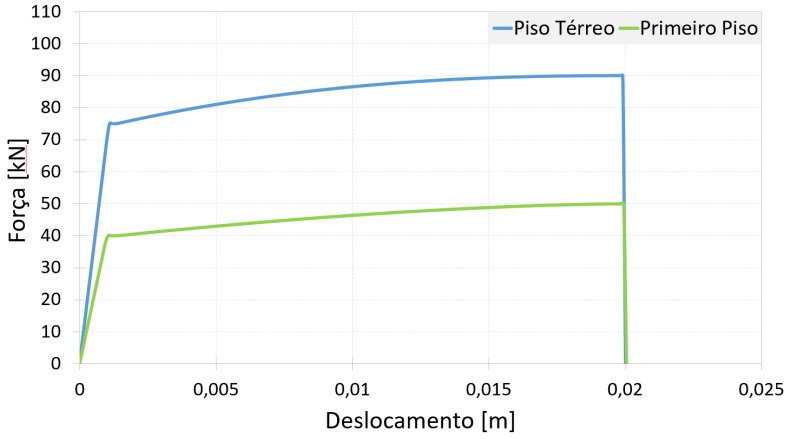

Figura 13: Curvas força-deslocamento do ensaio de tração do modelo numérico do BRB isolado.

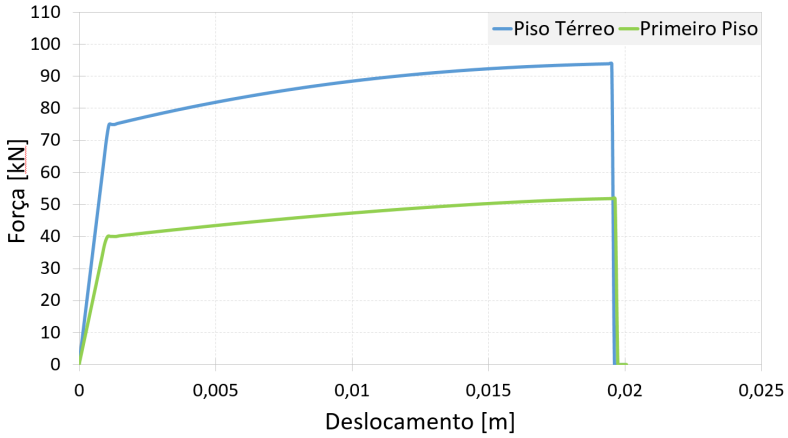

Figura 14: Curvas força-deslocamento do ensaio de compressão do modelo numérico do BRB isolado.

Modelo Numérico do Conjunto Tubo e BRB

Com os BRBs calibrados procedeu-se à adição dos tubos estruturais no *SeismoStruct*. Foi adotada uma secção tubular de 101.6mm de diâmetro exterior,

e 6.3mm de espessura, constituído por um aço de classe de resistência S275. Nas Figuras 15 e 16 estão representadas as curvas força-deslocamento para os dois ensaios numéricos conduzidos, onde se pode observar que a presença dos tubos não prejudica de maneira alguma o comportamento dos BRBs.

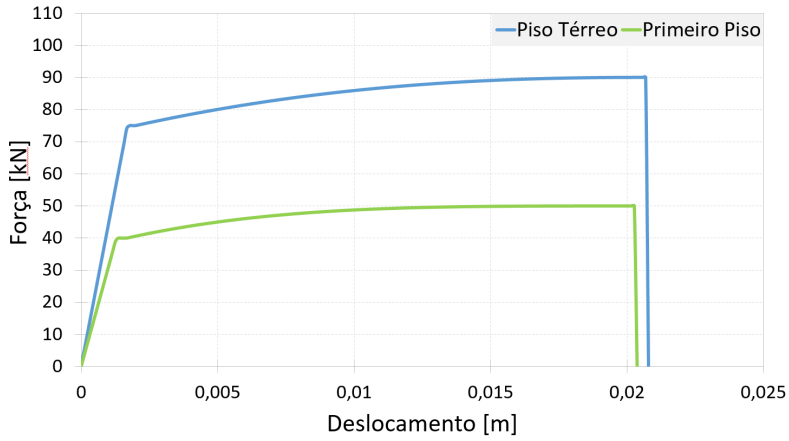

Figura 15: Curvas força-deslocamento do ensaio de tração do modelo numérico do conjunto tubo e BRB.

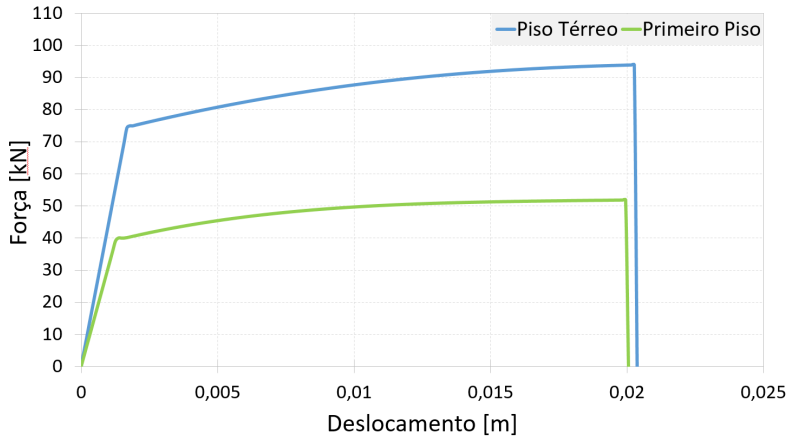

Figura 16: Curvas força-deslocamento do ensaio de compressão do modelo numérico do conjunto tubo e BRB.

Modelo Numérico Equivalente

No modelo anterior era necessário um nó estrutural a fazer a ligação entre o tubo e o BRB, sendo que este pormenor levanta problemas em termos de compatibilidade de deslocamentos, uma vez que este nó de ligação tem de restringir todas as rotações nas três direções ortogonais. Para tal, foi considerada uma solução equivalente, composta por um só elemento de treliça capaz de substituir os dois componentes, mantendo o mesmo comportamento mecânico. Foi adotada uma secção circular sólida com os mesmos 101.6mm de diâmetro.

Nas Figuras 17 e 18 é apresentada uma comparação entre os resultados dos

ensaios numéricos do modelo do conjunto tubo e BRB, e o modelo equivalente. Pode ser observado que o modelo equivalente representa bem o comportamento do conjunto.

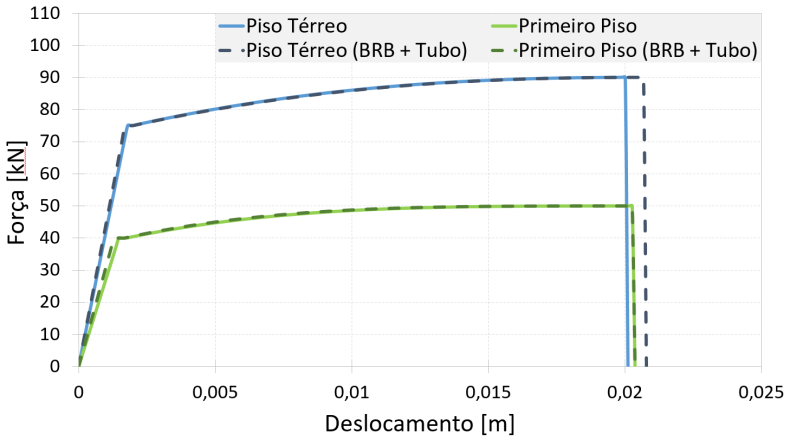

Figura 17: Curvas força-deslocamento do ensaio de tração do modelo equivalente.

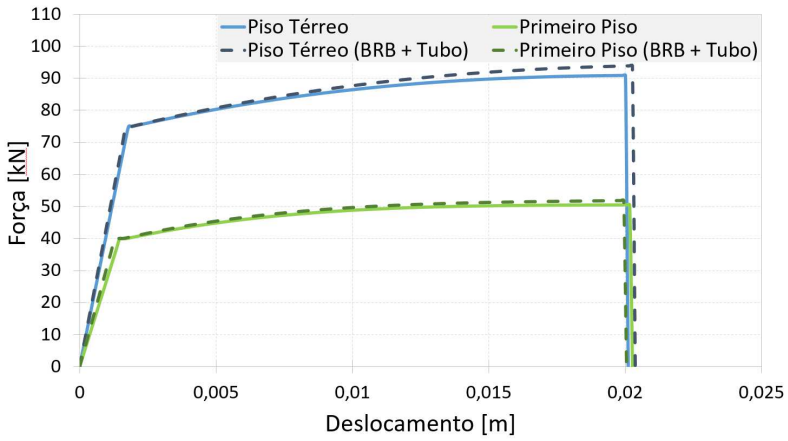

Figura 18: Curvas força-deslocamento do ensaio de compressão do modelo equivalente.

Com o sistema de reforço devidamente calibrado, procedeu-se à validação da Estrutura BRB, começando por recriar o esquema de reforço experimental e, posteriormente, proposta uma nova solução de reforço.

Validação do Esquema de Reforço Experimental

No trabalho experimental de Di Sarno e Manfredi [10] a estrutura foi reforçada somente na direção longitudinal e apenas num pórtico. Este esquema de reforço foi reproduzido e ensaiado numericamente, tendo sido realizada uma análise modal e pushover. Na Tabela 5 é apresentada uma comparação entre os valores das frequências de vibração dos ensaios experimentais e numéricos, sendo possível observar que o erro relativo se mantem sempre abaixo dos 10%, e nos três primeiros modos abaixo dos 3%, o que se considerou aceitável.

Tabela 5: Frequências de vibração: Estrutura real reforçada vs. Modelo numérico reforçado

Modo	Estrutura real [Hz]	Modelo numérico [Hz]	Erro [%]
1	3.15	3.157	0.233
2	3.30	3.261	1.183
3	4.84	4.695	2.989
4	8.76	8.280	5.484
5	9.25	8.383	9.369
6	12.94	12.046	6.908

Na Figura 19 é apresentada uma comparação das duas curvas de capacidade, tanto da estrutura real como do modelo numérico, podendo ser constatado que as curvas têm um traçado similar nunca passando um erro relativo de 8%.

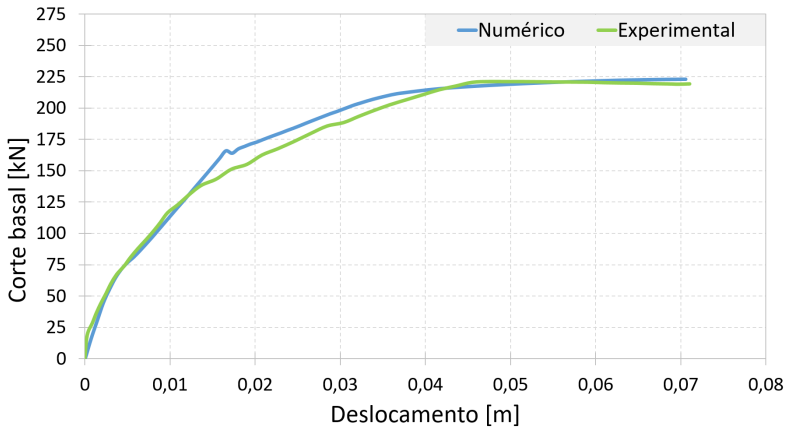

Figura 19: Comparação entre as curvas de capacidade da estrutura real e do modelo numérico.

Validação dos Esquema de Reforço Proposto

O esquema de reforço proposto consiste em aplicar a mesma "'quantidade"' de BRBs nas duas direções ortogonais, sendo que na direção longitudinal o reforço é aplicado nos dois pórticos. Esta proposta surge no sentido de mitigar os efeitos de torção resultantes da excentricidade entre o centro de massa e o centro de rigidez que ocorre no esquema experimental. Foi realizada uma análise modal e pushover para comparar o esquema proposto com o esquema experimental. Na Tabela 6 são comparados os valores das frequências de vibração. Na Figura 20 é apresentada uma comparação entre as curvas de capacidade da estrutura real reforçada, do modelo numérico reforçado com o esquema experimental e o modelo numérico reforçado com o esquema proposto.

Assim como para a Estrutura Simples, foi realizada uma análise pushover na direção transversal. Na Figura 21 é apresentada uma comparação entre os dois

Tabela 6: Frequências de vibração: Esquema de reforço experimental vs. Esquema de reforço proposto.

Mode	Experimental scheme [Hz]	Proposed scheme [Hz]	Difference [%]
1	3.157	3.119	1.205
2	3.261	3.221	1.222
3	4.695	4.567	2.735
4	8.280	8.152	1.551
5	8.383	8.255	1.531
6	12.046	11.645	3.330

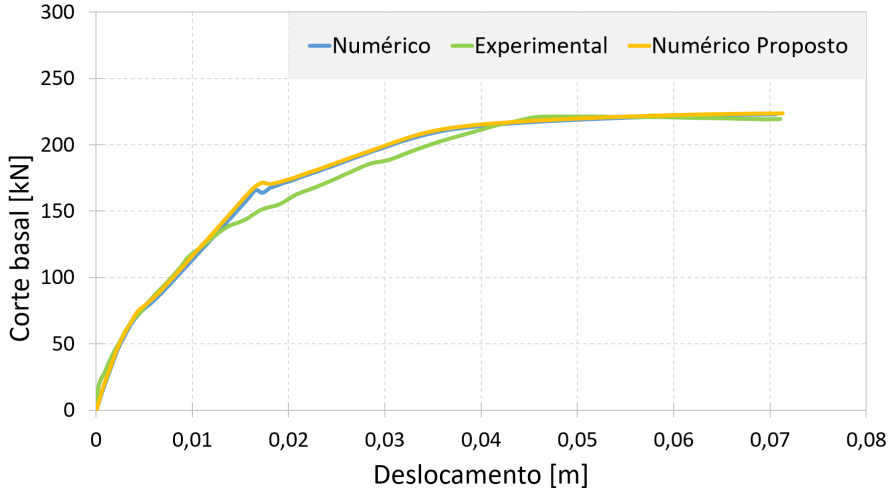

Figura 20: Comparação entre as curvas de capacidade da estrutura real reforçada, do modelo numérico reforçado com o esquema experimental e o modelo numérico reforçado com o esquema proposto.

esquemas de reforço, ficando evidente a disparidade de comportamento entre as duas direções no esquema de reforço experimental.
A Estrutura BRB foi então validada e considerada como ponto de partida para criação dos 50 modelos para o estudo de fragilidade.

Avaliação da Vulnerabilidade Sísmica

Uma vez validados os modelos numéricos, o passo seguinte passou pela realização da avaliação da vulnerabilidade sísmica.

Ação Sísmica

Foram considerados dois cenários sísmicos distintos, com probabilidade de acontecer na região de Faro, Portugal. Os cenários são referentes às falhas do Marquês de Pombal e da Ferradura, ambas localizadas no Oceano Atlântico. A simulação numérica dos cenários foi realizada com base no método estocástico

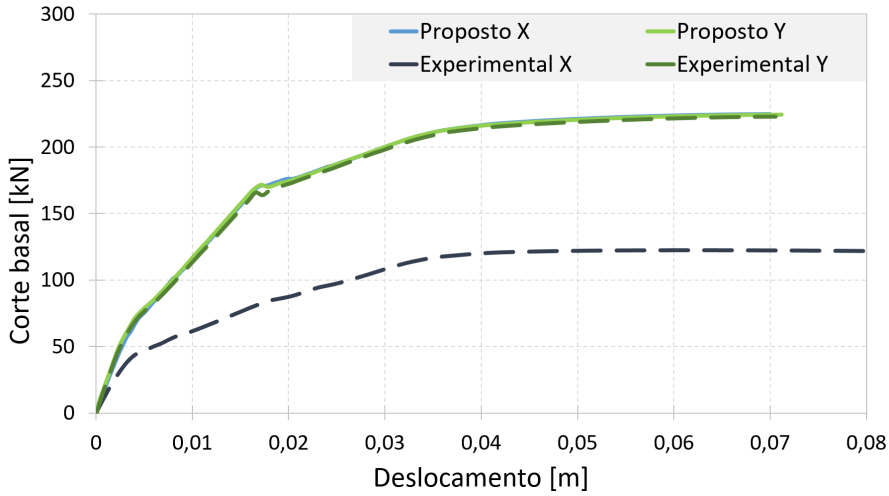

Figura 21: Comparação entre as curvas de capacidade para os dois tipos de reforço, nas duas direções ortogonais.

não-estacionário considerando os efeitos de falha finita, através do programa RSSIM integrado no simulador LNECloss desenvolvido pelo LNEC [15]. Foram consideradas várias direções de rutura, norte-sul, sul-norte e aleatória ao longo da extensão das falhas, assim como magnitudes de 7.2 e 7.5 para a falha de Marquês de Pombal, e de 7.8 para falha da Ferradura, na escala de Richter. A título de exemplo, é apresentado na Figura 22 um dos acelerogramas gerados.

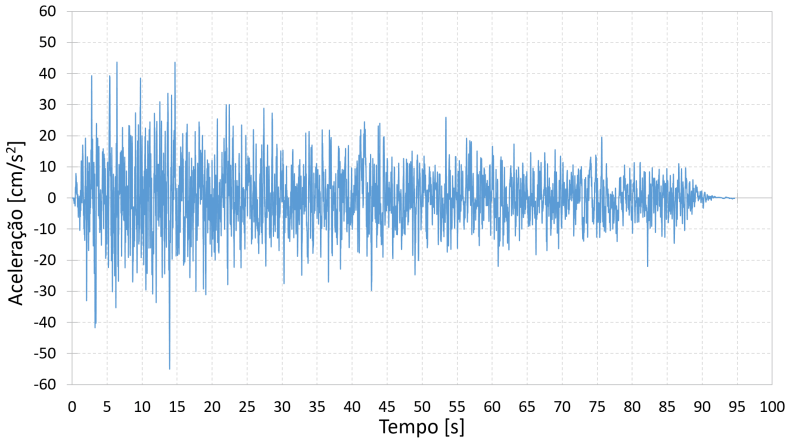

Figura 22: Acelerograma Faro falha da Ferradura direção Norte-Sul

Com os acelerogramas gerados, 50 cenários sísmicos foram considerados, com durações entre 20.57s e 94.64s. Todos os acelerogramas foram escalados para uma aceleração máxima de 1g, por forma a serem introduzidos no *SeismoStruct* e poderem assim ser escalados durante a análise dinâmica incremental (IDA).

Parâmetros Chave e Variabilidade Probabilística

Para entrar em consideração com incertezas físicas e mecânicas, os modelos numéricos foram desenvolvidos assumindo para alguns parâmetros chave uma distribuição probabilística, de acordo com o *JCSS model code* [16]. A Tabela 7 aprensenta esses parâmetros chave e as respetivas distribuições.

Tabela 7: Caraterização probabilística dos parâmetros chave.

Parâmetros chave	Distribuição	Média	DP	Unidades
Resistência à compressão do betão (f_c)	Lognormal	19.4	1.3	MPa
Peso volúmico do betão (ρ_c)	Normal	24	0.96	kN/m^3
Tensão de cedência do aço (f_y)	Normal	341.4	12.6	MPa

Assim, 50 cenários foram gerados, com os paramêtros a variar segundo as respetivas distribuições probabilísticas, estando estes apresentados na Figura 23.

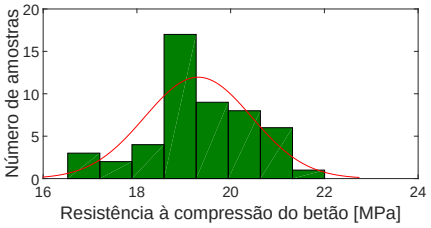

(a) Resistência à compressão do betão

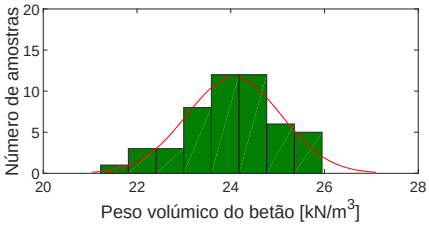

(b) Peso volúmico do betão

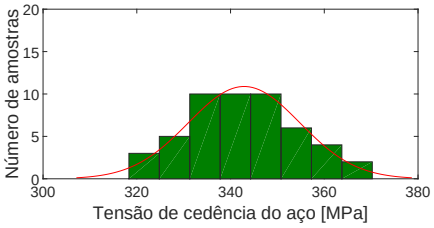

(c) Tensão de cedência do aço

Figura 23: Distribuição probabilística dos parâmetros chave.

Para saber se um espaço amostral de 50 amostras seria estatisticamente confiável em termos de resultados, foi realizado um estudo da variação e erro relativo do desvio padrão à medida que o espaço amostral aumentava. Nas Figuras 24 e 25 podemos observar que o desvio padrão estabiliza perto dos valores inicialmente pretendidos à medida que o espaço amostral aumenta, e que, o erro relativo baixa dos 1% quando é atingido um espaço amostral de 50 amostras. Os resultados demonstram tratar-se de um espaço amostral adequado e que os resultados subsequentes serão confiáveis e relevantes estatisticamente.

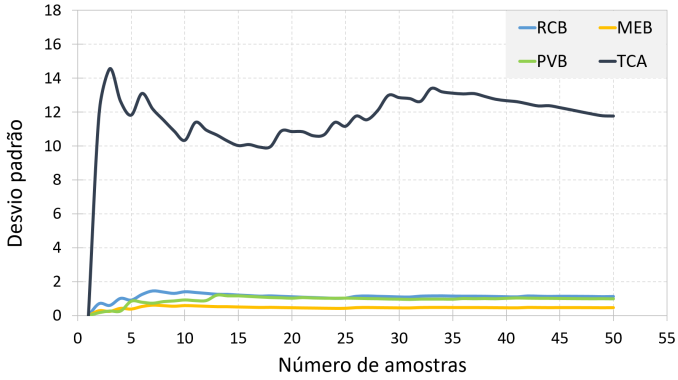

Figura 24: Evolução do desvio padrão ao longo do espaço amostral.

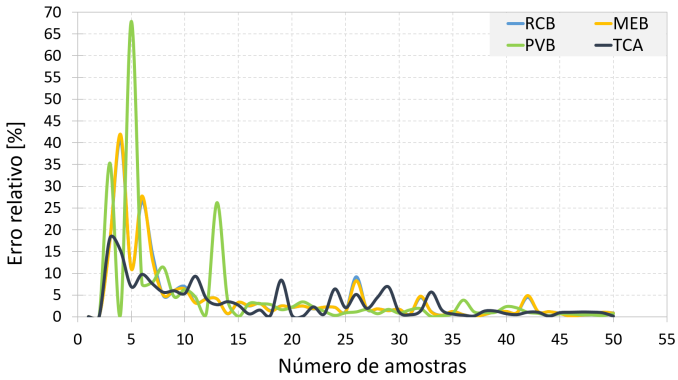

Figura 25: Evolução do erro relativo do desvio padrão ao longo do espaço amostral.

Análise Dinâmica Incremental

Definidos os 50 cenários sísmicos e os 50 modelos numéricos, de acordo com as variações probabilísticas, podem ser realizadas as 150 análises dinâmicas incrementais. Numa análise dinâmica incremental a estrutura é submetida a um série de análises dinâmicas não lineares no tempo de intensidade crescente. É depois gerado um gráfico que relaciona o valor máximo de deslocamento com o correspondente valor da força de corte basal para cada análise não linear no tempo de diferente intensidade, dando origem à curva IDA ou pushover dinâmico, Figura 26.

Estados de Dano

Com as curvas IDA definidas, definiram-se os estados de dano associados a cada curva, de acordo com Vargas [17], sendo que a definição de cada estado de dano pode ser consultada na Tabela 8 e na Figura 26.

Curvas de Fragilidade

As curvas de fragilidade são descritas por uma função de distribuição de probabilidade do tipo lognormal, dada pela Equação 1:

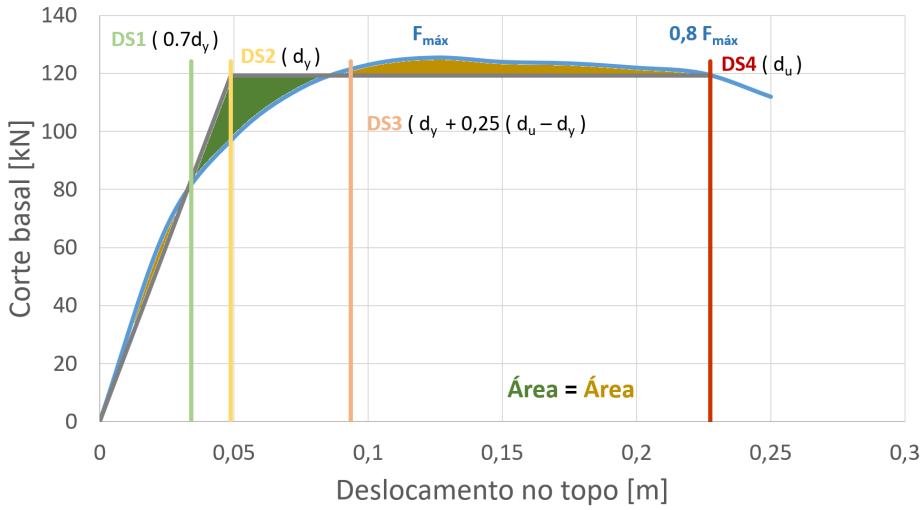

Figura 26: Curva IDA, juntamente com a sua representação bilinear e respetivos estados de dano.

Tabela 8: Definição dos estados de dano.

Estados de dano
$DS_1 = 0.7 \cdot D_y$
$DS_2 = D_y$
$DS_3 = D_y + 0.25 \cdot (D_u - D_y)$
$DS_4 = D_u$

$$P\left[DS|S_d\right] = \Phi\left[\frac{1}{\beta_{DS}} \cdot ln\left(\frac{S_d}{\overline{S_d}_{,DS}}\right)\right] \quad (1)$$

e os valores de probabilidade para cada estado de dano são dados por:

$$P(D_0) = 1 - P\left[d_{s_1}|S_d\right] \quad (2)$$

$$P(D_k) = P\left[d_{s_k}|S_d\right] - P\left[d_{s_{k+1}}|S_d\right] \quad (3)$$

$$P(D_4) = P\left[d_{s_4}|S_d\right] \quad (4)$$

com k = 1, 2 e 3.

Foram construídos três conjuntos de curvas de fragilidade para cada uma das estruturas (Simple e BRB), uma na direção X, na direção Y e uma combinando as duas direções, contemplando o estado de dano mais gravoso. Daqui resultaram três conjuntos de curvas globais para cada uma das estruturas.

Resultados e Comparação

Após a realização de 150 análises dinâmicas incrementais, perfazendo mais de 1000 horas de trabalho computacional, e análise de mais de 300 curvas IDA e respetivos estados de dano, foram construídas as curvas de fragilidade. Para todas as curvas foi evidenciado o nível de aceleração de pico do movimento do

solo (*Peak Ground Aceleration* - PGA) de 0,3g, para o qual foram calculadas as probabilidades de atingir determinado dano. Este nível de PGA corresponde ao nível de projeto estipulado no Eurocódigo 8 [18], na região de Faro, Portugal. Devido a problemas de análise de resultados as curvas de fragilidade foram refeitas ao nivel dos pilares da estrutura em vez da estrutura global.

Nas Figuras 27 e 28 apresentam-se as curvas de fragilidade globais e os valores das probabilidades de cada estado de dano para um nível de PGA de 0,3g para a Estrutura Simples.

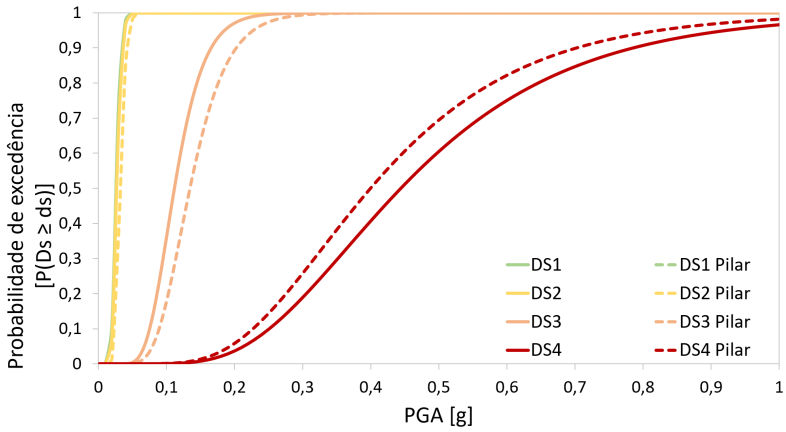

Figura 27: Comparação entre as curvas de fragilidade ao nível do topo e ao nível dos pilares da Estrutura Simples.

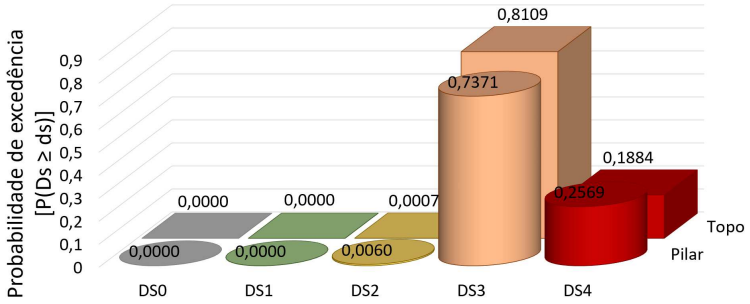

Figura 28: Comparação entre os valores de probabilidade de excedência dos estados de dano ao nível do topo e ao nível dos pilares da Estrutura Simples, para um nível de PGA de 0,3g.

No caso da Estrutura BRB podem ser observadas nas Figuras 29 e 30 as respetivas curvas de fragilidade e os valores de probabilidade de excedência dos estados de dano.
Foi realizada uma verificação com a finalidade de aferir se as estruturas

xxx

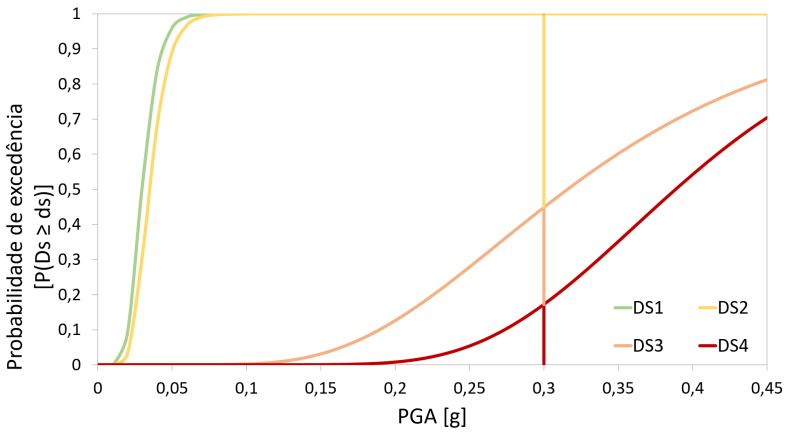

Figura 29: Curvas de fragilidade da Estrutura BRB.

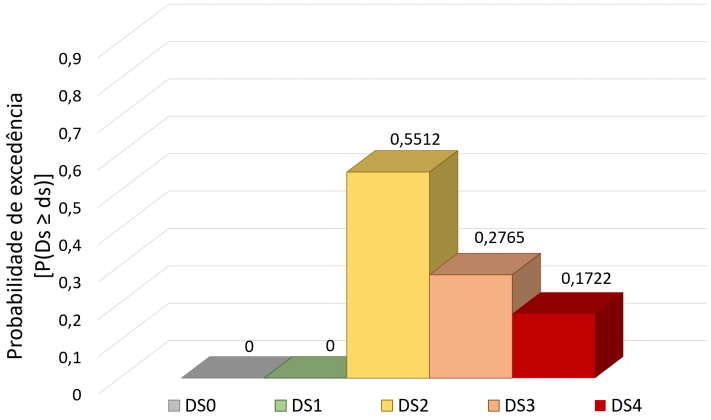

Figura 30: Valores de probabilidade de excedência dos estados de dano para um nível de PGA de 0,3g, da Estrutura BRB.

verificavam os valores máximos admissíveis de probabilidade de atingir os estados limites últimos, p'_{fu}, de acordo com a regulamentação inglesa [19] e Henriques [20]. Na Tabela 9 são apresentados os valores máximos admissíveis calculados para a estrutura em estudo.

Tabela 9: Máxima probabilidade de excedência admissíveis, p'_{fu}, for K_s = 0,05

Nível de segurança, n_p	**Período de vida da estrutura,** T_r **50 anos**
Reduzido (0.1)	2.5×10^{-3}
Normal (1.0)	2.5×10^{-4}
Elevado (10)	2.5×10^{-5}

Considerando que:

$$P_{fu;Simple} = 2.57 \times 10^{-1}$$
$$P_{fu;BRB} = 1.72 \times 10^{-1}$$

Realizou-se a seguinte verificação:

- Se $p'_{fu} \geq P_{fu;Simple;BRB}$ Verifica
- Se $p'_{fu} \leq P_{fu;Simple;BRB}$ **Não Verifica**

Nas Tabelas 10 e 11 são apresentadas as verificações para a Estrutura Simples e BRB, respetivamente.

Tabela 10: Verificação Estrutura Simples

Nível de segurança, n_p	**Período de vida da estrutura,** T_r **50 anos**
Reduzido (0.1)	**2.5×10^{-3}**
Normal (1.0)	**2.5×10^{-4}**
Elevado (10)	**2.5×10^{-5}**

Tabela 11: Verificação Estrutura BRB

Nível de segurança, n_p	**Período de vida da estrutura,** T_r **50 anos**
Reduzido (0.1)	**2.5×10^{-3}**
Normal (1.0)	**2.5×10^{-4}**
Elevado (10)	**2.5×10^{-5}**

Conclusão

A avaliação da eficiência do uso de contraventamentos de encurvadura impedida (BRB) como reforço sísmico de um edifício porticado de betão armado foi realizada com sucesso. Após a calibração do modelo numérico no programa de elementos finitos *SeismoStruct*, baseado nos resultados experimentais de Di Sarno e Manfredi [10], uma abordagem probabilística permitiu contemplar incertezas ao nível da ação sísmica, das propriedades dos materiais e do comportamento estrutural, e, juntamente com as curvas IDA, definir os respetivos estados de dano e por fim gerar as curvas de fragilidade.

A subsequente análise das curvas de fragilidade permitiu concluir que, para um PGA de projeto de 0,3g definido para a região de Faro, a estrutura sem qualquer tipo de reforço tem elevada probabilidade de sofrer danos extensos e até mesmo

de colapsar, evidenciando assim a necessidade deste tipo de estruturas sofrerem uma intervenção de reforço sísmico.

Após a instalação dos BRBs, a estrutura continuou a exibir 100% de probabilidade de sofrer danos para um PGA de 0,3g. Apesar de se verificar uma redução dos valores de excedência nos estados de dano mais gravosos e um aumento nos mais leves, a estrutura não se encontra em cumprimento do exigido pelos códigos em termos dos estados limites últimos.

Concluindo, a avaliação da vulnerabilidade e estudo de fragilidade conduzido na estrutura sem reforço e reforçada com BRBs foi conduzida com sucesso, revelando claramente a capacidade dos BRBs de mitigar o dano face a solicitações sísmicas severas.

Contents

List of Figures

List of Tables

List of Abbreviations, Acronyms and Symbols

Abbreviations

DT-BRB	Double-Tee Double Tube BRB
EC2	Eurocode 2
EC8	Eurocode 8
iBRB	Inspectable BRB
PMC	Probabilistic Model Code

Acronyms

AISC	American Institute of Steel Construction
BRAD	Buckling Restrained Axial Damper
BRB	Buckling Restrained Braces
BRBF	Buckling Restrained Braced Frame
CEN	European Committee for Standardization
DCBRB	Double-core buckling restrained braces
DM	Damage Measure
DS	Damage State
FE	Finite Element
FEM	Finite Element Method
FEMA	Federal Emergency Management Agency
GBF	Gorringe Bank Fault
HAZUS	Hazards United States
HF	Ferradura Fault
IDA	Incremental Dynamic Analysis
IM	Intensity Measure
JCSS	Joint Committee on Structural Safety
JSCA	Japan Structural Consultants Association
JSSI	Japan Society of Seismic Isolation
LTVF	Lower Tagus Valley Fault
MPF	Marquês de Pombal Fault
NEHRP	National Earthquake Hazards Reduction Program
NGBF	Northern Guadalquivir Bank Fault
PAF	Príncipes de Avis Fault

PGA	Peak Ground Acceleration
PGD	Peak Ground Displacement
PGV	Peak Ground Velocity
PSNF	Pereira de Sousa Normal Fault
RC	Reinforced Concrete
SD	Standard Deviation
SDOF	Single degree of freedom
SEAOC	Structural Engineers Association of California
SF	Scale Factor
SGBF	Southern Guadalquivir Bank Fault
SW	South West
UC	University of California
VM	Vinyl Mastic
WT	Wire transducers

Symbols

α_2	Fraction of building height at location of pushover mode displacement
β	Imperfect unbonding factor
β_c	Compression strength adjustment factor
β_C	Random variable related to the response and resistance capacity of the element uncertainties
β_D	Random variable related to the earthquake input motion uncertainties
β_{DS}	Random variable related to the damage state definition uncertainties
$\beta_{M(DS)}$	Uncertainty on the definition of the damage state threshold
β_{tot}	Total standard deviation
Γ	Axial load difference
δ	Fault dip
δ_y	BRB's yield axial deformation
Δ_b	Deformation quantity used to control the loading of the test specimen
Δ_{bm}	Design story drift of the bay in which the BRB will be located
Δ_{by}	Deformation at the first significant yielding in the brace
Δ_{DS}	Inter-story drift ratios threshold values of a damage state
ΔL	Subfault length
Δ_u	Ultimum drift
ΔW	Subfault width
Δ_y	Yielding drift
ε	Axial strain
ε_{DS}	Lognormally distributed variable with standard deviation β_{DS}
ζ	Damping
η	Cumulative inelastic axial deformation
λ	Load factor
λ_{yield}	Lowest scaling factor needed to cause yielding for a given record and structural model
ν	Poison Ratio
σ	Standard deviation
ϕ	Fault strike

Φ	Reinforcement bars diameter
Φ	Standard cumulative probability function
ω	Tension strength adjustement factor
Ω	Steel core's material over-strength factor
Ω_h	Steel core's material strain hardening factor

A	Brace's deformed cross section area
A_0	Brace's original cross section area
A_{sc}	Cross sectional area of the BRB core plate
c	Center of subfault
C_{max}	Maximum compressive brace forces
d_2	Collapse prevention limit state
d_{bL}	Minimum diameter of longitudinal rebars
d_{bW}	Stirrup's diameter
D_{by}	Brace's yield axial elongation
D_u	Ultimum spectral displacement
D_y	Yielding spectral displacement
E_0	Encasing member's Young Modulus
E_{cm}	Concrete's Young Modulus
E_h	Total hysteretic energy
E_i	Steel core's Young Modulus
EA	Axial stiffness
EI	Flexural stiffness
EI_{trans}	Flexural stiffness
f_{cm}	Concrete's mean compressive cylinder strength
F_{ysc}	Nominal yield strength of the core material
f_y	Nominal yield strength
$F_{y,1}$	Ground floor BRB's yield force
$F_{max,1}$	Ground floor BRB's maximum force
$F_{y,2}$	Upper floor BRB's yield force
$F_{max,2}$	Upper floor BRB's maximum force
GJ	Torsional stiffness
h	Depth to fault upper edge
h	Typical roof height
H_W	Beam's height
I_0	Encasing member's moment of inertia
I_i	Steel core's mnoment of inertia
IM_{mi}	Median threshold value of the earthquake IM required to cause the i_{th} DS
$k_{el,1}$	Ground floor BRB's elastic axial stiffness
$k_{el,2}$	Upper floor BRB's elastic axial stiffness
K_s	Coefficient responsible of translating society's aversion to accept structural rupture occurrence
KL	Brace's effective/equivalent length
L	Brace's deformed length
L_0	Brace's original length

n_p	Average number of people victimized in case of structure rupture/ security threshold
N_e	Encasing member's Euler buckling load
N_y	Steel core's yielding force
O	Origin
Os	Surface projection of origin
P	Applied incremental load
P	Axial load
P	Observation point
P_{cr}	Brace's critical buckling load
$P_f()$	Probability of being present or exceeding a particular damage state
$P_{fu;Simple}$	Probability value of reaching the ultimate limit states for the Simple Frame
$P_{fu;BRB}$	Probability value of reaching the ultimate limit states for the BRB Frame
$P_{fu;CBF}$	Probability value of reaching the ultimate limit states for the CBF Frame
P_y	Nominal yield strength of the core section
P_y^+	Brace's effective compressive yield capacity
P_y^-	Brace's effective tensile yield capacity
P_y^*	Brace's average of the effective compressive and tensile yield capacities
P^o	Nominal loads pattern
p'_{fu}	Maximum admissible probability value of reaching the ultimate limit states
q(x)	Unknown distributed load
r	Distance from hypocenter to subfault center
R	Distance from subfault to observation point
s	Stirrup's spacing
S_a	Spectral acceleration
S_d	Spectral displacement
$\overline{S_d}_{,DS}$	Median value of S_d of damage state, DS
T_e	True elastic fundamental-mode period of the building
T_{max}	Maximum tensile brace forces
T_r	Lifetime period of structures to consider in the design
V	Rupture velocity
$\star$	Hypocenter

Chapter 1

Introduction

1.1 Background

During their life time, structures are susceptible to various solicitations that endanger their stability and, therefore, their function and safety. Firstly, vertical loads and displacements were the major concern for engineers when designing building structures. Afterwards, the concern with the lateral loading and displacements caused by wind and seismic actions was developed.

Seismic events are known to cause major problems to societies, specially in regions with high seismicity. They are one of the most dangerous natural phenomena, not only because of the structural damage in the building stock and human causalities, but also because of its unpredictability. Therefore, it becomes necessary to design buildings capable to resist ground motion solicitations.

One important seismic event, in Portugal, was Lisbon's 1755 earthquake. On November 1st 1755 an earthquake of approximately 8.5 on the moment magnitude scale struck Lisbon, causing major fires throughout the city and a Tsunami. The 1755 earthquake was one milestone in the Portuguese seismology development, since in the city's reconstruction special structural systems were employed to grant some resistance to seismic actions. Two structural systems were used to replenish the building stock, which already contemplated the contemporary concept of ultimate limit state and service limit state:

- Wood framed structures, which resisted the gravitational loads but also provided the necessary flexibility to not be significantly damaged when subjected to seismic action;
- Masonry walls which assured comfort and privacy in normal situations, but in case of intense ground motions their collapse was acceptable.

It was one of the first times that seismic mitigation systems were applied in buildings and these solutions remained to be used in the following decades. Afterwards, with the RC boom these solutions were abandoned and, the wood and masonry gave place to cement, steel and aggregates.

Since then, seismic engineering came a long way and many design guidelines and retrofitting techniques were developed and proposed for mitigation of the seismic induced damage. Solutions vary according to the solicitation intensity, building type and function.

Currently, in Europe, the Eurocode 8 (EC8) is the seismic code applied. It contains all the guidelines and recommendations for a proper structural design of seismic resistant structures. In EC8, structures are assigned a importance class and coefficient, according to their functional needs before a seismic event, as well as the consequences of its collapse in social, economical and human loss terms. This way, and according to this importance class, the importance coefficient is applied to the seismic action. Being superior to one, increasing the seismic action, for structures with a higher importance class and one, or lower, for lower importance classes. This way, structures with a higher class can withstand more severe earthquakes reducing the damages due to seismic action.

However, not all the current building stock was build recently, and respects the EC8 guidelines. Many old RC buildings lack adequate lateral resisting systems. These structures do not include closed-spaced stirrups in beams, columns and structural joints, thus endangering the shear capacity of these elements. Smooth bars, insufficient percentage of longitudinal steel reinforcement, low strength concrete, inadequate lap splices and anchorage, low concrete confinement, are typically found in many existing deficient buildings.

One currently used retrofitting technique is the use of bracing systems to add lateral stiffness to structures. Many configurations of these systems exist and are used in many types of buildings. The most common one consists on steel profiles added to RC frames, with various patterns, to allow them to have some lateral resistance, Figure 1.1. This system performs well to a certain degree, since the buckling behaviour of steel slender profiles reduces their load carrying capacity.

Figure 1.1: Typical retrofitting using concentric steel braces [21]

One significant technique used nowadays is the use of steel braces with their buckling restricted by an encasing member. The basic principle is to restrict the

buckling occurrence and therefore allow the brace to continue to absorb the horizontal loads. In Figure 1.2 is presented an illustration of the typical so called buckling restrained brace (BRB) along with its basic components.

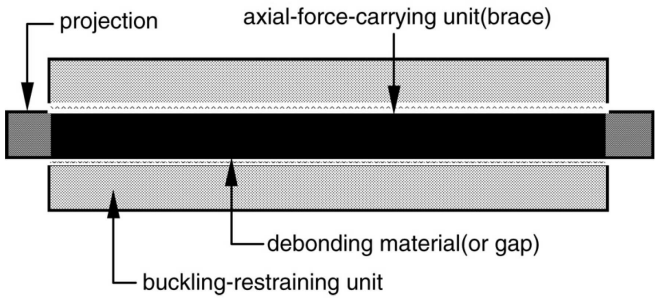

Figure 1.2: Typical composition of a buckling restrained brace [1]

As mentioned before, seismic events cause major losses both in terms of human lives and building stock, translating into major social/economic losses. Therefore, the study and research of not only seismic design, but also seismic retrofitting is of major importance in Civil Engineering. Currently, due to the advances in technology, computers are capable of accurately simulate seismic scenarios and predict the structural behaviour of buildings, allowing engineers to study many retrofitting configurations, materials and design strategies. In the present dissertation those advances were used and through numerical simulation, vulnerability assessment and a fragility analysis we seek to study the efficiency of BRBs.

1.2 Objectives and Scope

Taking into account what was previously mentioned, this dissertation aims to assess the efficiency of Buckling Restrained Braces in reinforced concrete (RC) structures through vulnerability assessment and fragility analysis. The objectives of the present document are:

- Literature research and review on Buckling Restrained Braces, their properties, behaviour and application.
- Development of a numerical model capable of reliably simulate the behaviour of a real RC framed structure.
- Literature research on Seismic vulnerability assessment and fragility analysis.
- Perform a vulnerability and fragility analysis of the structural frames, both without and with BRB retrofitting.

1.3 Dissertation Outline

In this section, an overview of the dissertation structure is provided. The text is organized in the following five chapters:

- **Chapter 1** Introductory overview on the subject of the dissertation, its objectives and structure;
- **Chapter 2** Review on Buckling Restrained Braces, addressing six main subjects: a brief history, configurations, key issues and detailing, design overview, histeretic behaviour and application cases.
- **Chapter 3** Description of the experimental campaign developed by Di Sarno and Manfredi [10]. Development and calibration of numerical models to accurately simulate the test specimens.
- **Chapter 4** Description of the considered seismic action. Seismic vulnerability study and description of the required procedures, such as the Incremental Dynamic Analysis and Fragility Curves. Results presentation and comparison.
- **Chapter 5** Summary and conclusions of the research, followed by suggestions of future work.

Chapter 2

Buckling Restrained Braces

The present chapter presents a review of buckling restrained braces. A brief introduction of these devices is provided, along with the various configurations developed and studied along the years. Afterwords, key topics of BRB's functionality and design are addressed, such as debonding between components, global stability and connections. Design codes and provisions are also briefly reviewed. Finally, the global hysteric behaviour of BRBs is assessed and examples of practical applications worldwide are provided.

2.1 BRB. The early years

Throughout the years, concentric steel braces have been used to counteract both wind and seismic actions in structures. However, the high slenderness of such braces results in global buckling under compression due to seismic excitation, causing strength and stiffness degradation. To prevent this behaviour, concentric steel braces have been applied using two opposed braces, so that when one is in tension the other is in compression. Nonetheless, the braces still exhibit pinched hysteretic cycles [2], as ilustrated in Figure 2.1.

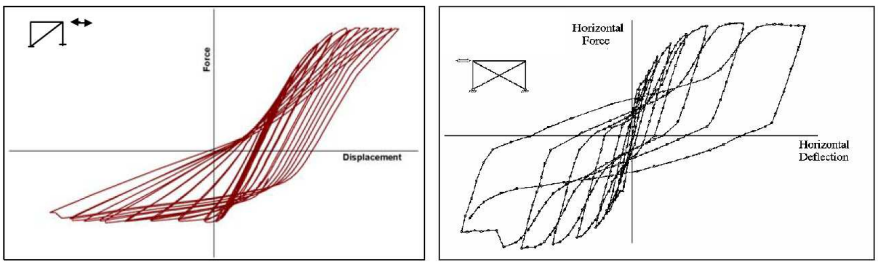

Figure 2.1: Typical behaviour of concentric brace frames (adapted from [2])

In order to avoid this behaviour, alternative systems have been developed and suggested. One alternative device is the buckling restrained brace (BRB). As the name implies, it consists of a steel brace with its buckling inhibited by an appropriate system. By restraining buckling, the braces exhibit the same strength in compression as they do in tension, displaying a better hysteretic behaviour

and increased energy absorption capability [1]. A comparison between the typical behaviour of both concentrically braced and BRB frames is illustrated in Figure 2.2.

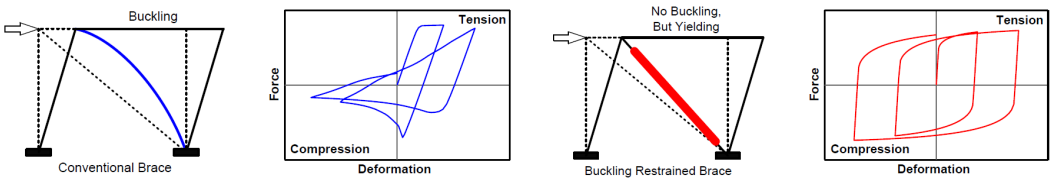

Figure 2.2: Conventional brace vs. BRB hysteretic behaviour [4]

Many configurations of BRBs have been proposed, but they generally follow the same principle and components: a yielding core, responsible for withstanding the axial forces; a restraining/casing member, capable of preventing the core buckling; a separation system between the former two components, to ensure the yielding core can slide freely inside the restraining member and that transverse expansion can occur in case of yielding in compression; and a strengthened transition segment, which is responsible for the link between the brace and the connections to the structure, and also ensures the yielding occurs along the length of the steel core and never in the transition segments.

According to Xie Q. [1] the first scientific appearance of a bracing system with its buckling behaviour inhibited was in 1971, in a study carried out by Yoshino et al. [22]. Two specimens consisting of a flat steel plate encased by RC panels with some debonding materials between them where cyclically tested. One with a 15mm gap between the plate and restraining panel whilst the other was not provided with any spacing. The former specimen displayed larger deformations and energy dissipation capacity than the later.

Years later Wakabayashi et al. [23, 24] thoroughly tested very similar systems in which, braces made of steel flat plates were encased by RC panels with an unbonded layer between them. A multi-step experimental campaign was carried out, which consisted of: firstly, testing debonding materials to explore the unbonded effects; secondly, brace testing to examine the effects of reinforcement at the concrete panel boundaries; thirdly, tests on reduced scale braced systems encased by concrete panels were conducted; and lastly, large scale tests on two story frames with the proposed brace systems were carried out. Eleven specimens with different debonding materials were tested trough pull-out tests. A two layer coating of a silicon resin on top of an epoxy resin one showed the best performance and was afterwards used in the following experiments. In the second stage, twenty one specimens with many combinations of reinforcing details around the plate and details between the exposed and embedded parts were tested for monotonic compressive loading. Tests showed, that in order to avoid restrained deformation of the stiffened ends in the panel, small styrol foam should be applied in the gap. In order to assess the hysteretic behaviour, fourteen 1/5 scale specimens of X-shape and diagonal shape braces encased in pre-cast panels were tested under cyclic loading. The test set-up and hysteresis of a test specimen is shown in Figure 2.3.

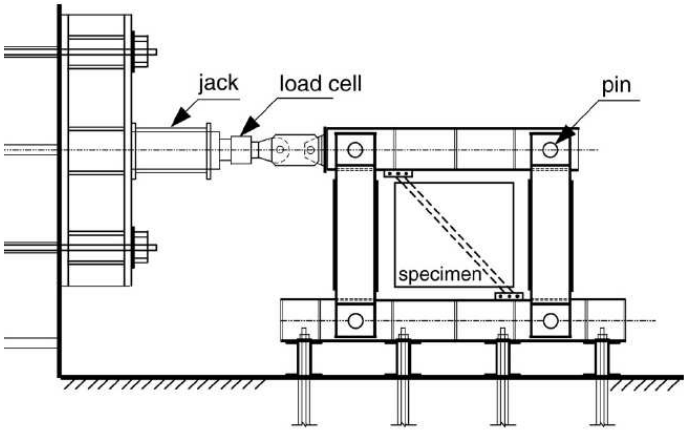

(a) Test set-up

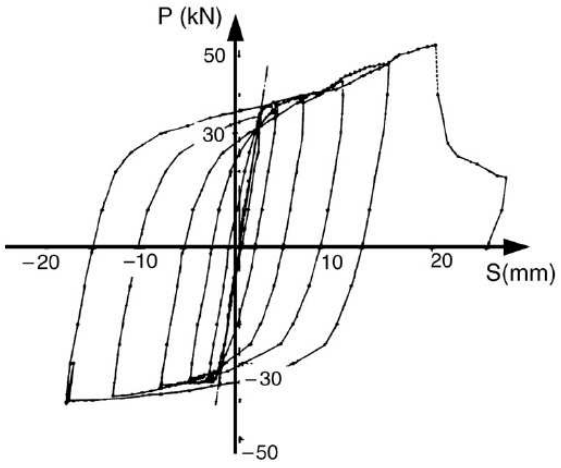

(b) Result hysteresis

Figure 2.3: Wakabayashi et al.'s 1973 experiment of a concrete panel encased steel brace [23, 24]

The authors show that the load carrying capacity of the unbonded brace was higher than that of the bonded brace. In terms of lateral drift, test results showed that the maximum lateral drift of the unbonded brace was almost four times that of the bonded brace. Finally two 1/2 scale, two story and two spans, steel frames equipped with such devices were tested cyclically, one with the braces arranged diagonally and the other arranged in a chevron pattern. As shown in Figure 2.4 the hysteretic behaviour prior to local buckling was stable, showing good absorption capacity with spindle shape loops. From the conducted study the authors concluded that the debonding layer on the brace's surface was crucial to allow the steel brace to resist the horizontal loading while the concrete panels only prevent the brace from buckling.

Pioneering research on BRBs was also conducted by Kimura et al. [25], being the first to test steel braces encased in mortar infilled steel tubes. The proposed

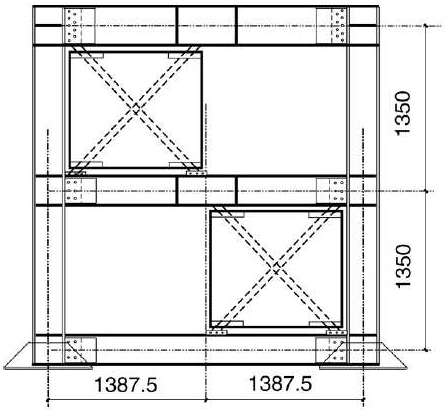

(a) Test set-up

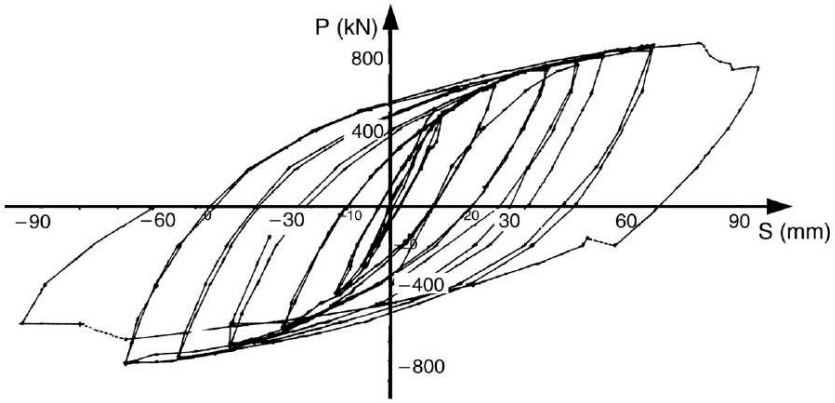

(b) Result hysteresis

Figure 2.4: Wakabayashi et al.'s 1973 experiment of a X configured BRB frame [23, 24]

system consisted of a conventional brace encased in a square steel pipe filled with mortar. No gap or debonding material was applied between the core brace and the mortar. However, the system showed some buckling restrainment of the core brace during the first loading cycles. Tests demonstrated that the brace showed higher resistance in compression than in tension and longitudinal strains on the encasing tube were proximately 85-90% less than the measured in the steel core plates. In their following research [26], four full-scale specimens were tested under cyclic loads, with two of them having a gap between the core brace and the enclosing mortar. The results showed that if the ratio between the outer tube's Euler load and the yielding strength of the core brace were larger than 1.9 no buckling would take place and a good hysteretic behaviour would be observed.

Similar tests were conducted by Mochizuki et al. [27] on RC wrapped steel braces, with the use of a separation layer of shock absorbing material between the core brace and the surrounding RC. A coefficient factor was used to account for the RC cracking and resultant stiffness degradation. Fujimoto et al. [28] and Watanabe

et al. [29] carried further research on this concept leading to the refinement of the now called unbonded brace [30], Figure 2.5. The unbonded brace is the most common type of BRB and typically consists in a low yielding steel core encased in a concrete infilled tube. Both the steel core brace and encasing member can have multiple cross sections, and throughout the years many different configurations varying these two elements have been proposed and tested.

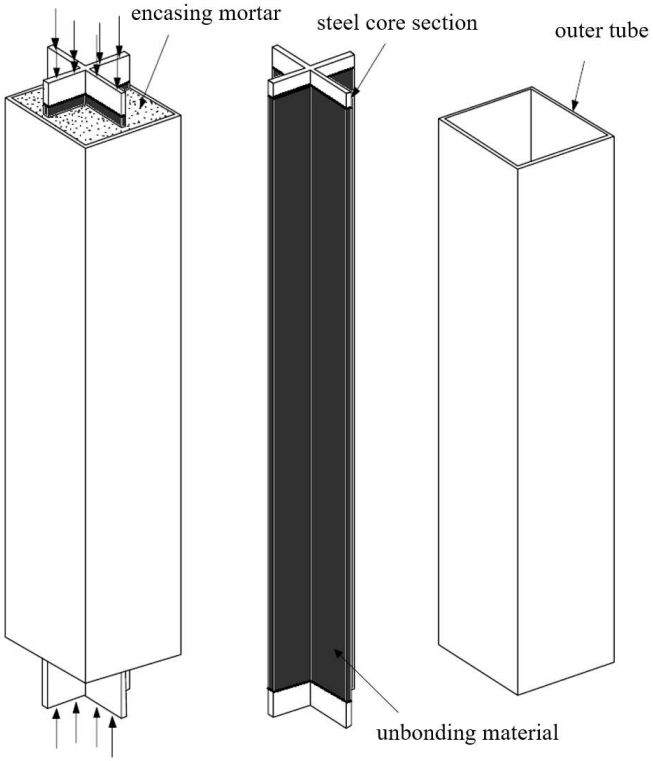

Figure 2.5: Typical unbonded brace configuration [31]

2.2 BRB Configurations

Although buckling restrained systems can have multiple configurations, according to Xie [1] they can be summarized in two large categories: one consists of a steel brace core encased by either RC, mortar infilled steel tube or steel profiles, the other consist of the same steel brace core encased by concrete panels. Figure 2.6 shows an example of the first and second categories respectively.

Many researchers tested, developed and proposed various cross sections configurations for restrained braces, all following the concept of using infilled steel tubes/steel profiles to restrain transversal displacements while allowing axial deformations to occur on the core. Figure 2.7 shows some of those cross sections.

Watanabe et al. [29] performed tests on five unbonded brace specimens to study

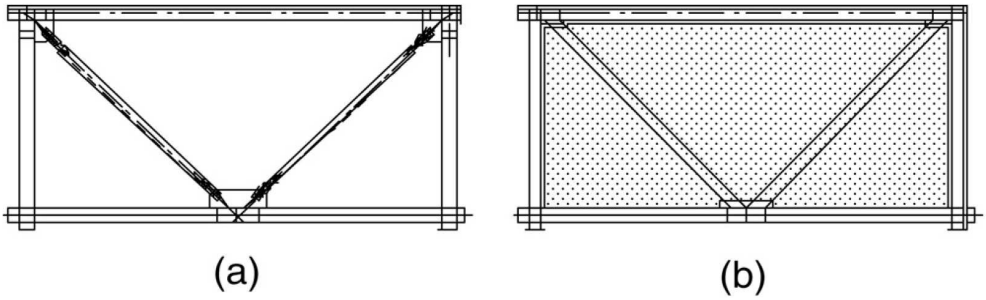

Figure 2.6: Two categories of BRBs: a) Steel brace encased by RC or steel element and b) Steel braced encased by concrete panels [1]

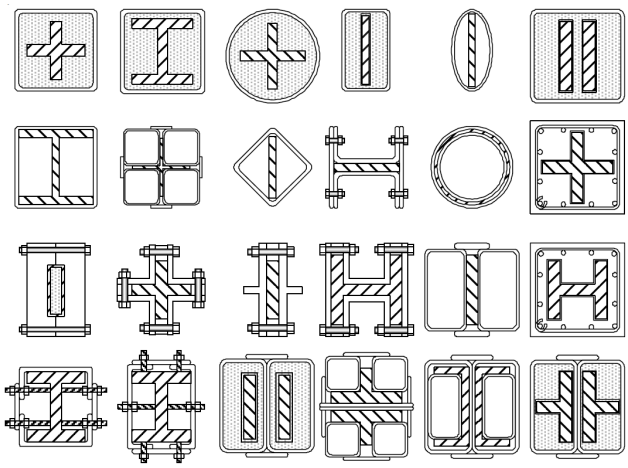

Figure 2.7: BRB cross sections configurations [3]

the effect of the ratio between the encasing member's Euler buckling load and the steel core's yielding force, N_e/N_y. Two of the five specimens were designed with said ratio below 1 and the remaining three specimens were designed with a ratio superior to 1. After being cyclically tested both specimens with the ratio below 1 buckled under compression, revealing the same behaviour as a conventional brace, while the other three specimens remained stable, displaying symmetric behaviour under both tension and compression. For practical approaches, the authors suggested that a N_e/N_y ratio should be, at least, 1.5.

Nagao et al. [32, 33, 34, 35, 36] developed, tested and theoretically studied BRBs either with wide flanges H-section steel cores or square steel tubes cores covered by RC members, Figure 2.7, and evaluated the reinforcement, strength and stiffness requirements of the concrete casing.

In the following years many configurations, apart from the "unbonded brace", were suggested, i.e., among many others a steel core encased in a hollow steel tube of numerous configurations [37, 38, 39, 40], a steel core restrained with bolted steel profiles [41] and even a steel core restrained by two, to four, connected steel

tubes [3]. Many researchers studied all steel BRB configurations using a steel tube as a restraining unit. Through the careful selection of the material strengths and the lengths of the portions expected to yield and the ones to remain elastic a wide range of braces can be designed [30].

According to D'Aniello [30], Kuwahara and Tada in 1993, Suzuki et al. in 1994, Manabe et al. in 1996 and Shimizu et al. in 1997 were some of the first investigators to study the use of an all steel BRB configuration, recurring to the use of hollow steel tubes as a restraining member. Besides these, more configurations of only steel braces have been suggested, such as the use of two to four steel tubes connected together, either by bolted or welded connections, in direct contact with the axial forces bearing steel core. The use of bolted connections offers the possibility of relatively easy inspection, maintenance and replacement of the devices after a seismic event or even during its life time [3]. As it happens in the "unbonded brace" an appropriate gaping space between the core brace and the restraining unit should be kept in "all steel" BRBs, to allow the relative deformation between both elements.

With the aim to reduce the connections dimensions Tsai and his co-workers [3, 42, 43, 44], studied extensively a new configuration of all steel BRB. The brace was composed of a double tee core, each encased in a steel tube (DT-BRBs: Double-Tee Double Tube BRBs).

More recently An-Chien et al. [45] proposed a new configuration of all steel BRB, the so called inspectable BRB (iBRB) which consisted of a steel core member and a pair of identical restraining members connected by bolted connections, Figure 2.8. Six specimens with different core plate cross-sections were tested with 6 different loading protocols.

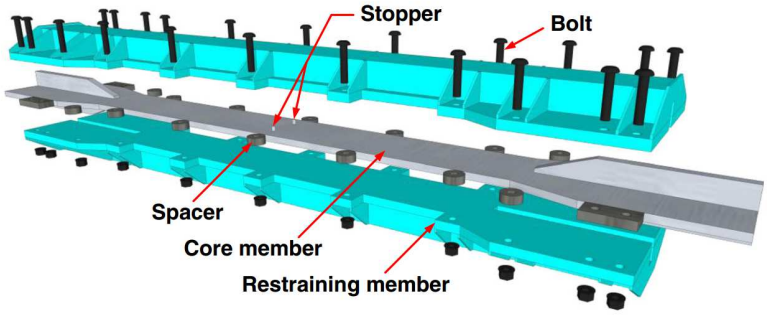

Figure 2.8: iBRB assembly [45]

Although "all steel" BRB have been thoroughly studied, the design simplicity and performance of the "unbonded" brace attracted the industry's interest, and were firstly made commercially available by Nippon Steel Corporation [30]. These are the type of BRBs considered in the present dissertation.

2.3 Key Issues and Detailing

2.3.1 Debonding Materials

To allow the brace core to slide freely inside the restraining unit and to expand in the transverse direction when yielding in compression, a separation gap should be kept between the two components. As a result, gap and debonding are of great importance to ensure a good performance of BRBs. This separation is obtained resorting to a debonding material or applying a small gap between components.

A large variety of debonding materials can be used when concrete is employed as a restraining element. Wakabayashi et al. [23, 24] firstly tested numerous possible debonding materials, such as epoxy resin, silicon resin, vinyl tapes, among others, and opted for coating a silicon resin layer on top of an epoxy resin one. Mochizuki et al. [27] also studied some types of debonding materials with different thickness in steel plates encased by RC BRBs. Many more methods to achieve debonding were investigated by researchers, such as applying a silicone painting on the core brace [46], Vinyl Mastic (VM) tape or styrol foam [29, 28, 47, 48], coiling of two 0.15-0.2mm thick layers of polyethylene film sheet [38], silicon rubber sheets with a thickness of 2 mm [43], among many others. Depending on the material employed, thickness varies from 0.15 to 2mm.

As an alternative to the debonding material, a small gap between the core brace member and the encasing mortar/concrete should be provided in order to accommodate the relative deformation between them, resulting from the transversal expansion of the brace core due to the action of Poisson's effect combined with axial deformation under compressive loads. According to Xie [1], typical dimensions of the gap for real application in BRBs are 3mm each side.

In 2004, Tsai et al. [3] tested the effects of various unbonding materials, in order to find out which kind of material possessed satisfactory unbonding effects. A total of ten BRBs, varying singularly in the unbonding material, were tested under increasing cyclic displacement. The test specimens characteristics referring to the load protocols and debonding material are summarized in the table 2.1.

Test results of the ten specimens are summarized in the Figure 2.9.

With the axial load difference, Γ, defined as follows:

$$\Gamma = \frac{(C_{max} - T_{max})}{T_{max}} \tag{2.1}$$

where C_{max} and T_{max} are the maximum compressive and tensile brace forces at the same absolute axial deformation level, respectively. Theoretically speaking, after the core member is yielded, the Poison ratio ν = 0.5 can be applied in the following calculations [3]. Also, the volume of the yielding steel segment should remain constant, that is:

$$A_0 \cdot L_0 = A \cdot L \tag{2.2}$$

Table 2.1: Summarized Test Specimens Characteristics [3]

Specimen	Unbonding material	Unbonding material tickness [mm]	Loading history
AS-1	Asphalt paint	n.a.	Standard
VF-1	Vinyl sheet + foaming tape	2	Standard
VK-1	Vinyl sheet + kraft tape	2	Standard
R2-1	Rubber sheet	2	Standard
R5-1	Rubber sheet	5	Standard
SR1-1	Silicone rubber sheet	1	Standard
SR2-1	Silicone rubber sheet	2	Standard
SR2-2	Silicone rubber sheet	2	Low-cycle fatigue*
SR2-3	Silicone rubber sheet	2	Near-fault**
SR5-1	Silicone rubber sheet	5	Standard

*The specimen is submitted to alternating cycles of plastic deformation, it is characterized by high amplitude, low frequency plastic strains.

**Loading history simulating near-field earthquakes, characterized usually by higher accelerations and frequencies.

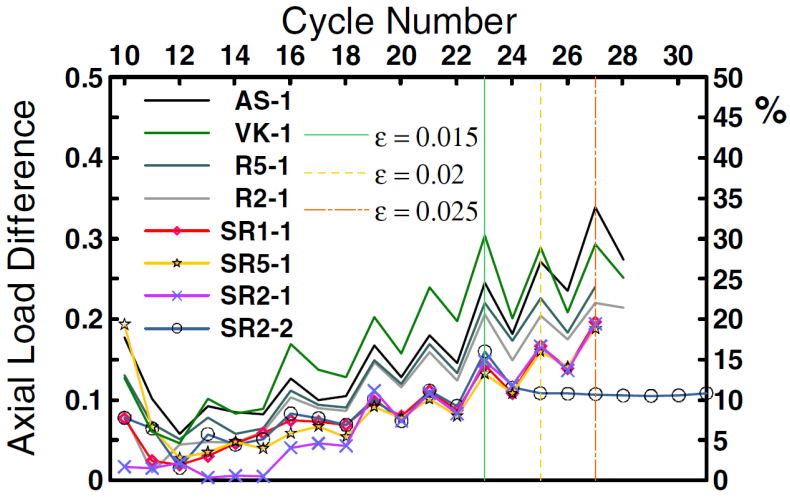

Figure 2.9: Axial load difference under cyclic loading [3]

where A_0 and L_0 are the original cross sectional area and length, respectively, while A and L correspond to the those after the brace is deformed. Therefore, the axial strain comes as:

$$\varepsilon = 1 - \frac{L_0}{L} = 1 - \frac{A}{A_0} \;\; and \;\; A = A_0 \left(1 - \varepsilon\right) \tag{2.3}$$

Thus, the ratio between the compressive and tensile brace forces for a giving absolute strain level could be:

$$\Gamma = \frac{\left(C_{max} - T_{max}\right)}{T_{max}} = \frac{A_0 \left(1 + \varepsilon\right) - A_0 \left(1 - \varepsilon\right)}{A_0 \left(1 - \varepsilon\right)} = \frac{2\varepsilon}{1 - \varepsilon} \approx 2\varepsilon \tag{2.4}$$

The equation above suggests that the Γ is about 4% for an ε = 2%. However, test results shown in Figure 2.9 exhibit much higher Γ values. The authors proposed that this phenomena should be due to the imperfect unbonding mechanism and a substantial friction developed between the steel core member and the restraining unit. In Figure 2.9 it can be observed that the 2mm thick silicone rubber sheet has the least axial load difference under the cyclic increasing displacements and, therefore, it was the unbonding layer used by the authors in their future work.

In case of all-steel BRBs it is common to not apply any infilling material. Therefore, no debonding material has to be applied. Nonetheless, an adequate gaping space should be provided between the core brace and restraining member, in order to produce the necessary space for relative deformation between both members and prevent the core braces from buckling. Depending on the type of BRB, gap sizes vary from 0.7 to 3.5mm [1].

It is now evident that the achievement of a efficient debonding between the core brace and the restraining system is one of the main steps to obtain a good overall performance of the BRB. Another important aspect that affects the efficiency of a BRB system is the configuration of the connection between the BRB device and the structure.

2.3.2 Connections and Contraction Allowance

In early 2002, three full-scale BRB braced frames were cyclically testes in Berkeley, California [49]. The specimens had different BRB dispositions but similar connections, with the single difference being the added stiffeners in the gusset plates of the third specimen. Yielding of the gusset plates was observed in all test specimens. In the second specimen apart from yielding, the buckling of the gusset plate became evident. Finally, in the last test subject the gusset-to-beam connection failed by fracture of the beam flange, causing out of plane deformation on the BRB. The results showed that the buckling in the second specimen and the fracture in the third, both worsen the overall performance of the frame. These test campaigns will be thoroughly described in section 2.5.

According to Tsai et al. [3] a BRB connection to a gusset plate is typically a butt joint using several splice plates and two set of connecting bolts, as illustrated in

Figure 2.10. As such, these connections may suffer flexural buckling under large compression strains [50], and it is recommended that the following stability criterion must be met for this type of connection details:

$$P_{e\_trans} = \frac{\pi^2 EI_{trans}}{(kL_b)^2} \geq P_{max} \text{ and } P_{max} = \Omega \cdot \Omega_h \cdot \beta \cdot P_y \tag{2.5}$$

where P_y=$A_c F_y$ is the nominal yield strength of the core section, Ω and Ω_h take into account the possible material over-strength and strain hardening factors of the steel core, respectively, β represents the imperfect unbonding and EI_{trans} is the flexural stiffness of the core member at a section near the steel tube.

In order to reduce the connection's length and the number of connecting bolts in the brace-to-gusset connection, Lai and Tsai [51] developed the so called double-core buckling restrained braces (DCBRBs), illustrated in the Figure 2.11.

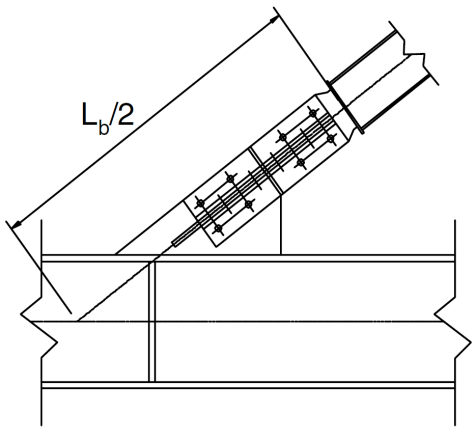

Figure 2.10: Typical single core BRB connection detail [3].

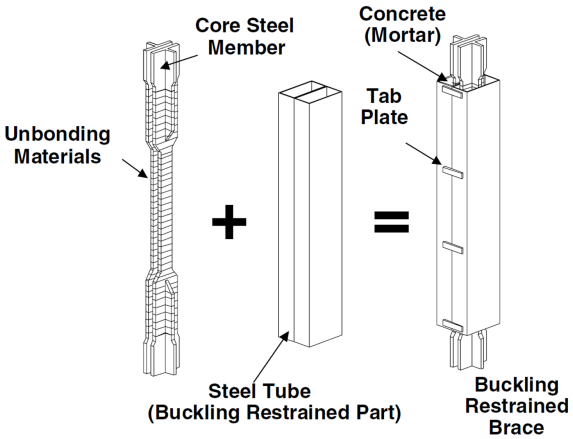

Figure 2.11: Schematic representation of double-cored buckling restrained brace (DCBRB) (Adapted from [3]).

In the following years further research was carried out in with the DCBRBs, being

extensively tested in [51, 52, 53, 54].

In 2007, Fahnestock et al. [55] conducted pseudo-dynamic earthquake simulations using the explicit Newmark algorithm to solve the time-discretized equations of motion for the displacements to be imposed to a large-scale 4-story frame. In response to the results of previous Buckling Restrained Braced Frames (BRBFs) tests, additional attention was given to the beam-column-brace connections. A true pinned connection was used for the brace-gusset plate connection, which limits the moment developed in the BRB due to the beam-column rotation. Additionally, a bolted beam splice using double structural tees was introduced between the beam and the beam stub to transfer axial force, while providing minimal flexural resistance. This allows to limit the moment developed in the beam and column at the beam-column connection region. A illustration of the proposed connection is given in Figure 2.12.

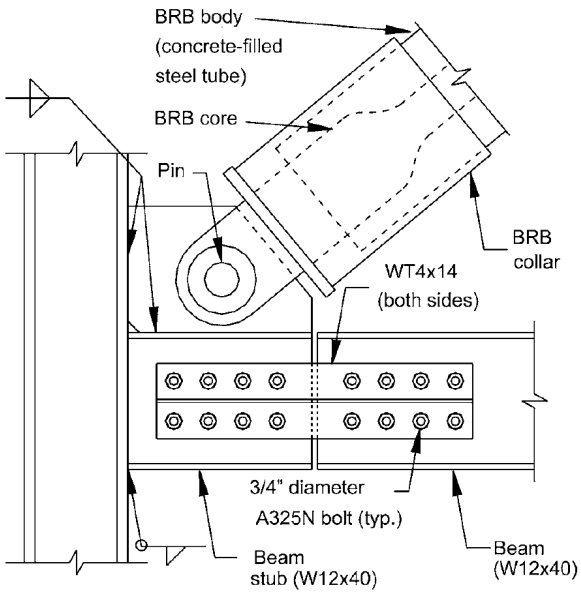

Figure 2.12: Beam-column-brace connection detail [55]

The program conducted four hybrid pseudo-dynamic earthquake simulations and a quasi-static cyclic test. The overall frame system exhibited excellent performance and sustained no strength or stiffness degradation during the earthquake simulations, or during the significant demands imposed by the subsequent quasi-static cyclic test [55]. Beam-column-brace connections exhibited excellent performance, and sustained only minor yielding at storey drifts up to 4.8%. Additionally, no damage or distortion was observed in the gusset plates. Even though the bolted beam splices allowed significant relative rotations between the beam and the beam stubs, the experimental results demonstrated that the pinned connections, the end collars of the BRBs (Figure 2.12), and the thick gusset plates, had a major contribution to both the connection's and overall system's good performance.

Berman and Bruneau [56] suggested a different type of connection in which the gusset plate is provided with an offset from the column face, and is connected only to the beam. The intent was, to counteract the negative effects on seismic performance of the elevated beam-to-column connection stiffness, and increase the BRB efficiency. A three-story frame with the proposed connections and BRBs was tested under quasi-static loading. The connection consisted of a stiffened gusset plate bolted to the beam flange with a spacing from the column's face, as represented in the Figure 2.13.

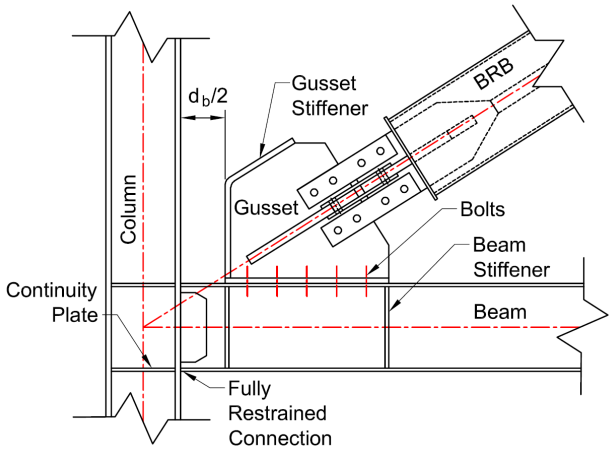

Figure 2.13: Proposed gusset connection detail [56]

The connection was shown to accommodate frame drifts as large as 3%, and satisfy the buckling restrained brace performance requirements of the 2005 AISC *Seismic Provisions for Steel Buildings* [57]. The three-story BRBF specimen demonstrated excellent ductility. BRB yielding occurred at 0.2% roof drift and reached an element ductility of almost 5 prior the initiation of frame yielding at 1% roof drift [56]. Ultimately, the specimen reached a roof drift of 3.75% and a cumulative BRB inelastic deformation of over 1,500δ_y, with δ_y being the yield axial deformation of the BRB, when failure of the first floor beam-to-column connection occurred and the testing was stopped. Results showed that the tested BRBF specimen displayed excellent ductility and proved the proposed gusset connection to be a possible alternative to traditional BRB gusset plate configurations. However, the test was performed at 1/3 scale. Full scale testing should be performed to verify the performance of this type of connection prior to implementation. The authors also concluded that the proposed connection configuration could be particularly relevant in the context of seismically deficient moment resisting frames retrofitting [56].

2.3.3 General Stability

According to Black et al. [31], the global stability of the unbonded brace can be estimated from the Euler theory of buckling. In Figure 2.14 (a) a schematic layout of an unbonded brace in compression is presented, and Figure 2.14 (b) and 2.14 (c)

show the distributed forces on the steel core and the encasing mortar/outer tube in the deformed configuration.

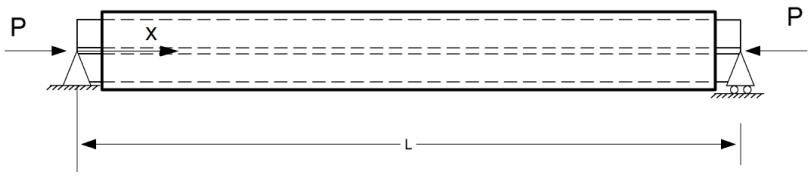

(a) Unbonded brace under axial loading

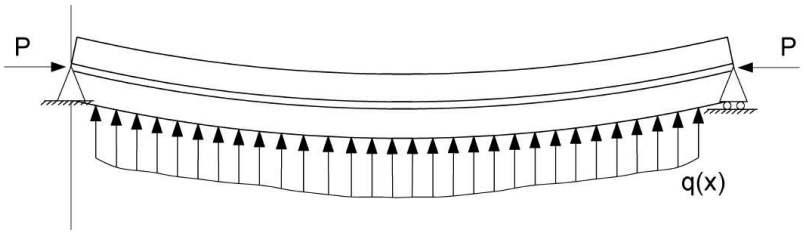

(b) Distributed load along the inner core in the deformed configuration

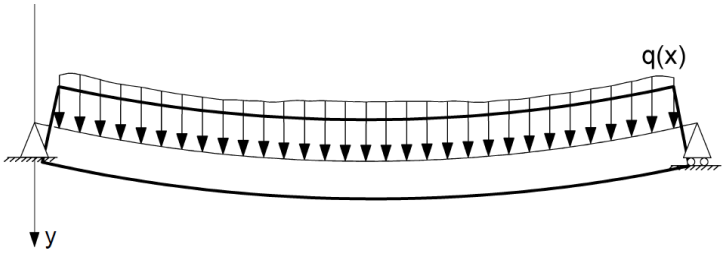

(c) Distributed load along the encasing mortar/outer tube

Figure 2.14: Schematic configuration and forces of an unbonded brace under compression [31]

The unknown distributed load, $q(x)$, is the transverse reaction of the outer tube/encasing mortar along the inner steel core. Considering the displayed axes system in Figure 2.14, the equilibrium of the inner steel core in its deformed configuration is given by

$$E_i I_i \frac{d^4 y\,(x)}{dx^4} + P\frac{d^2 y\,(x)}{dx^2} = -q\,(x) \tag{2.6}$$

where $y(x)$ is the transverse deflection, P is the axial load, and E_i and I_i are the Young modulus and the moment of inertia of the inner steel core, respectively. The equal and opposite distributed load $q(x)$ is loading the encasing mortar/outer tube as shown in the Figure 2.14 (c). By equilibrium of a segment of the BRB we obtain

$$E_0 I_0 \frac{d^4 y\,(x)}{dx^4} = q\,(x) \tag{2.7}$$

where E_0 and I_0 is the Young modulus and moment of inertia of the encasing mortar/outer tube, respectively.

From equations 2.6 and 2.7 we obtain

$$E_i I_i \frac{d^4 y(x)}{dx^4} + P \frac{d^2 y(x)}{dx^2} = -E_0 I_0 \frac{d^4 y(x)}{dx^4} \tag{2.8}$$

which yields a homogeneous Euler equation

$$\frac{d^4 y(x)}{dx^4} + \frac{P}{E_i I_i + E_0 I_0} \frac{d^2 y(x)}{dx^2} = 0 \tag{2.9}$$

Considering a buckling length of L, equation 2.9 returns the critical buckling load of the brace

$$P_{cr} = P_e = \frac{\pi^2}{(KL)^2} (E_i I_i + E_0 I_0) \tag{2.10}$$

where KL is the effective/equivalent length, with K=1 for pinned end and K=0.5 for fixed end conditions. Since the bending rigidity of the inner steel core, $E_i I_i$, is two to three orders of magnitude smaller than the bending rigidity of the encasing mortar/outer tube, $E_0 I_0$, equation 2.10 simplifies to

$$P_{cr} = P_e \approx \frac{\pi^2 (EI)_{tube}}{(KL)^2} \tag{2.11}$$

Therefore, equation 2.11 indicates that the critical load of the unbonded brace is merely the Euler buckling load of the outer tube, and that the global stability of the brace is ensured when the Euler buckling load of the tube, P_{cr}, exceeds the yielding load of the steel core, $P_y = \sigma_y A_{core}$.

2.4 Design Overview

2.4.1 Codes and Provisions

According to Almeida et al. [5], in Japan, BRBs are regarded as seismic dampers and, therefore, are considered as a type of passive control system for damage mitigation. According to Kasai [58], with the publication of the JSCA (Japan Structural Consultants Association) Specifications in December 2000 and the publication of the JSSI (Japan Society of Seismic Isolation) Manual in October 2003, BRBs became a viable mean of enhancing the seismic performance of buildings. The JSSI Manual refers to damper mechanism's, design, fabrication, testing, quality control and analytical modelling, as well as design, construction, and analysis of passively controlled buildings. More than fifty members, comprising university researchers, structural designers and engineers from about twenty damper manufacturing companies contributed to the document.

In the United States of America, BRBs have been regulated since the release of the NEHRP (National Earthquake Hazards Reduction Program) *Recommended Provisions for Seismic Regulations for New Buildings and Other Structures* (FEMA 450-1) in 2003 [59]. This document has the intent to provide the minimum

recommended requirements necessary for the design and constructions of new buildings and other structures to resist earthquake ground motions throughout the United States. As such, it provides specific rules for BRBs and other structural elements of steel BRB frames, as well as qualifying cyclic tests. As stated in [59], the document's recommended provisions should be used together with AISC *Seismic Provisions for Structural Steel Buildings* [60], despite the fact that this version of the AISC Seismic provisions did not contemplate any specific provisions regarding BRBs. Later in 2005 the AISC Seismic incorporated, in a later version, provisions for the use of BRBs in steel buildings [57]. However, no provisions were issued for the use of BRBs in composite steel-concrete or RC structures.

In Europe, BRB design is not present in the seismic design codes [5]. However, despite omitting design and detailing provisions, some codes allow the use of such devices in seismic building's protection. In Italy, the most recent normative is the NTC'08 [6]. This document allows the use of anti-seismic dissipative devices in both new and existing structures, setting general design rules and providing other relevant indications such as: compliance tests and installation, maintenance and replacement related requirements. A year later, in 2009 the European Committee for Standardization (CEN) released the European Standard EN15129 [7], which contains provisions for performance requirements, materials and testing of displacement dependent devices, besides other seismic devices such as velocity dependent devices and isolators [5].

2.4.2 Design Procedures

According to Bergami and Nuti [61], dissipative devices can be grouped into two major categories: displacement dependent behaviour devices, such as yielding metallic and friction dampers; and velocity dependent behaviour devices, such as visco-elastic solids or viscous fluid dampers. Similarly, dissipative devices design methods can be grouped into two categories according to the scope of the design process: optimization of global response parameters (such as the dissipated energy), or limiting maximum displacement (so called performance based design). Hereafter some proposed design procedures present in the literature are briefly described.

In the first categorie, Filiatrault and Cherry [62, 63] proposed a design criteria for dissipative braces that aimed at minimizing the difference between the seismic input energy and the dissipated energy. The procedure was based on non-linear time history analysis and the existing structure was supposed to remain elastic. Ciampi et al [64, 65] defined a design method that consisted of minimizing a cumulative structural index, such as the kinematic ductility or the cumulative ductility. The structure is represented by an equivalent elasto-plastic SDOF with one equivalent dissipative brace.

More recently many researchers have developed procedures based on the displacement based design. Vulcano and Mazza [66] suggested that the brace distribution should maintain strength and stiffness distribution of the original

unbraced structure, and guarantee that the modal shapes don't change after the braces insertion. Kim and Choi [67] assumed that all the required additional damping was provided by the additional braces whose distribution, and therefore strength and stiffness distribution, is not discussed. Ponzo et al. [68] proposed a method in which the characteristics of the bracing systems is determined by imposing the equivalence between, the energy stored in an equivalent elastic single degree of freedom system (the original structure), and in the elasto-plastic system (the dissipative bracing system). The method results were verified using the N2 method by Fajfar and Gaspersic [69, 70].

Both the procedures proposed by Kim and Choi [67] and Ponzo et al. [68] based their method calibration on a single target performance point without considering any other parameters. These procedures, together with the one proposed by Vulcano and Mazza [66], work for the design of new buildings, which are usually designed regular both in plan and in elevation, and whose seismic response can be controlled by few parameters [61]. In fact, Vulcano and Mazza [66] assume that the structure has not to change its modal shapes. On the other hand, Kim and Choi [67], as well as Ponzo et al. [68], base their evaluation on global parameters, such as top displacement, and do not care of other significant parameters usually relevant for retrofitting design. Therefore, these don't seem sufficiently manageable for interventions on existing buildings [61].

In 2013, Bergami and Nuti [61] developed a design procedure based on the Capacity Spectrum Method, which takes in consideration the energy dissipated by the analyzed structure. Therefore, the method is suitable for structures with additional dampers. In this new approach the computation of the energy dissipated by the devices is evaluated referring to the hysteretic cycle performed by each device of each braced level, while, the dissipation offered by the original structure, is computed in a global matter based on the pushover curve. Moreover, as well as the top displacement, also the interstorey drift, a good indicator of irregularity, is kept under control. After testing the procedure, including an application to a real building intervention, the authors concluded that it represents a substantial improvement of displacement based design for building's retrofit using dissipative braces. The method proved to be simple, though it permits to account for the nonlinear behaviour of the original structure, and determines stiffness and strength of all braces to be added to the structure.

2.5 Hysteretic Behavior

BRBs have been tested to full extend throughout the years [29, 31, 71, 72, 73], and consistently shown good performance with full spindle shape and close to symmetric hysteretic curves, as represented in the Figure 2.15.

In July 2000 the Nippon Steel & Sumitomo Metal Corporation released a technical report [8] in which practical-scale unbonded braces were tested to assess its fatigue properties. Five test programs were tried out with different shape configurations and different core steel grades. Table 2.2 shows the material

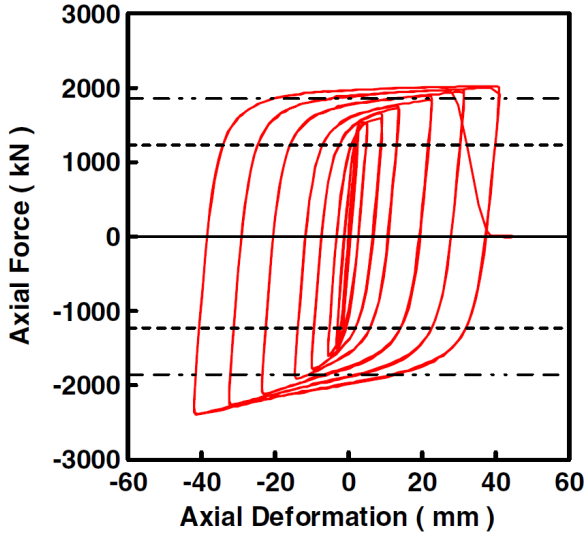

Figure 2.15: Example of hysteretic behaviour of BRBs (adapted from [3])

mechanical properties employed in each test program.

Table 2.2: Material mechanic properties [8]

Series	Steel grade	Thickness [mm]	Yield point [N/mm^2]	Tensile strength [N/mm^2]	Enlongation [%]
TP-1,2	LYP100	25	95	249	84
TP-3	SN400B	25	259	426	35
TP-4	LYP235	16	239	334	60
TP-5	LYP235	28	222	324	69

SN400B is a rolled structural steel and LYP100 and LYP235 are two low yield point steels from Nippon Steel Corporation. The detail drawings of test specimens are exhibited in Figure 2.16.

A total of eleven specimens distributed over 5 test series were studied. Parameters such as, core section shape, thickness and length, concentration ratio α, yield axial force, controlled displacement, among others varied between specimens. For a full detailed test specimens data report to [8].

The specimens were tested under cyclic loading and the cycles to failure were counted once the controlled displacement was reached for each specimen, following the loading protocol schematically presented in Figure 2.17.

Tests results showed that the unbonded brace can withstand roughly 200 cycles of loading at an axial strain of $\pm 0.75\%$ on the core, corresponding to a story drift angle of 1/100, before material failure occurs. The authors concluded that the test results clarified the fatigue properties of the test specimens and confirmed the sufficient hysteretic performance of the unbonded brace to be applied as hysteretic damper. For further details on testing protocols and results refer to [8].

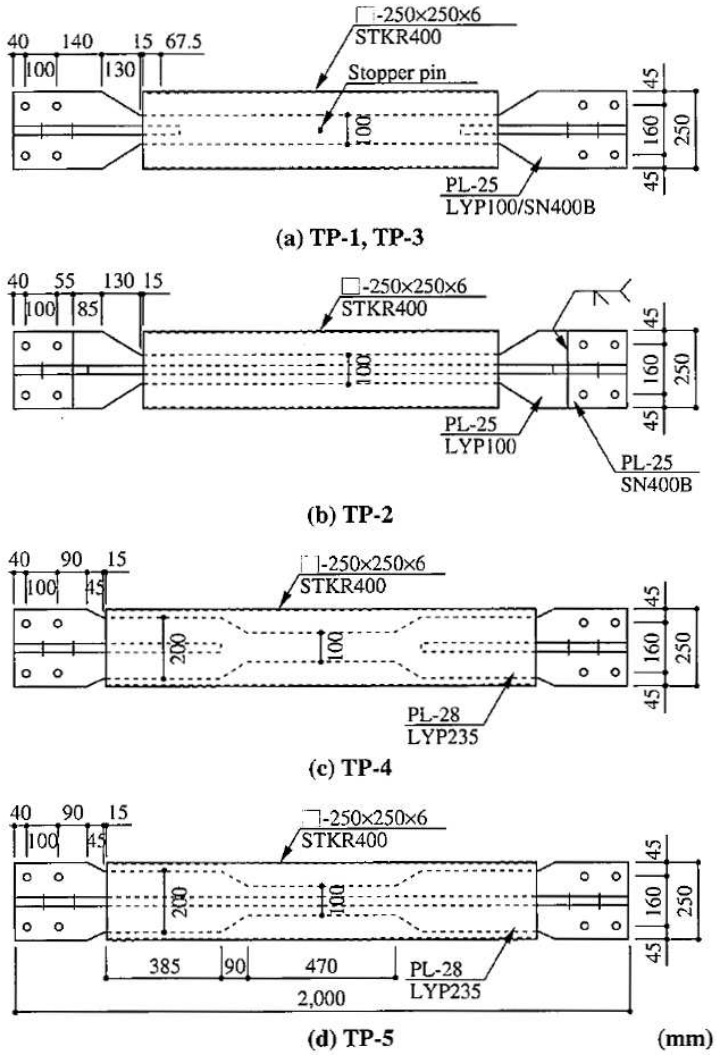

Figure 2.16: Detail drawings of Nakamura et al. test specimens [8]

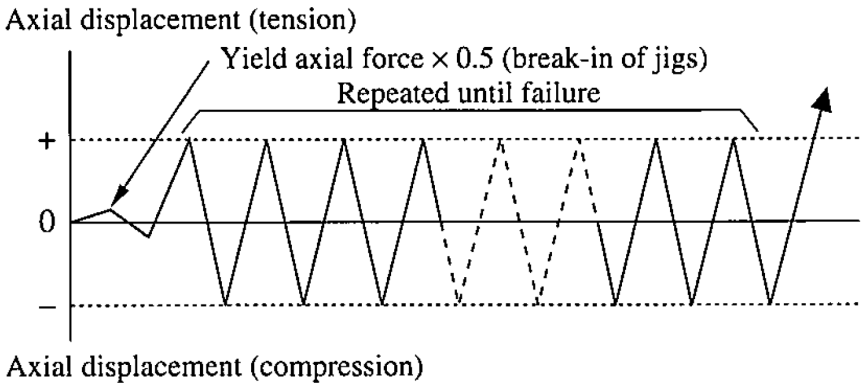

Figure 2.17: Loading protocol applied by Nakamura et al. in the test campaign [8]

Three years later, three test campaigns were conducted by Merritt et al. [71, 72, 73] that clearly show the seismic retrofitting potential of the Unbonded brace. At the time, and since the tests were performed in the University of California in the United States, BRB design was performed following the guidelines presented in the Structural Engineers Association of California and American Institute of Steel Construction (AISC/SEAOC) provisions entitled “Recommended Provisions for Buckling-Restrained Braces Frames” [74]. Accordingly, the BRB specimens were designed to satisfy the strength, inelastic deformation and energy dissipation requirements provided from the AISC/SEAOC. To determine de adequacy of a BRB three measurements should be assessed: the compression strength adjustment factor, β_c, the tension strength adjustment factor, ω, and the cumulative inelastic axial deformation capacity, η. The following equations define these measures.

$$\beta_c = \frac{C_{max}}{T_{max}} \tag{2.12}$$

$$\omega = \frac{T_max}{F_{ysc}A_{sc}} \tag{2.13}$$

Where C_{max} and T_{max} are the maximum compression and tension forces measured in the specimen upon testing, respectively, F_{ysc} is the nominal yield strength of the core material and A_{sc} is the cross sectional area of the BRB core plate. The cumulative inelastic axial deformation is defined by a normalized ratio of the total hysteretic energy (E_h), to the average of the effective compressive (P_y^+) and tensile (P_y^-) yield capacities of the brace.

$$\eta = \frac{E_h}{P_y^* D_{by}} \tag{2.14}$$

$$P_y^* = \frac{(P_y^+ + P_y^-)}{2} \tag{2.15}$$

D_{by} is the yield axial elongation of the brace, and the parameter that enables the normalization of the cumulative inelastic axial deformation [71]. E_h is simply the sum of the areas surrounded by each hysteretic loop of a test. The AISC/SEAOC provisions [74] specify boundary values for β_c and η, a maximum of 1.3 is specified for β_c and a minimum of 140 for η for uni-axial testing [2]. Apart from uni-axial testing, BRBs must be qualified under sub-assemblage testing which impose the BRB connection to rotational demands combined with axial loading. The following loading protocols are provided by the AISC/SEAOC Appendix T [74] for the qualification tests.

- 6 cycles of loading corresponding to $\Delta_b = \Delta_{by}$;
- 4 cycles of loading at the deformation corresponding to $\Delta_b = 0.5\Delta_{bm}$;
- 4 cycles of loading at the deformation corresponding to $\Delta_b = 1.0\Delta_{bm}$;
- 4 cycles of loading at the deformation corresponding to $\Delta_b = 1.5\Delta_{bm}$; (Additional complete cycles of loading at the deformation corresponding to $\Delta_b = 1.0\Delta_{bm}$ as required for the braces test specimen to achieve a cumulative

inelastic axial deformation of at least 140 times the yield deformation, this step is not required for subassemblage testing)

Δ_{by} is the deformation at the first significant yielding in the brace, Δ_{bm} is the design story drift of the bay in which the BRB will be located, and Δ_b is the deformation quantity used to control the loading of the test specimen.

With the purpose to demonstrate the typical behaviour of the buckling restrained brace two test campaigns will be described hereafter. Both campaigns were carried out in 2003 by Merritt and his co-workers. One consists of sub-assemblage tests on six CoreBrace BRB specimens [71], the other comprises uni-axial tests on two Associated Bracing BRB specimens [73]. The proprieties and results of each campaign are presented in table 2.3 and 2.4, respectively. The β_c and ω values presented refer to a drift level of $1.5\Delta_{bm}$.

Table 2.3: Properties and Results of CoreBrace Subassemblage Tests [71]

Specimen	**Core Plate Type**	A_{sc} [in^2]	F_{ysc} [kip]	ω	β_c	E_h [k-in]	η
1	Flat	10	388	1.48	1.058	110000	1100
2	Flat	10	388	1.49	1.06	120000	1175
3	Cruciform	16	712	1.61	1.052	175000	700
4	Cruciform	16	712	1.63	1.055	130000	600
5	Cruciform	23.125	897.3	1.52	1.044	390000	1400
6	Cruciform	23.125	897.3	1.52	1.046	330000	1200
			average	1.54	1.052	209000	1025

Table 2.4: Properties and Results of Associated Bracing Uniaxial Tests [73]

Specimen	**Core Plate Type**	A_{sc} [in^2]	F_{ysc} [kip]	ω	β_c	E_h [k-in]	η
1	Flat	10	460	1.68	1.2	140000	700
2	Flat	10	460	1.67	1.12	240000	1200
			average	1.68	1.16	209000	950

The values of β_c for the CoreBrace tests varied from 1.044 to 1.058 with an average value of 1.052, and the for the cumulative inelastic axial deformation capacity, η, values ranged from 600 to 1400 with an average value of 1025. The Associated Bracing tests had 1.2 and 1.12 for β_c values, and 700 and 1200 for η values.

From Tables 2.3 and 2.4 one can be observe that the values of β_c easily verified the AISC/SEAOC specification with all of them being bellow 1.3. Also for η, the cumulative inelastic axial deformation capacity, the values verify the minimum of 140 required by the AISC/SEOC provisions. Additionally the average maximum

strains measured during the BRB tests stood between 0.025 and 0.035 [31, 71, 72, 73]. All BRB specimens showed good performance under the standard loading protocols from the qualification tests.

Isolated component testing is of great importance for the performance assessment of the buckling restrained braces. However, it is only part of the overall action these devices are subjected to during their life span. To properly replicate the actual conditions BRB are subjected to, buckling restrained braced frames must be tested. A description of some of these tests and the associated results is provided in the following paragraphs.

A series of three full-scale braced frames with unbonded braces were conducted in the University of California, in Berkeley [49]. Two different dispositions of the BRB were tested, one with two specimens assembled in a chevron or inverted V pattern (BRBF-1), the other two with a single BRB disposed diagonally (BRBF-2 and BRBF-3). Although they comprise different BRB dispositions all three tests used the same testing apparatus and structural frame. The test disposition is provided in the Figure 2.18 and their general characteristics are summarized bellow:

- The bay was 130.5 inches (2.639m) high by 240 inches (6.096m) wide;
- The bay comprises W14x176 columns and a W21x93 beam, Figure 2.19;
- The upper level "'hat bracing"' is responsible for the horizontal loading transfer and was designed to remain elastic during the excitation;
- Beam-to-column connections had full penetration welds on the flanges, and fillet welds on the beam web;

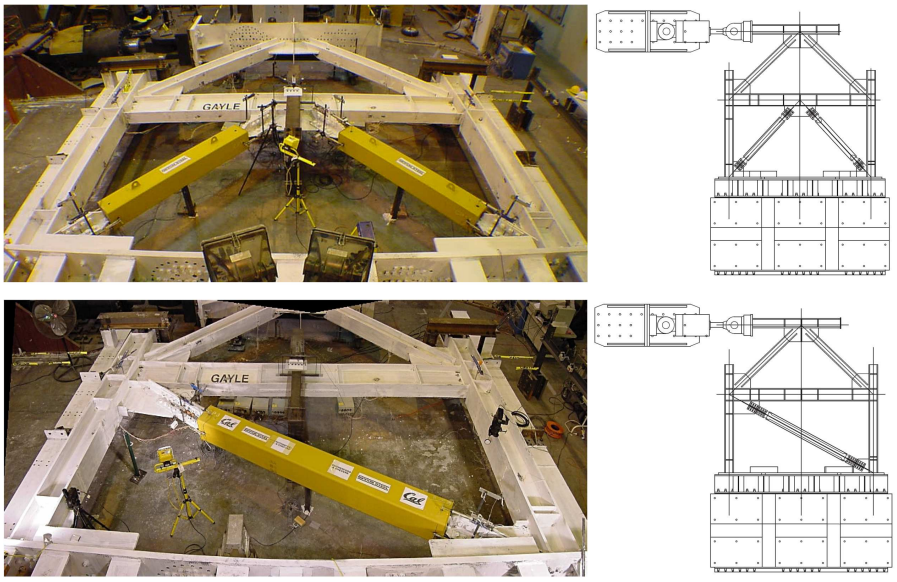

Figure 2.18: UC Berkeley Full-Scale Tests [49]

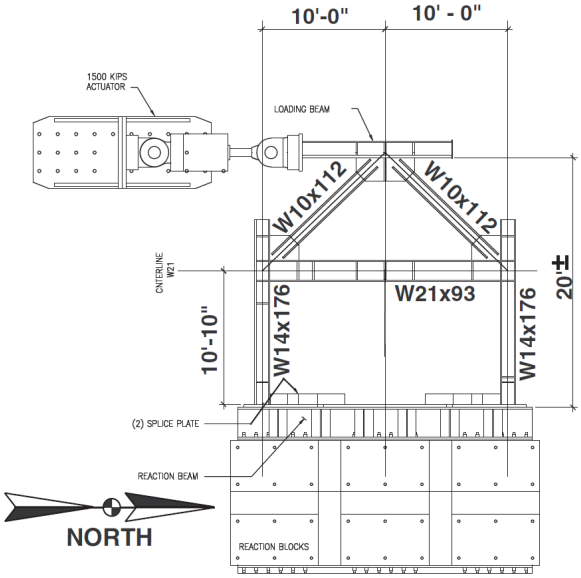

Figure 2.19: UC Berkeley tests bare frame structural drawing [49]

Test BRBF-1 and BRBF-2 used a slip-critical bolted/splice plate BRB-to-gusset plate connection and fillet welded gusset-to-frame connections and the BRB specimens had a single plate core with a cross section area of 6 in^2 (38.71 cm^2). Test BRBF-3 used a similar type of connections. However, almost twice the cross sectional area was used, 11.5 in^2 (74.19 cm^2), since a cruciform shape core cross section was used. Additionally, steel stiffeners were added to the gusset plate in BRBF-3 specimen.

The loading protocol adopted for the specimens followed the loading protocol provisions outlined in the AISC/SEAOC [75]. It suggests that six cycles be performed at a displacement corresponding to Δ_b=Δ_{by} (or the displacement that corresponds to the first yield of the BRB); four cycles applied corresponding to Δ_b=0.5Δ_{bm} (where Δ_{bm} is the estimated analytical target displacement taken for a specific site hazard); four cycles imposed corresponding to Δ_b=1.0Δ_{bm}; and four cycles applied corresponding to Δ_b=1.5Δ_{bm}. Despite the provisions recommendations the authors reduced the number of cycles corresponding to 1.5Δ_{bm} to two in an attempt to avoid damage to the moment frame that was to be re-used. In the Table 2.5 a brief definition on the terms used in the loading protocol is provided, and in Table 2.6 the values for each specimen are displayed. In Figure 2.20 a graphic illustration of the loading protocol for specimen BRBF-1 is provided, the loading protocol for the remaining specimens is similar varying only the values o story rotation according to the values defined before in Table 2.6. However, in the last campaign, BRBF-3, the last two cycles were replaced by one 1.5Δ_{bm} and two 1.0Δ_{bm} cycles due to some damage in the test set up.

In the BRBF-1 specimen testing no serious damage occurred in the BRB or in the gusset plate connections, although gusset plates yielded a fair amount no

Table 2.5: Loading protocol definitions [49]

Symbol	Definition
Δ_b	Deformation quantity used to control loading of the test specimen (total brace rotation for the subassemblage test specimen: total brace axial deformation for the brace test specimen)
Δ_{bm}	Value of deformation quantity, corresponding to the design story drift
Δ_{by}	Value of deformation quantity, at first significant yield of test specimen

Table 2.6: Deformation values for testing (Adapted from [49])

Specimen	Δ_{by} [in] ([cm])	Δ_{bm} [in] ([cm])
BRBF-1	0.37 (0.94)	1.75 (4.45)
BRBF-2	0.39 (0.99)	2.25 (5.72)
BRBF-3	0.33 (0.84)	2.25 (5.72)

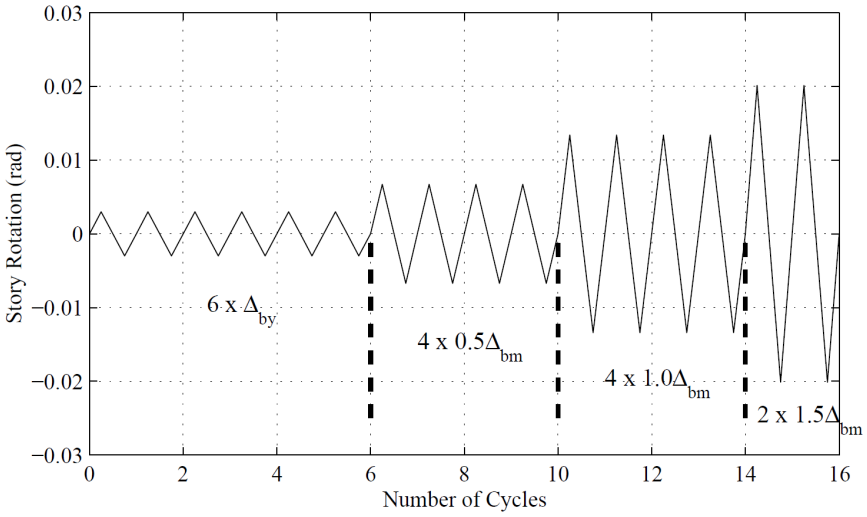

Figure 2.20: UC Berkeley loading protocol for specimen BRBF-1 [49]

fracture or buckling occurred. Frame yielding was observed in the first cycles and increased in the following cycles. In Figure 2.21 and 2.22 the BRBF-1 frame and buckling-restrained brace hysteresis, respectively, is presented.

In the first cycles of testing BRBF-2 no yielding in the frame or gusset plates were observed. In the following cycles yielding on the gusset plates was evident. During the last cycles, cracks began to form at the gusset plate-to-column connections. Finally, when the brace was tensioned buckling of the "'south"' plate became evident, phenomena which is pictured in Figure 2.23. In Figure 2.24 and 2.25 the BRBF-2 frame and buckling-restrained brace hysteresis, respectively, is presented.

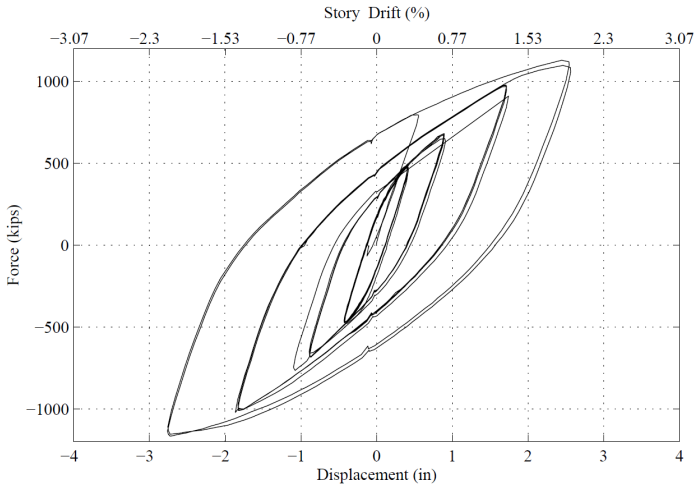

Figure 2.21: UC Berkeley BRBF-1 base shear versus lateral displacement [49].

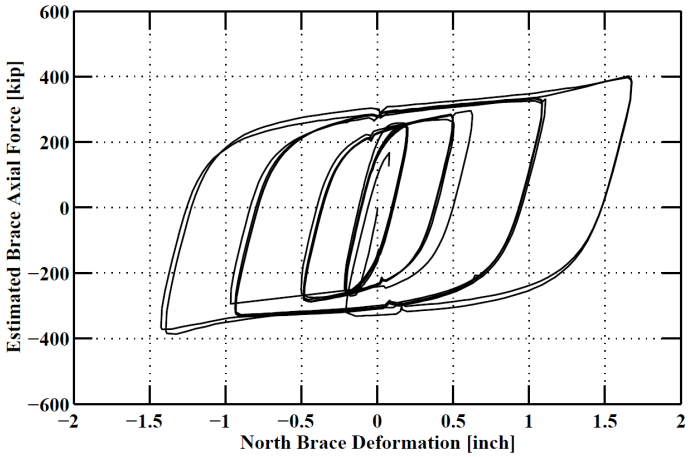

Figure 2.22: UC Berkeley BRBF-1 BRB estimated hysteresis [49].

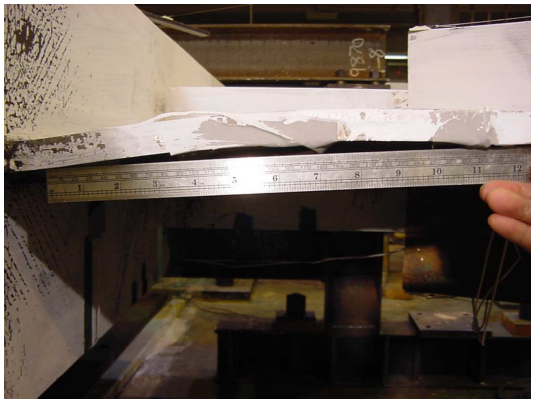

Figure 2.23: UC Berkeley BRBF-2 gusset plate buckling [49].

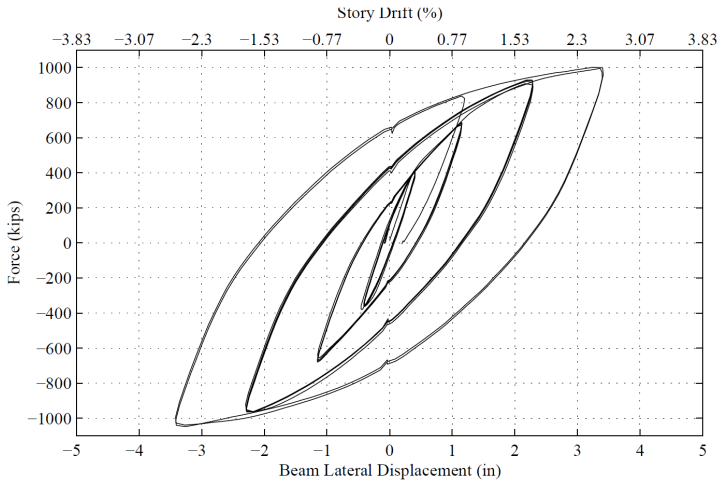

Figure 2.24: UC Berkeley BRBF-2 lateral beam displacement versus base shear [49].

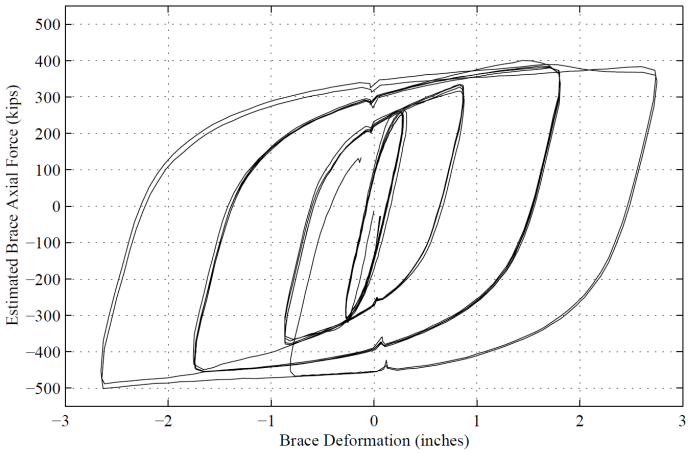

Figure 2.25: UC Berkeley BRBF-2 BRB estimated hysteresis [49].

In the third test campaign, during the $1.5\Delta_{bm}$ cycle, the entire bottom flange of the main beam fractured at the gusset plate-to-beam connection, this caused out of plane deformation in the BRB, pictured in Figure 2.26. In the last cycles, the fracture expanded into the beam's web and the BRB hinged out of plane as shown in the Figure 2.26. In Figure 2.27 and 2.28 the BRBF-3 frame and buckling-restrained brace hysteresis, respectively, is presented.

From the performed tests one can draw a number of considerations about the performance of BRBF. Tests demonstrated that the gusset plates and connected frame elements negatively affected the system's overall performance. The occurrence of the gusset plate buckling in the BRBF-2 test showed that the connections weren't able to withstand the large inelastic deformations, even though they were designed according to the available methods. The beam fracture that took place in the BRBF-3 testing also played a role in hindering the system's

Figure 2.26: (*left*) UC Berkeley BRBF-3 beam flange fracture (*rigth*) UC Berkeley BRBF-3 brace rotation at peak displacement [49].

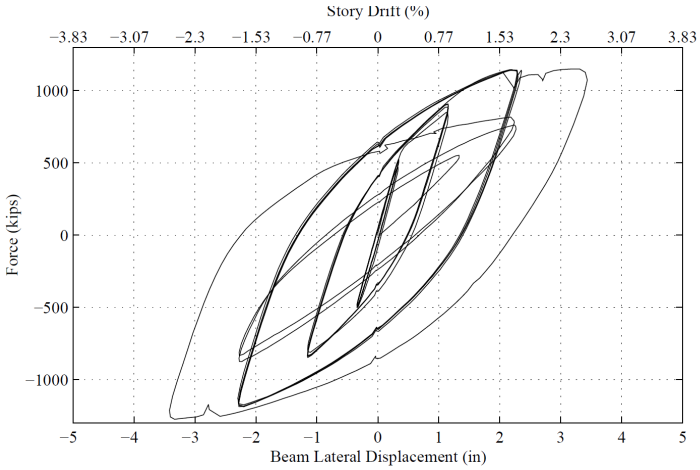

Figure 2.27: UC Berkeley BRBF-3 lateral beam displacement versus base shear [49].

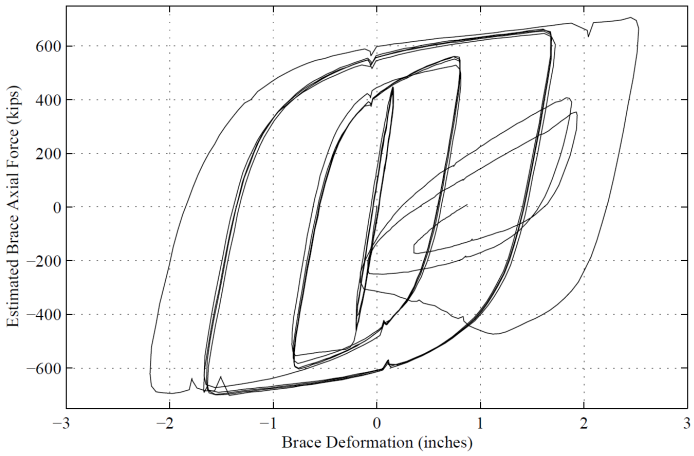

Figure 2.28: UC Berkeley BRBF-3 BRB estimated hysteresis [49].

performance, causing the BRB to hinge out of plane. It should be noted that, since the same structural frame was used in all the three tests, the frame was designed to be stronger and stiffer than what usually is present in an actual building, which could be the source of the connections poor performance.

2.6 Application Cases

There are many buildings where BRB have been used to counteract horizontal actions, either used as a reinforcement or since the building's conception. The first company to provide commercially BRBs was the Nippon Steel Corporation in Japan. They filed a patent for the unbounded brace and were responsible for the application of BRBs to more than 300 buildings by 2007 [30]. One successful example of BRB application in Japan is the Nittele Tower that serves as headquarters for Nippon Television [9], pictured in Figure 2.29.

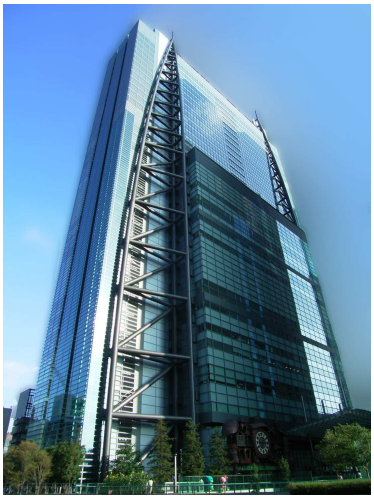

Figure 2.29: "'Nittele tower"' Shiodome, Japan. Head office building of Nippon Television Network Corporation.

In the United States of America, COREBRACE, LLC filed the first patent for an unbonded brace [30]. It consisted of a flat or cruciform steel core with bolted end splice connections, as pictured in Figure 2.30. The second filed patent was submitted by Star Seismic, LLC, and featured a pin-and-collar assembly at each end of the brace [9], as shown in the Figure 2.31.

After tests carried out in 1999 at the University of California, Berkeley, BRBs started being applied in the US for seismic retrofitting. There are two relevant examples of BRB use for seismic retrofitting in the US, one was the UC Davis Plant and Environmental Sciences building, the other was the retrofitting of the Wallace F. Bennett Federal Building in Salt Lake City, Utah. The second consists of an 8 story RC building constructed in the early 1960s and afterwards retrofitted with BRBs. In this case besides its use as a seismic retrofit, BRBs were also used as architectural elements [30], as pictured in the Figure 2.32.

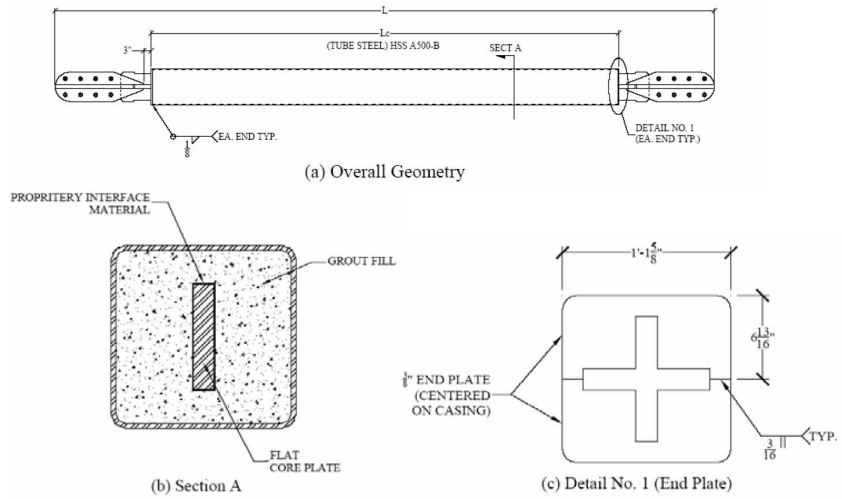

Figure 2.30: COREBRACE, LLC patent, the first in the USA [30].

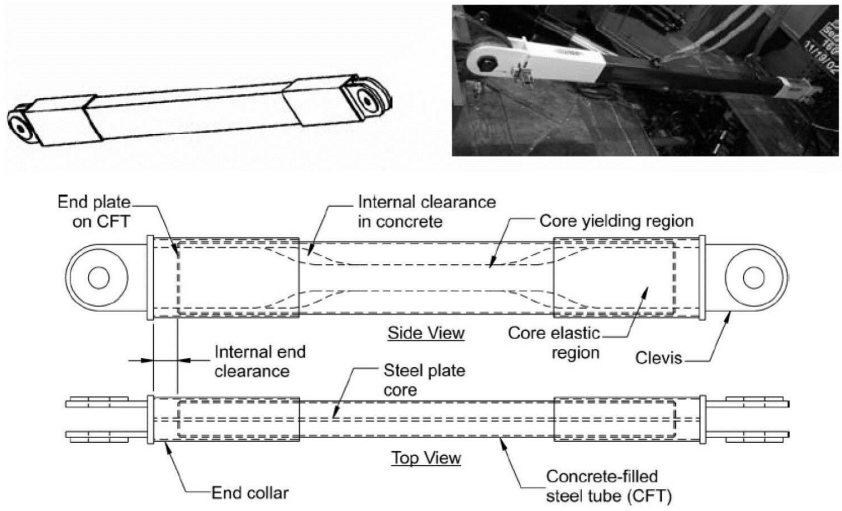

Figure 2.31: STAR SEISMIC, LLC patent, the second in the USA [30].

Figure 2.32: Wallace F. Bennet Federal Building, USA: *(left)* Before BRB seismic retrofitting, *(right)* after BRB seismic retrofitting

In Europe, most specifically in Italy, FIP INDUSTRIALE S.r.l. also filed a patent for a type of unbonded brace, the so called Buckling Restrained Axial Damper (BRAD). They consist of a steel plate core encased in a steel tube infilled with high strength mortar, as shown in Figure 2.33. BRADs have been successfully applied for the seismic protection of one building of the Faculty of Engineering of Ancona, Italy, as displayed in Figure 2.34. This application represents the first of this type of devices in Italy and Europe [76].

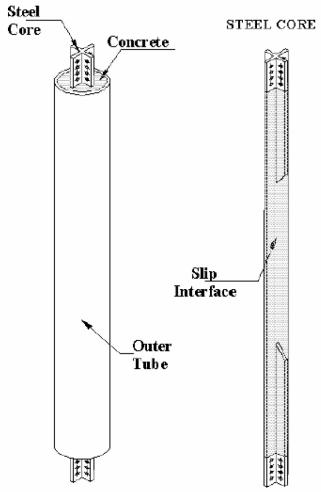

Figure 2.33: FIP INDUSTRIALE S.r.l. patent, the Buckling Restrained Axial Damper (BRAD) [30].

Figure 2.34: Building of the Faculty of Engineering of Ancona, Italy, retrofitted with BRADs [76].

Chapter 3

Case Study

In the present section, the experimental models and test campaign performed by L. Di Sarno and G. Manfredi [10], which served as base for the numerical model calibration, are presented. Afterwords, a full description of the model calibration procedure is given.

3.1 Experimental Models

For the assessment of the seismic reinforcement potential of BRBs, two identical, full scale multi-storey, RC structures were built and tested by Sarno and Manfredi [10]. One was tested with no type of additional reinforcement, from hereinafter named “unretrofitted frame”, and the other was retrofitted with BRBs, from hereinafter named “retrofitted frame”.

3.1.1 General Description

The test structures consist of two identical full scale, two storey, RC structures. The foundations consist of a 6 by 7m, 50cm thick, shallow RC mat, resulting in an implementation area of 42m^2. The structures combine two 2.55m bays in one direction and a single 4.40m bay in the other orthogonal direction. The interstorey heights are 3.50m and 3.44m for the first and second floor respectively, resulting in a total height of 7.65m. The structural frames incorporate rectangular 30 by 50cm cross section beams and 30 by 30cm square section columns. In order to avoid the use of additional weights to simulate vertical loads and seismic masses, 25 and 20cm thick RC solid slabs were employed in the first and second floors respectively. The floor plans and cross sections views of the test structures are provided in Figure 3.1. The test frames employ typical details of gravity load design, with application of smooth bars, large spacing stirrups, hooks and low concrete compression strength.

3.1.2 Material properties and Details

The RC structures were deliberately designed with structural deficiencies, not compliant with the modern codes of practice. The materials of construction, both

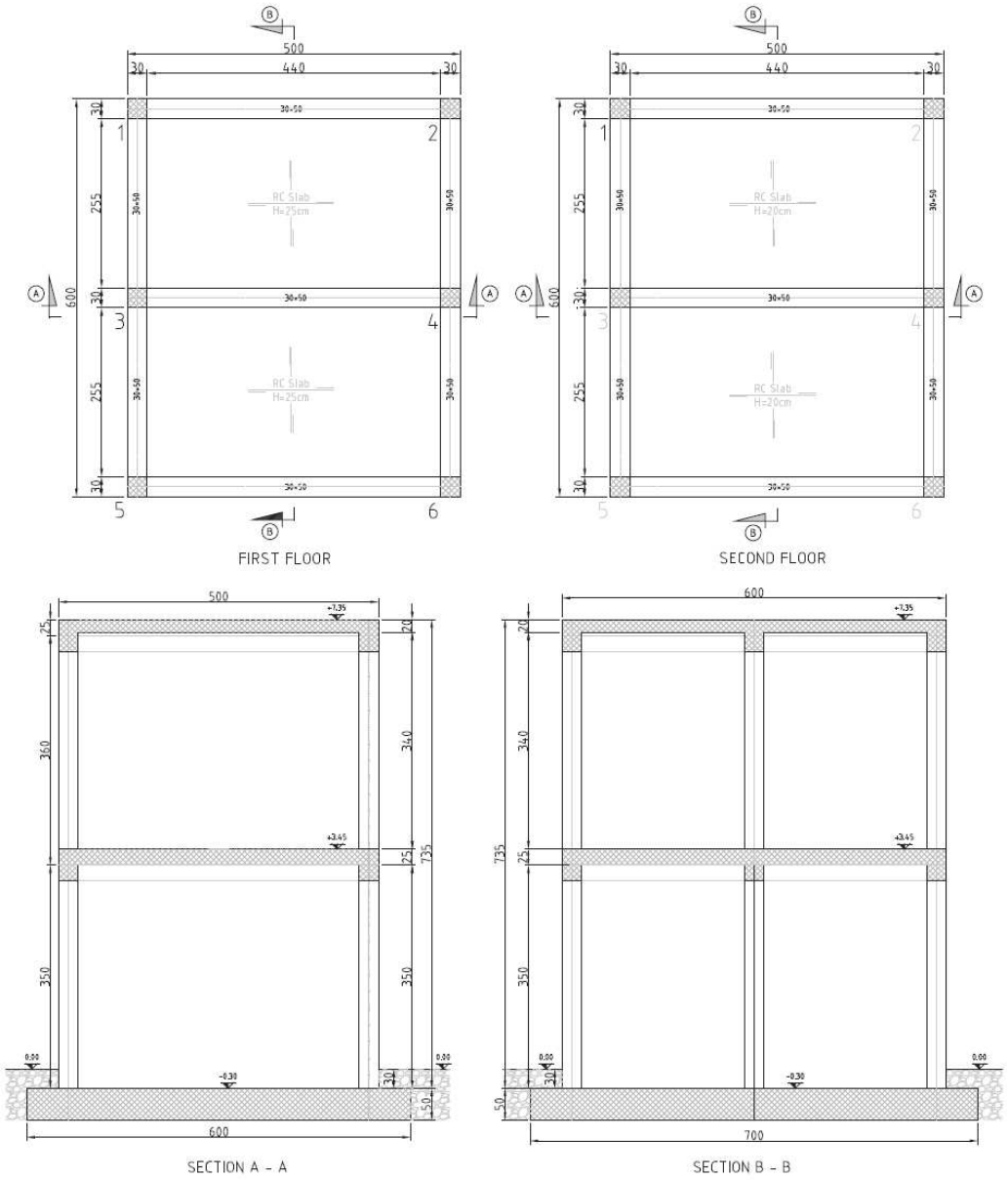

Figure 3.1: Floor plans and cross sections of the RC test frames [10]

concrete and reinforcement steel bars, possessed low strengths compared to the response of modern code-compliant grades.

Concrete

The mean compressive cylinder strength of the concrete was f_{cm}=19.4MPa, computed from 21 crushing tests on cubic specimens extracted from the casting of beams, columns and floor slabs. The concrete cubes crushing tests also presented a standard deviation of 1.3MPa, and a Young modulus of E_{cm}=26672MPa.

As it can be observed the concrete doesn't fulfil the modern code-compliant grades required for structural components in earthquake prone regions [10]. For example, the lowest compressive mean strength of a concrete compliant with Eurocode 2 [77] (EC2) is 20MPa (C12/15) and it is recommended for concrete elements without reinforcement, and no risk of corrosion or attack from ambient conditions.

Reinforcement Bars

Tensile tests were performed in six reinforcement bars with the different diameters (Φ) employed in the structures. The mechanical properties of the rebars are presented in Table 3.1.

Table 3.1: Mechanical properties of the reinforcement bars [10]

				Ultimate-to-yield stress ratio		
Φ	**Low yield stress***	**Upper yield stress**	**Ultimate strength**	**Low yield**	**Upper yield**	**Ultimate elongation**
[mm]	[MPa]	[MPa]	[MPa]	[-]	[-]	[%]
6	338.7	358.6	433.9	1.28	1.21	50
8	345.9	355.8	438.3	1.27	1.23	42
10	350.8	354.1	515.1	1.47	1.45	34
12	322.3	342.2	415.4	1.29	1.21	38
14	334.1	348.1	444.0	1.33	1.28	41
16	312.7	329.7	417.5	1.34	1.27	43
Mean	334.1	348.1	444.0	1.33	1.28	41
SD	14.4	10.8	36.62	0.07	0.09	5
COV (%)	4.3	3.1	8.25	5.55	7.21	13

*Low and upper yield stresses correspond to the lower and upper bounds of the yield stress of the bars during tensile tests.

Along with the concrete, from Table 3.1, one can conclude that the reinforcement steel bars possess low strength compared to the grades required by modern codes for structural components in earthquake prone regions [10]. For example, in EC2 [77], Portuguese annexe C it is stated that the yield strength of steel rebars should be between 400 and 500MPa.

Design Considerations

As mentioned before the RC frame structures weren't designed in compliance with the recent codes of practice, especially with the seismic specifications. In fact, they were designed according to the allowable stress method as implemented in the Italian standards of the 1960s [11].

As such, smooth reinforcement bars were adopted in the structures. The diameter of the longitudinal bars of the columns is ϕ14 and ϕ12, for the first and second floor

respectively, along with a $\phi 6//300$mm spaced stirrups. For the beams, longitudinal bars vary from $\phi 8$ to $\phi 16$, and employ $\phi 6$ stirrups with spacing varying from 250 to 300mm. The reinforcement bar's layout shows that the frame doesn't fulfil the modern seismic codes. The stirrup spacing, the beams, columns and joints detailing do not fulfil the seismic code requirements. For example, Eurocode 8 [18] (EC8) specifies that in critic regions, such as beam to column connections, the stirrup's spacing should satisfy the following spacing criteria

$$s = min\left\{\frac{h_W}{4}; 24d_{bW}; 225; 8d_{bL}\right\} \tag{3.1}$$

where,

- h_W is the beams height in millimetres
- d_{bW} is the diameter of the stirrups, which should not be inferior to 6mm;
- d_{bL} is the minimum diameter of the longitudinal rebars;

The reinforcement details employed in the RC frames are presented in the Figure 3.2.

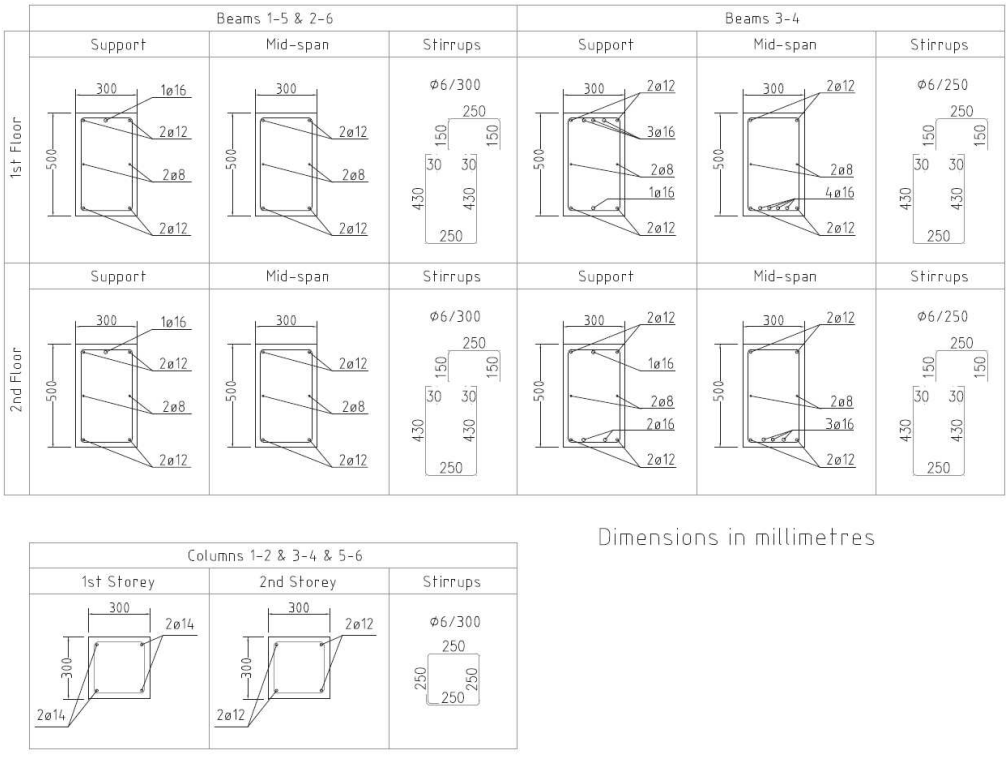

Figure 3.2: Beam and column cross-sections layout and steel reinforcement of the RC frames [10].

In compliance with [11], the structure was designed exclusively for gravity loads. The live loads for both floors were assumed equal to 3kN/m^2. The first floor

25cm thick slab includes the weight of dead loads, comprising the 16cm cast in situ slab, mat, plaster and partition walls, adding to a total design load of 8.13kN/m^2. The same was applied to the roof level were the total design loads added to 5.43kN/m^2. The total seismic mass of the building is 33.61 tons, divided in 18.66 and 14.95 tons for the first and second floors, respectively. The frames were designed to withstand gravity loads and as such they lack sufficient lateral resistance. The RC frames are typical substandard structures that do not fulfil any capacity-design guidelines implemented in the modern seismic design standards, for example [18], and don't present the required seismic detailing. The RC framed structures were assumed representative of typical residential buildings located in seismic zones of moderate earthquake hazards, with peak ground acceleration of about 0.25g and the response spectra of a typical building in a seismic zone close to Naples, South of Italy [10].

Retrofitting System and Configuration

Two types of BRB systems were applied to the retrofitted structure, one to the first floor and another to the second. The bracing was applied in one bay per floor only. The system is a combination of a BRB and a standard structural tubular steel pipe with 101.6mm exterior diameter and a thickness of 6.3mm, as pictured in Figure 3.3. The steel grade of the pipes is S275, with a nominal yield strength f_y=275MPa. The system exhibits maximum strokes of $\pm$20mm based on the maximum seismic displacement demand and component testing. The total length of the braces, both dissipative (BRB) and non-dissipative (steel pipe) parts, is 405cm ate base and 385cm at the upper story. The dissipative component is 91cm at the base and 110cm at the top story. At the lower story the BRB exhibit a yield force of $F_{y,1}$=75kN, a maximum force of $F_{max,1}$=90kN and an elastic axial stiffness of $k_{el,1}$=70kN/mm, trough component testing. At the upper story BRBs demonstrated a yielding force of $F_{y,2}$=40kN, a maximum force of $F_{max,2}$=50kN and an elastic axial stiffness of $k_{el,2}$=40kN/mm. The braces were designed within the framework of displacement-based methods [12]; the target interstorey drift was assumed equal to 0.3% along with an inverted linear triangular lateral deformed shape of the frame. The tubular steel pipes were capacity designed, with an ultimate strength higher than the dissipative parts at both storeys. The non-dissipative elements slenderness is about 170 and stability checks were performed to avoid the pipes buckling, which, could jeopardize the energy dissipation capacity of the diagonal braces.

The BRBs implemented in the retrofitted frame were tested according to the 2008 protocol required by the Italian seismic design code of practice [6]. The experimental protocol used for the qualification of the brace is based on the benchmark value of the total axial displacement of the device estimated at collapse prevention limit state (d_2), which is the limit state corresponding to the maximum credible earthquake. The three loading tests included in the protocol consist of:

- Preliminary test: five cycles of loading at deformations not less than $\pm$0.1 d_2, $\pm$0.2 d_2, $\pm$0.3 d_2, $\pm$0.5 d_2, $\pm$0.7 d_2 and at least 10 cycles at deformation amplitudes equal to $\pm$1.0 d_2;

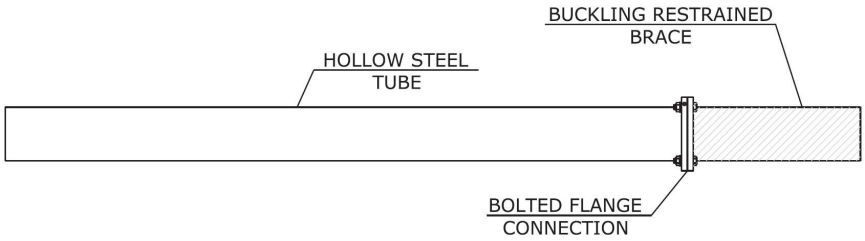

Figure 3.3: Schematic sub-assemblage of the diagonal braces: Conventional steel tube brace and BRB (adapted from [78].

- Quasi-static test: five cycles of loading at deformations of $\pm$1.0 d_2;
- Dynamic test: five cycles of loading at deformations of $\pm$1.0 d_2.

  The rate of the loading should be similar to the velocity of the expected earthquake ground motion. For BRBs, i.e. steel hysteretic dampers, such test can be, however, replaced by a series of quasi-static tests.

The acceptance criteria requires variations less than $\pm$10% of the initial stiffness evaluated at a deformation of $d_2/20$.

3.2 Experimental Test Campaign

The experimental models described in the previous section were tested using displacement-controlled pushover by Di Sarno and Manfredi, using both static and cyclic lateral loads [10]. Additionally, modal response properties of the RC frames were also determined. The monotonic lateral response, obtained from the static pushover test, along with the modal response of the structures, served as foundation for the calibration of the numerical models developed in the present work. As such, only the previous two test campaign will be described hereinafter. For further discussion on the experiments carried by Di Sarno and Manfredi please refer to [10].

3.2.1 Experimental Set-up and Loading Protocol

The RC structures were dynamically tested to identify their modal properties: periods of vibrations, mode shapes and equivalent inherent structural damping. The structures were tested before and after the lateral loading. The frames were subjected to an incremental lateral loading, pushover, until collapse was reached. The structures were pushed to about 159mm and 80mm roof lateral displacements for both the unretfrofitted and retrofitted frame, respectively. Cyclic response was also investigated by means of reversal pushover[1] at target roof displacements.

[1]Cyclic type of pushover analysis, where the structure is pushed to certain target displacement and afterwards reverses the displacement.

The structure's modal frequencies were estimated through the analysis of ambient noise and impulsive vibrations caused by instrumented impact hammer.

In order to retrieve the structures response to the excitations the RC frames were highly instrumented with sensors for vibration measurements, including accelerometers with a $1 \times 10^{-}6$g tolerance. The accelerometers were placed in the corners of the first and second floor of the test structures, as shown in the Figure 3.4. The X and Y directions defined in Figure 3.4 are the two orthogonal directions considered from hereinafter throughout this dissertation.

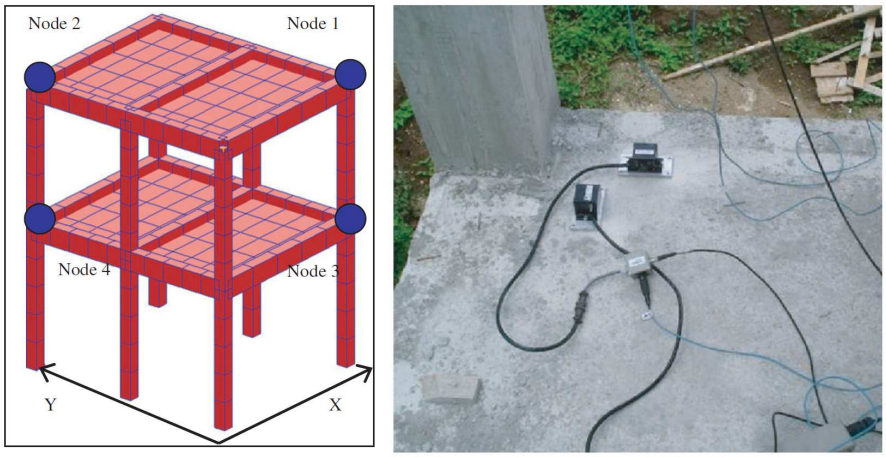

Figure 3.4: Accelerometers positioning for the experimental tests [10].

For the deformation control of the steel rebars 61 strain gauges were used for each of the full-scale structures. They were implemented in the bars of the foundation slab (12 gauges), columns (15 gauges) and beams (34 gauges). The beam-to-column connections were monitored with displacement transducers (DTs). The reaction wall and the BRBs were also instrumented with transducers, to monitor the deformations during the pushover tests and estimate the axial deformations of the added bracing system under lateral loads (6 wire transducers, WTs). Laser measurements were also conducted to characterize the deformed shapes of the RC frames and check the deformability of the steel reacting wall, if any, during the lateral loading. A total of eight measuring points were checked, five on the first and second floor slabs and three on the reaction wall.

Monotonic and cyclic lateral load patterns were applied to the structure to simulate the effects of horizontal earthquake ground motions. The load patterns were displacement controlled and were applied through two MTS hydraulic jacks connected to the steel reaction wall, as pictured in Figure 3.5. Both jacks possess a stroke of $\pm$250mm and a maximum force capacity of 500kN and 290kN for both compression and tension, respectively.

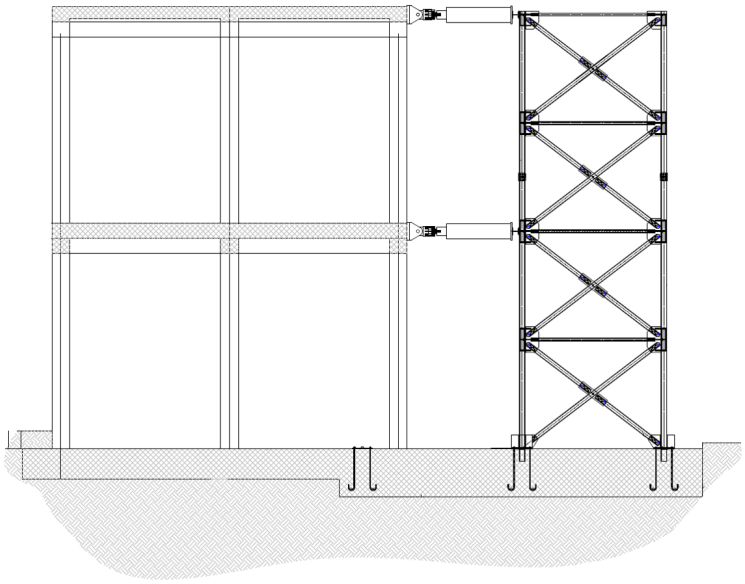

Figure 3.5: Schematic drawing of test set-up (adapted from [79]).

3.3 Experimental Test Results

3.3.1 Modal Response

In order to obtain the sample structures modal identification, dynamic loading was applied to the frames. The modal frequencies of the structure were estimated through ambient noise and impulsive vibrations caused by instrumented impact hammer. In the Table 3.2 a summary of the frequencies measured from the experimental modal identification is presented.

Table 3.2: Frequencies of vibration, in hertz, estimated with experimental methods for both the unretfofitted and retrofitted RC structures [10]

		Mode of vibration					
Input type	**RC frame**	**First Lateral X**	**Second Lateral Y**	**Third Torsional**	**Fourth Lateral X**	**Fifth Lateral Y**	**Sixth Torsional**
Ambient noise	Unretrofitted	3.15	3.30	4.75	8.80	9.31	13.10
	Retrofitted	3.15	3.30	n.a.	8.85	9.36	n.a.
Impulsive	Unretrofitted	3.15	3.40	4.75	9.13	9.24	13.08
	Retrofitted	3.15	3.30	4.84	8.76	9.25	12.94

3.3.2 Monotonic Lateral Response

As addressed before, both test RC frames were subjected to a displacement-controlled static pushover test. Capacity curves were obtained

for both the unretrofitted structure, and the retrofitted structure considering a linear inverted triangular displacement loading applied by the hydraulic jacks.

Unretrofitted Framed System

For the unretrofitted structure, the system was pushed close to 0.160m and the capacity curve obtained is presented in Figure 3.6.

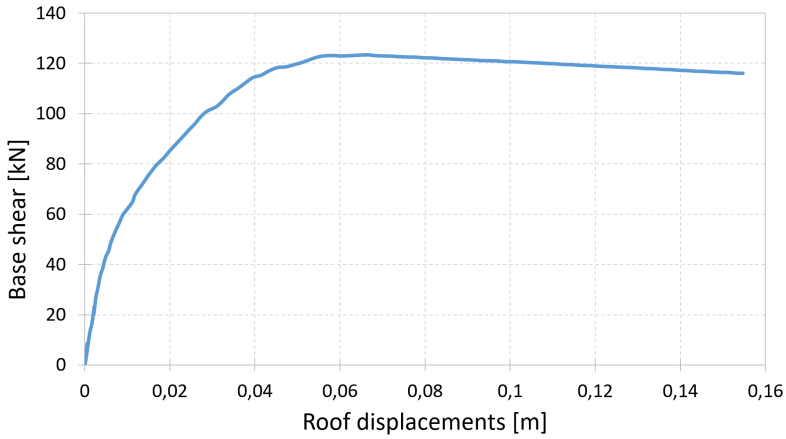

Figure 3.6: Unretrofitted frame capacity curve (adapted from [10])

From Figure 3.6, one can observe that the unretrofitted structure exhibits large inelastic deformations when subjected to horizontal forces simulating earthquake loading. However, the structure's stiffness and strength deteriorate rapidly [10]. The first yielding occurred in the bottom exterior columns when the structure reached a base shear capacity of 75kN at a correspondent roof displacement of 0.015m (≈0.2% top drift). When the structure reached a roof displacement of 0.030m (≈0.4% top drift), at a base shear of 102.2kN, the remaining first floor columns yielded. The RC frame reaches its maximum capacity of 123.7kN at a corresponding top roof displacement of 0.063m (0.82% top drift), and a ultimate capacity of 115.9kN for a ultimate top displacement of 0.155m (2.0% top drift). At high horizontal displacements, structural damage was observed at the top and bottom of the ground storey columns, such as deteriorated bond between the concrete and the smooth longitudinal steel rebars, with appearance of large cracks. The first floor beams exhibited plastic deformations at a lateral top displacement of 0.084m (≈1.1% roof drift). At the second storey, all beams and columns displayed an elastic behaviour.

Retrofitted Framed System

The retrofitted RC frame was pushed up to 0.080m and in Figure 3.7 the capacity curve obtained from the test is presented.

In the retrofitted frame, the bottom and top sections of the ground storey columns did not experience the damage observed in its unretrofitted counterpart. Beams

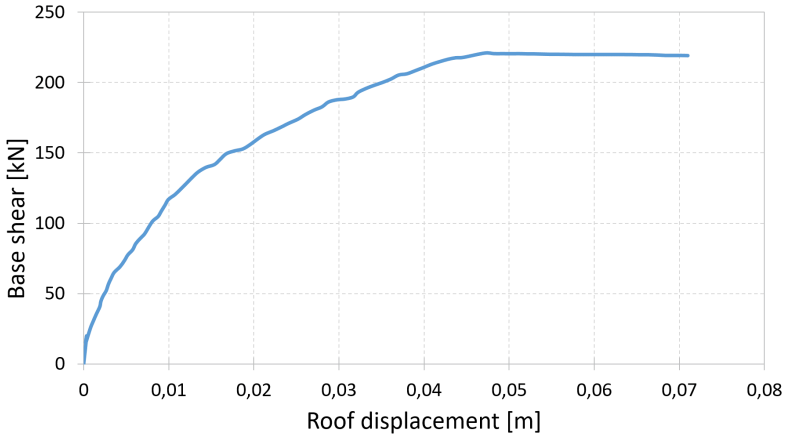

Figure 3.7: Retrofitted frame capacity curve (adapted from [10])

and columns of the retrofitted frame remained elastic throughout the pushover test, strain gauges attached to the longitudinal rebars showed the steel stress did not surpass the elastic stress thresholds. Even at roof drifts of approximately 1% (≈0.08m roof displacement), value when the BRBs reached their maximum axial displacement, the global stability of the frame was not endangered. The maximum reached base shear was 220.5kN at the ultimate roof displacement of 0.080m [10].

3.4 Numerical Model Development and Calibration

Adopting the results of the research conducted by DI Sarno and Manfredi [10], two numerical models of the RC frames were developed and calibrated, in order to establish a starting point for the fragility study conducted in the present work: one bare RC frame, hereinafter called “Simple frame”, and a BRB retrofitted RC frame, hereinafter called “BRB frame”. One additional model was developed, where the bare RC frame is retrofitted with concentric braces (CB), hereinafter called "‘CBF Frame"’. The numerical models were developed with the commercial nonlinear FE package SeismoStruct [80], based on the design drawings (Figures 3.1 and 3.2) and material properties defined in 3.1.2.

The present section provides a description of the development procedures and structural properties monitored to achieve a proper representation of the full-scale structural behaviour.

3.4.1 Simple Frame

Initially, all materials were properly defined and implemented in the SeismoStruct. An uniaxial nonlinear constant confinement model (con_ma), initially programmed by Madas [81] that follows the constitutive relationship suggested by Mander et al. [82] and the cyclic rules proposed by Martinez-Rueda and Elnashai [83], was adopted to model the constitutive relationship of the concrete. In the model, constant confining pressure, provided by the lateral transverse reinforcement

and implemented through the rules proposed by Mander et al. [82], is assumed throughout the entire stress-strain range. For the complete definition of the concrete behaviour five concrete characteristics must be inputted in the FE package. Table 3.3 provides these characteristics along with their adopted values. The values presented in Table 3.3 were directly retrieved from Di Sarno and Manfredi's research [10].

Table 3.3: Concrete characteristics implemented in the numerical model

Mean compressive strength [kPa]	**Mean tensile strength [kPa]**	**Modulus of elasticity [kPa]**	**Strain at peak stress [m/m]**	**Specific weight kN/m^3**
19400.00	1572.00	2.6672×10^7	0.002	24.00

The steel rebar's constitutive relationship was modelled using an uniaxial steel model based on a simple, yet effective, stress-strain relationship proposed by Menegotto and Pinto [13], coupled with isotropic hardening rules suggested by Filippou et al. [14] (stl_mp). Its use should be restricted to the modelling of RC structures, specially those subjected to complex loading histories, in which significant load reversals might take place. Initially developed with ribbed reinforcements in mind, under the correct calibration, the present model can also be employed in the modelling of smooth bars [84], often present in existing structures such as the case in hand. To fully characterize the stress-strain curve of the steel rebar's model ten parameters must be inputted in SeismoStruct. Table 3.3 provides these parameters along with their adopted values.

The value assumed for the steel rebar's yield strength resulted from the tensile tests performed on some of the actual reinforcement bars batch used in the full-scale structure. Taking the low and upper yield strength mean values from Table 3.1 and averaging them out, a value of 341.1MPa was adopted for the steel's yield strength. The fracture/buckling strain was also adopted from Table's 3.1 ultimate elongation value. The remaining parameters were the program default ones or selected according to the software user manual [80].

With the materials properly characterized, the cross-sections and reinforcements of all structural elements were implemented in SeismoStruct, according to the details provided by Di Sarno and Manfredi's work (see Figure 3.1).

Afterwards, the proper element types were defined for each structural element of the model. An inelastic forced-based 3D frame element was adopted for the beams and columns of the numerical model. This forced-based 3D beam-column element type is capable of modelling space frame's members considering geometric and material nonlinearities. The sectional stress-strain state is obtained through the integration of the nonlinear uniaxial material response of the individual fibres in which the section was subdivided, fully accounting for the spread of inelasticity along the member length and across the section depth, as described in the Material

Table 3.4: Steel reinforcement characteristics implemented in the numerical model

Modulus of elasticity [kPa]	2.00×10^8
Yield strength [kPa]	341100.00
Strain hardening parameter [-]	0.001
Transition curve initial shape parameter [-]	20.00
A1 [-]	18.50
A2 [-]	0.15
A3 [-]	0.00
A4 [-]	1.00
Fracture/Buckling strain [-]	0.41
Specific weight [kN/m^3]	78.00

inelasticity section.

The capability of capturing the inelastic behaviour along the entire length of a structural member, even when employing a single element per member, makes the infrmFB element the most accurate among the four inelastic frame element types on SeismoStruct. Therefore, these elements are capable of very high accuracy in the analytical results.

For the element configuration a cross section, previously defined, along with the number of integration sections and number of section fibres must be chosen.

In the beams, around 200 individual fibres were selected along with 7 integration sections. The columns were subdivided in 300 longitudinal fibres and, as it was set for the beams, 7 integration sections were adopted.

For the modelling of the slabs, a combination of elastic frame elements combined with a rigid diaphragm type of constraint solution was adopted as displayed in Figure 3.8. A rigid diaphragm has the purpose to constraint certain degrees-of-freedom of slave nodes to a master node, by means of rigid planes. This means that all constrained nodes will rotate/displace in a given plane maintaining their relative position unvaried. As such, both master and slave nodes must be defined, with the master node usually corresponding to the barycenter of the diaphragm.

The elastic frame elements added possessed the same characteristics as the slab, such as, axial stiffness, both plane directions flexural stiffness and torsional

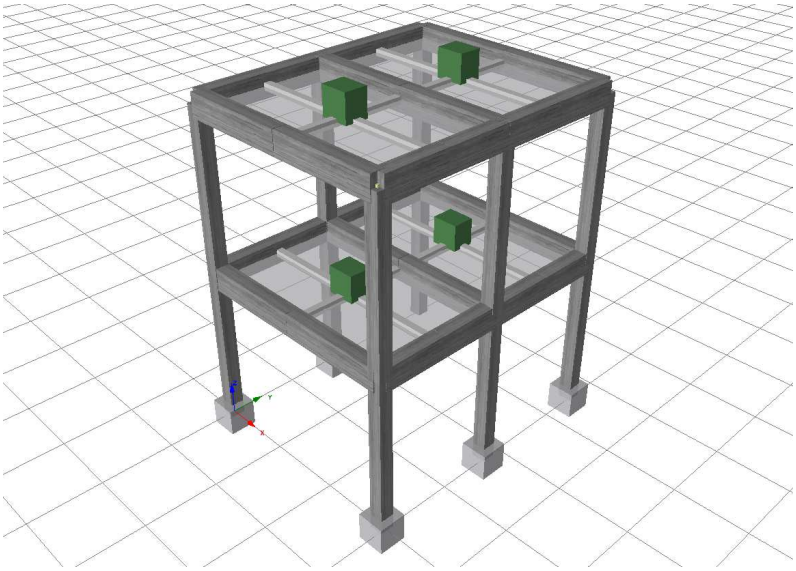

Figure 3.8: Adopted slab modelling solution.

stiffness. The values applied for both, the first and second floor slabs are presented in Table 3.5.

Table 3.5: Slab's elastic frame elements characteristics

	Direction	EA [kN]	EI_2 [kNm^2]	EI_3 [kNm^2]	GJ [kNm^2]
1st Floor	X	1.9125×10^7	99609.40	1.0363×10^7	143162.539
	Y	3.3000×10^7	171875.00	5.3240×10^7	254162.343
2nd Floor	X	1.5300×10^7	51000.00	8.2907×10^6	74303.002
	Y	2.6400×10^7	88000.00	4.2592×10^7	131147.122

Additionally, lumped mass elements were applied to the barycenter of the slab panels, to account for the slab's self weight and loads. As the name implies these elements allow to assign mass to a structural node of the model. Four lumped mass elements were applied, one for each slab panel of the structure, Figure 3.8. Since the structure is symmetric only two lumped mass elements were defined, one for each floor. The masses values applied in the model are presented in the Table 3.6.

Table 3.6: Slab's concentrated mass values

	Mass [tonne]
1st Floor	7.03782
2nd Floor	5.63026

Finally, to simulate the shallow RC mat foundation all columns were anchored at the base by restraining all displacements and rotations.

Following the numerical model definition the test campaign was recreated in order to proceed with the model calibration.

Modal Response

Firstly, we proceeded with a numerical eigenvalue analysis and retrieved the frequencies of vibration. In the following table a comparison between the real structure's frequencies of vibration and the ones obtained through numerical simulation is provided.

Table 3.7: Frequencies of vibration: Real Structure vs. Numerical Model

Mode	Real Structure [Hz]	Numerical Model [Hz]	Error [%]
1	3.15	3.157	0.233
2	3.30	3.261	1.183
3	4.75	4.695	1.151
4	8.80	8.280	5.913
5	9.31	8.383	9.952
6	13.10	12.046	8.045

From Table 3.7 we can observe a close correspondence between the first three modes of vibration, with all three with errors below 2%. In the later three modes, the numerical model stands more distant with errors below 10%, which was deemed acceptable.

Static Pushover

Additionally to the eigenvalue analysis, a numerical static pushover analysis in the longitudinal direction (Y) was carried out to compare the two capacity curves, the one from the real structure and the one from the numerical model. This comparison can be observed in Figure 3.9. Through the interpretation of Figure 3.9 we can conclude that the curves are sufficiently close to each other, with the biggest relative error around the 5% mark.

Although there is no data in Di Sarno and Manfredi's [10] work, a pushover analysis in the transverse direction was also carried out. The intent was to compare the capacity curves from both directions, since the columns have both doubly symmetric cross sections and reinforcement layout. In Figure 3.10 we can observe both the longitudinal and transversal capacity curves.

With assessment of the modal response and the capacity curves we can state that our numerical model for the Simple Frame represents the reality to an acceptable extent. Therefore, the model was deemed calibrated.

Before we could validate the BRB Frame it was needed to conduct a calibration process on the BRB itself.

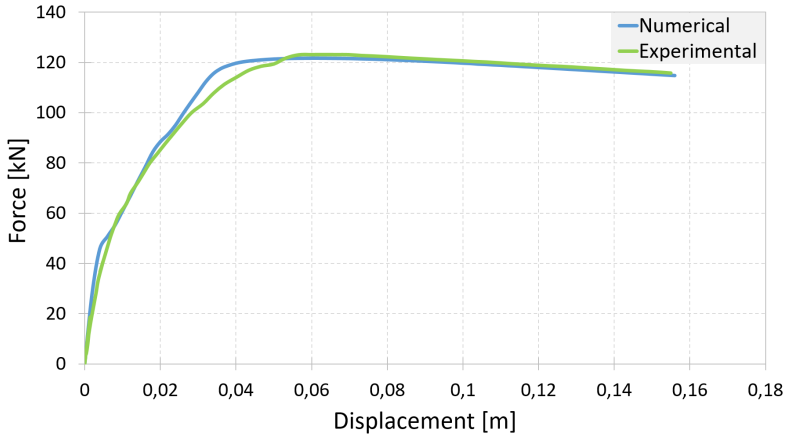

Figure 3.9: Comparison between the experimental and numerical pushover curves.

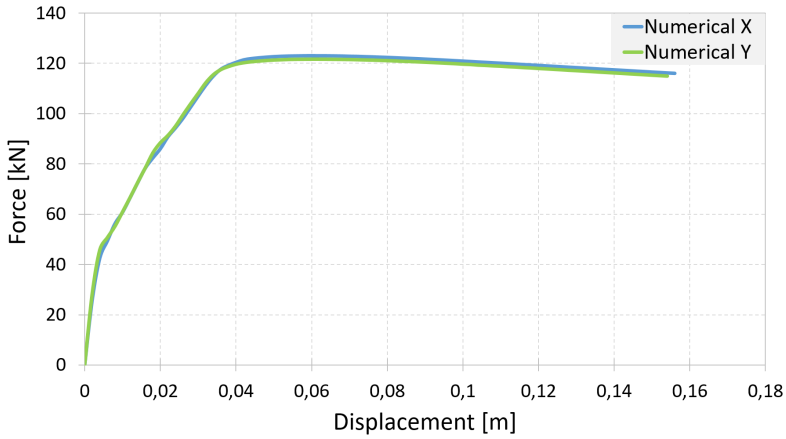

Figure 3.10: Comparison between the two orthogonal directions, X and Y, numerical pushover curves.

3.4.2 BRB Frame

In order to validate the BRB Frame it was crucial to proceed firstly with the proper calibration of the BRB device itself. Therefore, numerical tests were conducted in order to obtain the structural behaviour of the device.

BRB Calibration

In order to model the BRB Frame correctly it is of extreme importance that the BRBs are properly calibrated and match the behaviour of the ones used in the large scale test.

The parameters obtained through component testing, by Di Sarno and Manfredi [10], of the BRBs are presented in Table 3.8.

From component testing it is also known that the BRBs possess maximum strokes

Table 3.8: BRB's mechanical parameters for both the ground and first floor.

	Length [m]	Yield Force [kN]	Maximum Force [kN]	Elastic Axial Stiffness [kN/mm]
Ground floor	0.91	75	90	70
First floor	1.10	40	50	40

of $\pm$20mm.

Six numerical models were created in SeismoStruct [80], one of the following for each floor: one with only the buckling restrained brace component, one with the previously calibrated BRB and the steel pipe combination and, lastly, a single steel element equivalent to the previous set up. For each model a numerical compression and pull-test were conducted.

Single BRB Model

For the modelling of both the ground and first floor BRBs a solid circular steel cross-section with a 0.1016m diameter was used, along with a Dodd-Restrepo steel model. A truss element was used to represent the BRB in SeismoStruct, Figure 3.11. The steel mechanical properties are presented in Tables 3.9 and 3.10, for the first and second floors respectively.

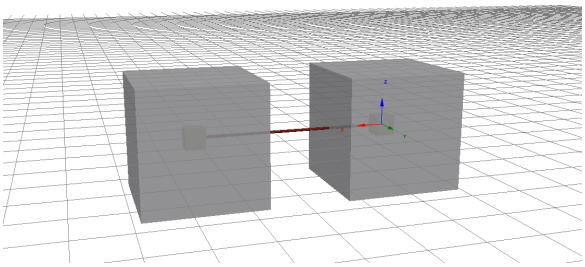

Figure 3.11: Numerical model of the single BRB

In Figure 3.12 and 3.13 the force-displacement curves of both the compression and pull-tests is presented for both floors, respectively. It can be seen that the BRB's behaviour is in compliance with the component testing results highlighted in Table 3.8. Therefore, the models were considered calibrated and a reliable representation of the real components.

Steel Pipe and BRB Combination

After the proper calibration of the BRBs, two numerical models of the experimental set-up were developed, one for the ground floor and another for the first floor. The set-up was composed of the calibrated BRBs connected with a regular circular

Table 3.9: Steel mechanical properties implemented on the ground floor single BRB model.

Modulus of elasticity [kPa]	7.857×10^6
Yield strength [kPa]	9250.90
Stress at peak load [kPa]	11101.10
Strain at initiation of strain hardening curve [-]	0.0015
Strain at peak load [-]	0.021978
Strain of the intermediate point of the strain hardening curve [-]	0.01
Stress of the intermediate point of the strain hardening curve [kPa]	10575.40
Specific weight [kN/m^3]	78.00

Table 3.10: Steel mechanical properties implemented in the first floor single BRB model.

Modulus of elasticity [kPa]	5.4274×10^6
Yield stress [kPa]	4934.01
Stress at peak load [kPa]	6167.51
Strain at initiation of strain hardening curve [-]	0.00125
Strain at peak load [-]	0.018182
Strain of the intermediate point of the strain hardening curve [-]	0.008
Stress of the intermediate point of the strain hardening curve [kPa]	5632.40
Specific weight [kN/m^3]	78.00

steel pipe, Figure 3.14, with a S275 steel grade. The pipes possess a nominal yield strength f_y=275MPa, an exterior diameter of 101.6mm and a thickness of 6.3mm. Figure 3.15 and 3.16 are a representation of the force displacement curves of the set-up's numerical testing. It can be observed that the presence of the structural steel pipes doesn't hinder in any way the performance of the BRB components.

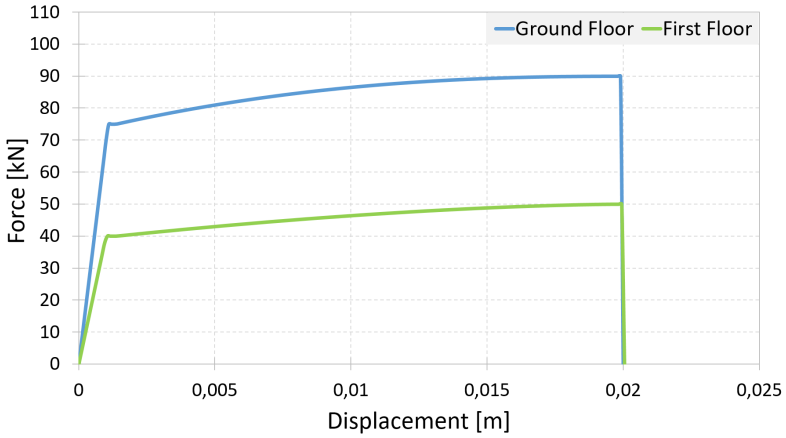

Figure 3.12: Force-displacement curve of the single BRB numerical pull-test

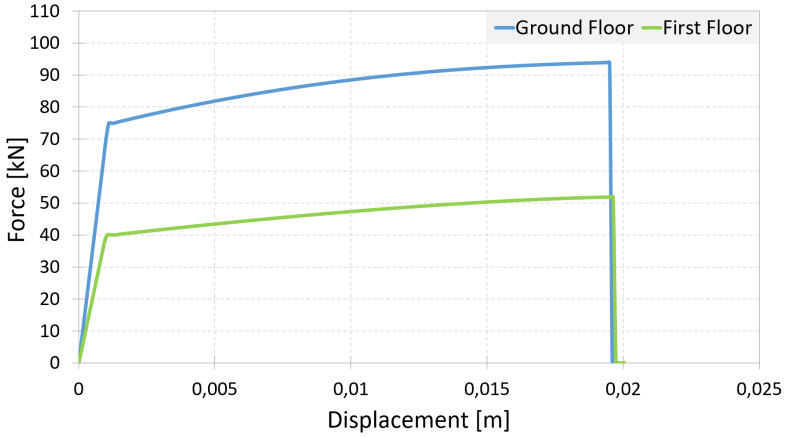

Figure 3.13: Force-displacement curve of the single BRB numerical compression test

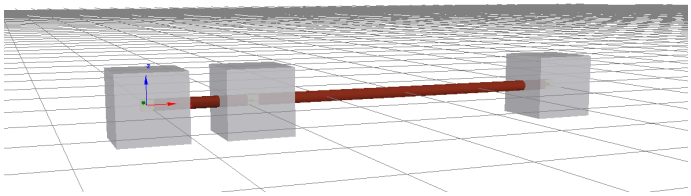

Figure 3.14: Numerical model of the BRB and steel pipe set-up

Equivalent Single Element Model

In the previous model a structural node was necessary in between the BRB component and the structural steel pipe, this originated problems in terms of displacement compatibility. It was necessary for the "'connection node"' to inhibit rotation between the elements in the three orthogonal directions. The adopted solution was to use an equivalent steel truss element to replace the two component

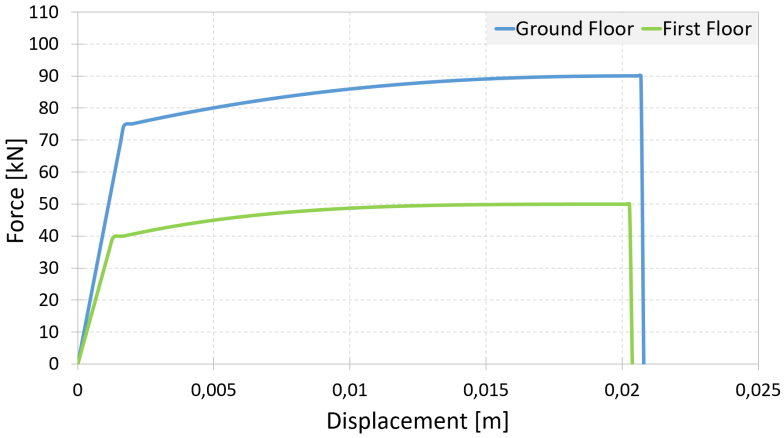

Figure 3.15: Force-displacement curve of the BRB and steel pipe set-up numerical pull-test

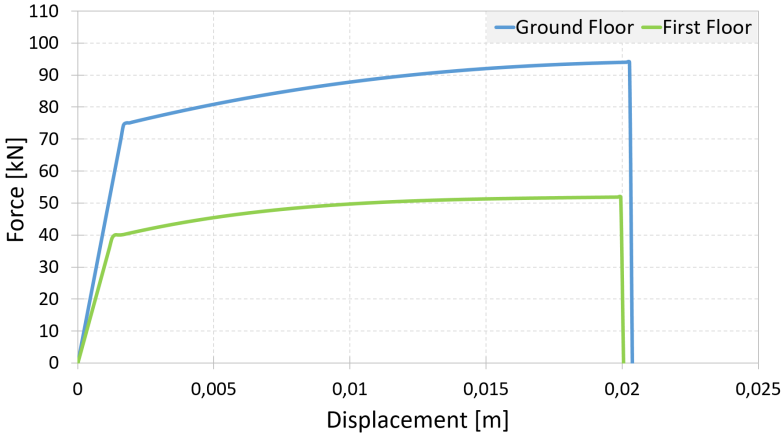

Figure 3.16: Force-displacement curve of the BRB and steel pipe set-up numerical compression test

set-up, maintaining the structural behaviour unaffected, Figure 3.17. The adopted cross-section diameter of the new equivalent steel element was the same as the structural pipe, 101.6mm, but a solid cross-section was considered instead of a hollow one. The mechanical properties of the steel were then altered so that the structural behaviour matches the one of the combined set-up. The steel mechanical properties assumed for the equivalent element are presented in Table 3.11 and 3.12, for the ground and first floor respectively.

In Figure 3.18 and 3.19 the force-displacement curves of the equivalent element's testing is presented along with the BRB-Pipe set-up. Comparing both curves it can be assumed that the equivalent steel element represents the BRB-Pipe set-up's behaviour precisely.

With the retrofitting devices properly calibrated, the next step was the validation of the retrofitted RC frame structure. Firstly, in order to validate the devices,

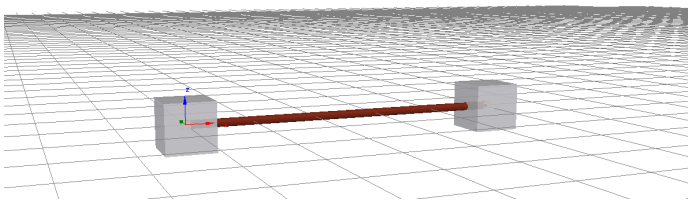

Figure 3.17: Numerical model of the equivalent single element model

Table 3.11: Steel mechanical properties implemented on the ground floor steel equivalent model model.

Modulus of elasticity [kPa]	2.0978×10^7
Yield stress [kPa]	9250.90
Stress at peak load [kPa]	11101.10
Strain at initiation of strain hardening curve [-]	0.00049
Strain at peak load [-]	0.005159
Strain of the intermediate point of the strain hardening curve [-]	0.002
Stress of the intermediate point of the strain hardening curve [kPa]	10375.40
Specific weight [kN/m^3]	78.00

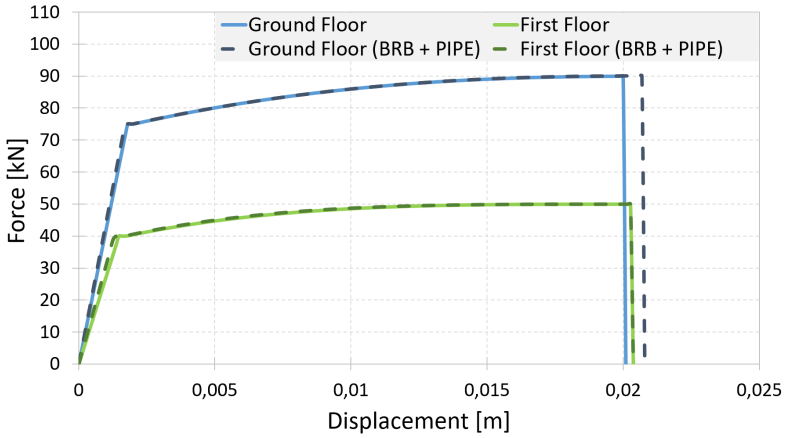

Figure 3.18: Force-displacement curve of the equivalent single element numerical pull-test

the retrofitting scheme adopted in the experimental protocol was recreated, and afterwards a new retrofitting solution is proposed.

Table 3.12: Steel mechanical properties implemented in the first floor steel equivalent model model.

Modulus of elasticity [kPa]	1.2923×10^7
Yield stress [kPa]	4934.20
Stress at peak load [kPa]	6167.75
Strain at initiation of strain hardening curve [-]	0.00045
Strain at peak load [-]	0.005264
Strain of the intermediate point of the strain hardening curve [-]	0.001
Stress of the intermediate point of the strain hardening curve [kPa]	5343.40
Specific weight [kN/m^3]	78.00

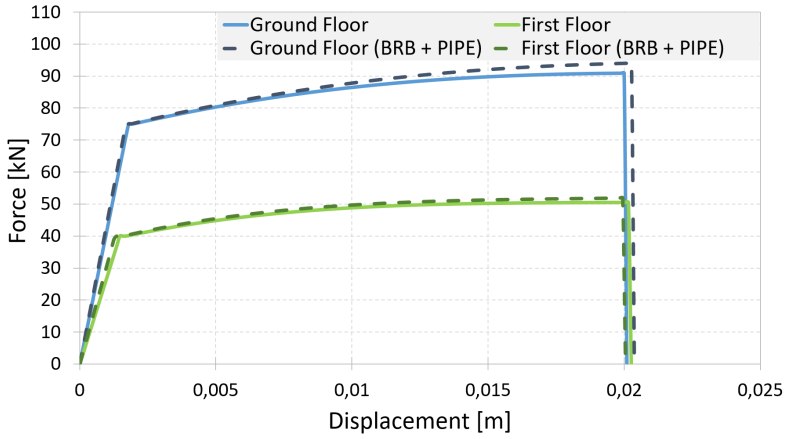

Figure 3.19: Force-displacement curve of the equivalent single element numerical compression test

Experimental Retrofitting Scheme Validation

In the experimental work by by L. Di Sarno and G. Manfredi [10] the RC structural frame was retrofitted in a single bay and single direction, Figure 3.20. Therefore, a numerical model with the previously calibrated equivalent element implemented as retrofitting was created, and an eigenvalue and pushover analysis were conducted in order to compare the numerical results with the experimental. In Table 3.13 a comparison of the frequencies of vibration between the real structure and the numerical model is presented. For the three first modes of vibration the relative error is bellow 3%, and for the three later modes the highest relative error is bellow 10%. Therefore, the results were considered acceptable.

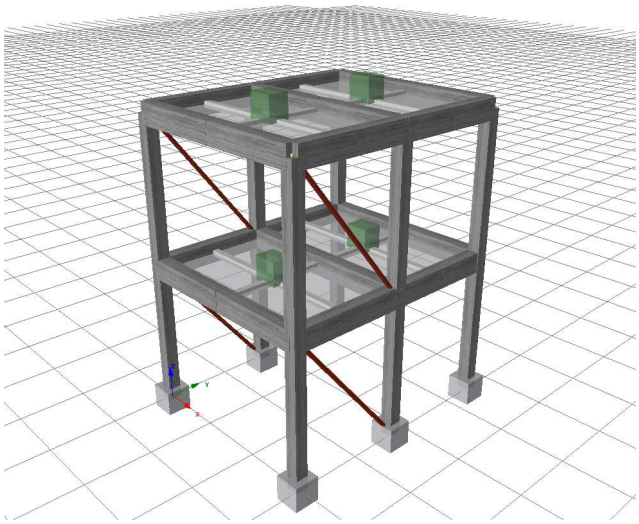

Figure 3.20: Experimental retrofitting scheme BRB distribution.

Table 3.13: Frequencies of vibration: Real Retrofitted Structure vs. Retrofitted Numerical Model

Mode	Real Structure [Hz]	Numerical Model [Hz]	Error [%]
1	3.15	3.157	0.233
2	3.30	3.261	1.183
3	4.84	4.695	2.989
4	8.76	8.280	5.484
5	9.25	8.383	9.369
6	12.94	12.046	6.908

As performed in the experimental campaign, in the numerical static pushover analysis the structure was pushed to 0.080m. In Figure 3.21 a comparison between the experimental and numerical curves of the retrofitted frame is presented.

From Figure 3.21 it can be observed that the behaviour of the numerical model is a sufficiently accurate representation of the real retrofitted RC frame, with a maximum of relative error below 8%.

After the verification and validation of the experimental retrofitting scheme a new approach was proposed for the numerical models retrofitting disposition.

New Retrofitting Scheme Proposition and Validation

The experimental campaign retrofitting scheme consisted of applying BRBs in a single direction and single bay of the the test structure. This originates an eccentricity between the structures centre of mass and centre of stiffness, resulting

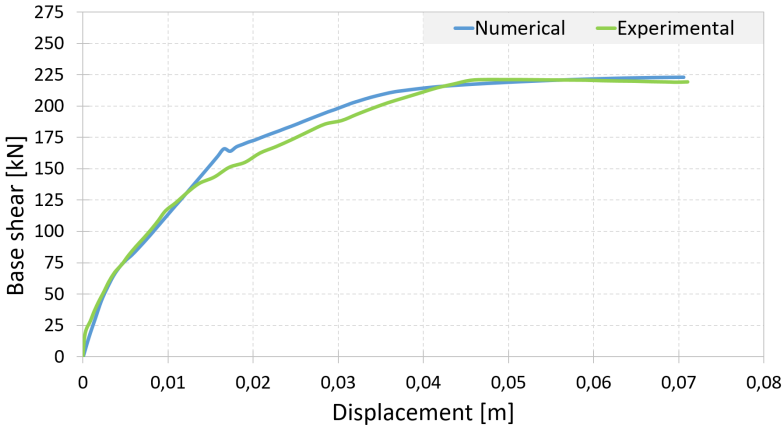

Figure 3.21: Comparison between the capacity curves of the real structure and the numerical model

on the arousal of torsional behaviours that can endanger the structure instead of improving it. With that in mind a new retrofitting scheme is proposed and validated.

The proposed scheme consists on not only applying BRBs in one direction but to both orthogonal directions, and in both longitudinal bays of the structure. The BRB cross section area was divided between both the longitudinal bays of the structure and the same total cross section area was applied in the orthogonal direction, Figure 3.22. This retrofitting scheme allowed to mitigate the torsional effects due to the eccentricity explained earlier.

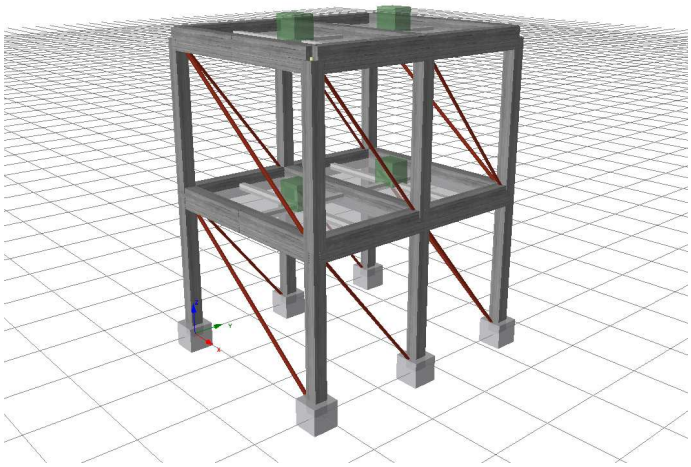

Figure 3.22: BRB frame brace distribution

In order to validate the retrofitting scheme both the eigenvalue and pushover analysis were performed to compare with the experimental retrofitting scheme. In Table 3.14 both the frequencies of vibration of the proposed retrofitting scheme and

experimental scheme are provided, along with the relative error between them.

Table 3.14: Frequencies of vibration: Experimental Retrofitting Scheme vs. Proposed Retrofitting Scheme

Mode	Experimental scheme [Hz]	Proposed scheme [Hz]	Difference [%]
1	3.157	3.119	1.205
2	3.261	3.221	1.222
3	4.695	4.567	2.735
4	8.280	8.152	1.551
5	8.383	8.255	1.531
6	12.046	11.645	3.330

In Figure 3.23 the comparison between the pushover curves of the real retrofitted structure, the numerical results of the experimental scheme and the numerical results of the proposed scheme is presented.

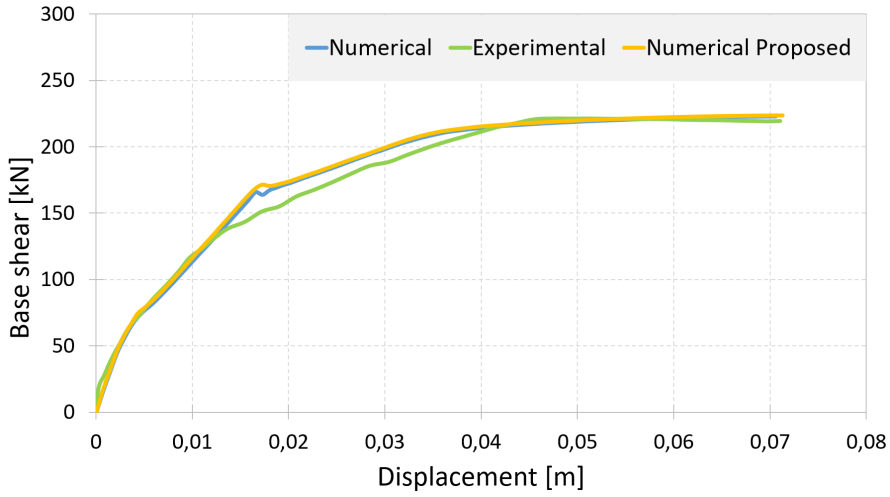

Figure 3.23: Comparison between the capacity curves of the real structure, the experimental numerical model and the proposed retrofitting scheme

Following what was carried out for the simple frame, a pushover analysis was also performed in the other orthogonal direction to assess if the capacity curve remained with a similar shape in both directions. In Figure 3.24 both the X direction and Y direction capacity curves are represented. It can be observed that the curves remain with similar shape, as it happened for the simple frame. Additionally, the pushover curves of the experimental scheme, in both directions, are also illustrated. By comparing both curves, it becomes obvious that, with the experimental scheme, the structure behaves distinctly for each of the orthogonal directions.

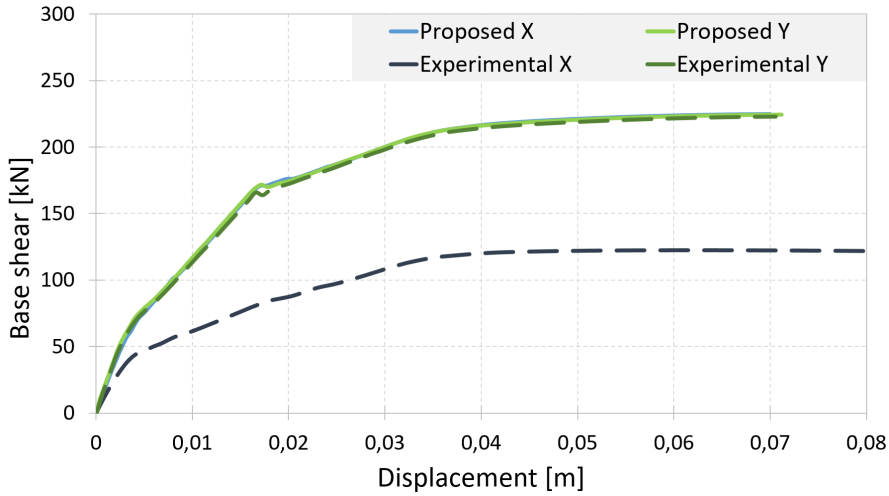

Figure 3.24: Comparison between the capacity curves of the proposed retrofitting scheme in both directions, X and Y.

Finally, the BRB Frame was deemed validated and was considered an accurate starting point for the development of the numerical models for the fragility study.

Chapter 4

Seismic Vulnerability Assessment

The response of RC structures under the effect of ground motions has always been a target of investigation, particularly in seismic prone regions. Moreover, the damage in buildings due to recent earthquakes has emphasized the need for risk assessment of the existing building stock to estimate the potential damage from future earthquakes. As such, seismic risk analysis of buildings is important, in order to identify the seismic vulnerability under the effect of potential seismic ground motions [85]. Therefore, a probabilistic methodology approach to seismic safety, based on vulnerability assessment, allows to quantify the collapse probability of a structure.

In the present chapter, a characterization of the seismic action is addressed, followed by the probabilistic variability of key parameters of the numerical model. Afterwords, the seismic vulnerability assessment of the three structures (Simple frame, BRB frame and CBF frame), along with all the procedures necessary, such as the incremental dynamic analysis (IDA) and fragility curves construction is presented.

4.1 Seismic Action

In order to perform the assessment of seismic vulnerability of the models, two distinct seismic scenarios were considered, both likely to occur in the Faro region, Portugal. These scenarios are related to the Marquês de Pombal fault (MPF) and the Ferradura fault (HF), both located in the Atlantic ocean, south-west of Cabo São Vicente, and historically responsible for severe earthquakes. A geographical map of both faults is presented in Figure 4.1

The numerical simulation of the seismic action was carried out, based on the stochastic non-stationary method considering finite fault effects, with the program RSSIM, developed in LNEC. This technique is particularly suitable for reproducing high frequency properties of strong ground motion [86]. The RSSIM is an integrating part of the seismic scenarios simulator LNECloss of LNEC [15].

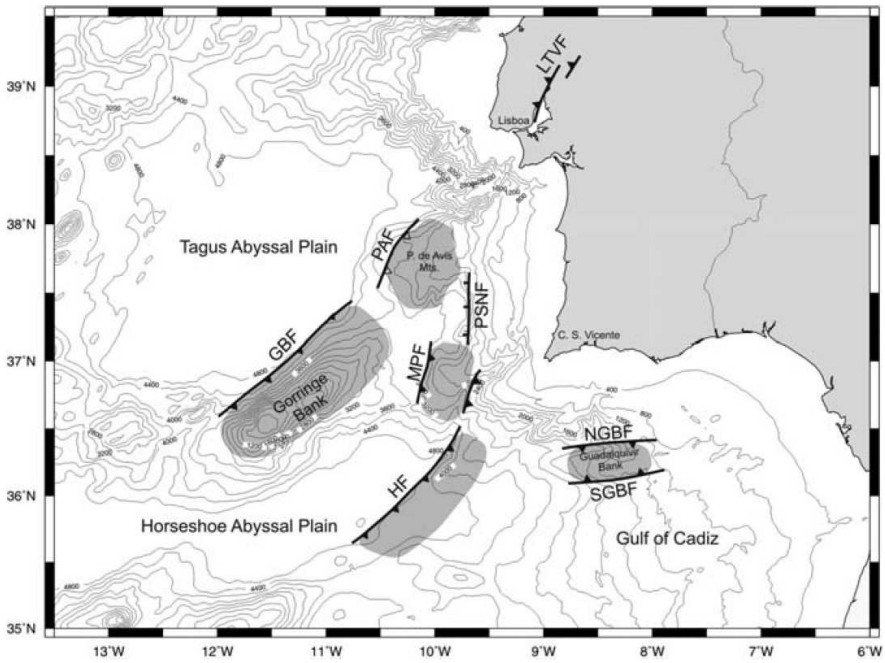

Figure 4.1: Major seismic zones in the SW of the Portuguese coast: GBF - Gorringe Bank Fault, PAF - Príncipes de Avis Fault, MPF - Marquês de Pombal Faut, HF - Horseshoe Fault, NGBF - Northern Guadalquivir Bank Fault, SGBF - Southern Guadalquivir Bank Fault, PSNF - Pereira de Sousa Normal Fault, LTVF - Lower Tagus Valley Fault [86].

LNECloss is an automatic calculus routine, integrated in a Geographic Information System, which allows to model the seismic action, building damage and, both economical and human losses for a specific seismic scenario defined by the user. The following parameters are to be imputed in the simulator by the user:

- Fault characteristics (fault starting location, length, width, incline, number of sub-faults along with its respective length, width,and starting location);
- Geographical coordinates of the location where the user wishes to preform the simulation;
- Magnitude of the desired simulated earthquake;
- Fourier spectrum function's parameters necessary for its calculations.

The effects of a large finite source may influence the amplitude, frequency and soil movement duration. For the modelling of a extensive source, the fault plane is subdivided in various sub faults, each one taken as a single point source. The ground motion at a given observation point is obtained by adding the contributions of all sub faults [15]. In Figure 4.2 this subdivision is illustrated.

The rupture propagation occurs radially from the hypocenter to the many sub elements and each sub elements contribution is afterwards added, considering

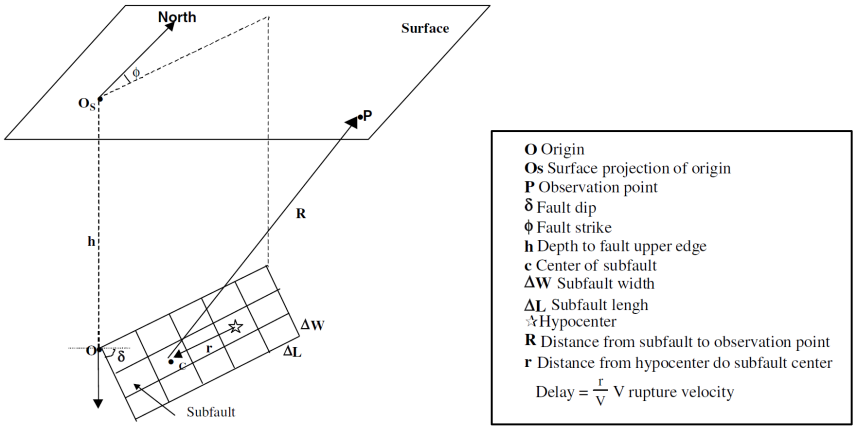

Figure 4.2: Finite-fault geometry [15]

a time delay in each element due to the fault rupture velocity (necessary time for the rupture to occur in the element, from the hypocentre) and the seismic waves propagation velocity in the considered propagation soil (propagation time of the seismic waves between the element and the receptor). A schematic explanation is pictured in Figure 4.3.

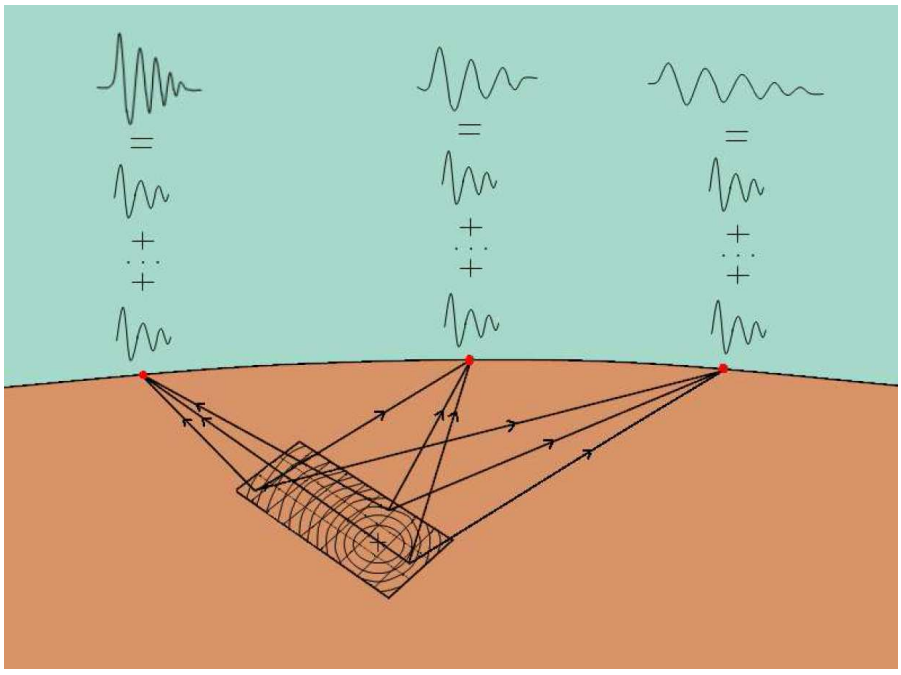

Figure 4.3: Schematic representation of the finite fault model [15]

Three rupture directions were considered for the earthquake simulation: North-South, South-Nort and random along the fault's extension. Magnitudes of M7.2 and M7.5 were considered for MPF, and M7.8 for the HF.

With the generated earthquakes, 50 seismic scenarios were assembled, with durations between 20.57 and 94.64 seconds. All the accelerograms were then scaled to a maximum acceleration of 1g, in order to be implemented in the FEM package for the incremental dynamic analysis (IDA). In Figure 4.4 and 4.5 two generated accelerograms are presented as example.

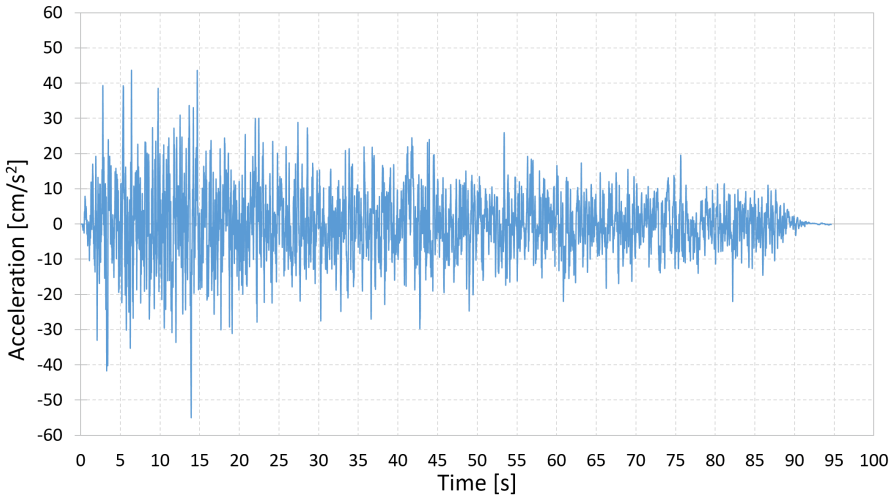

Figure 4.4: Faro HF M7.8 accelerogram

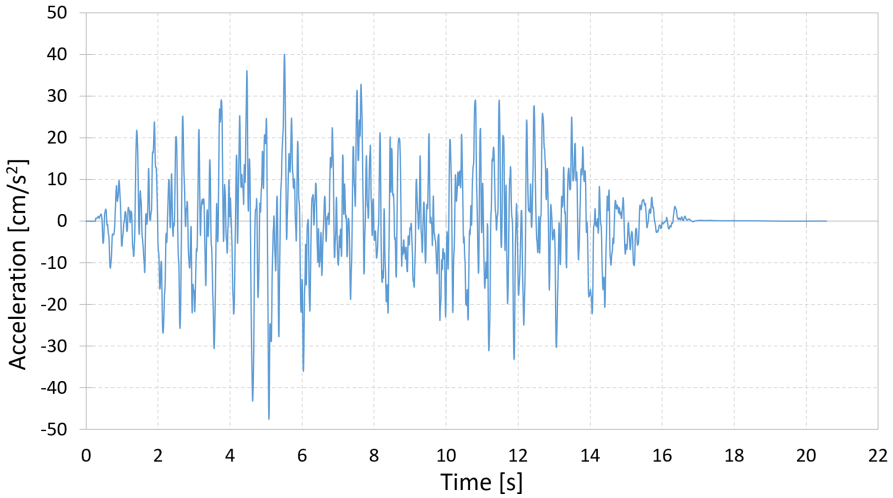

Figure 4.5: Faro MPF M7.2 accelerogram

4.2 Key Parameters Probabilistic Variability

4.2.1 Introduction

In general, the main focus for structural design lies on the response of structures to static and dynamic loading. However, the response to physical, chemical and

biological actions is also important as it may affect mechanical properties and general behaviour.

Since modelling is the art of reasonable simplification of reality such that the outcome is sufficiently explanatory and predictive in an engineering sense [16], models and values should follow from standardized tests, representing the actual environmental and loading conditions as good as possible.

For the classical building materials, knowledge about the various properties is generally available from past tests and experience. For new materials, models and values should be obtained from an extensive and properly defined testing program [16].

4.2.2 Material Properties

Material properties are defined as the resulting properties of material testing. Material specimens of defined size and conditioning, sampled according to given rules, subjected to an agreed testing procedure, the results of which are evaluated according to specified procedures.

The main mechanical behaviour characteristics are described by the stress-strain diagram. The modulus of elasticity and material strength represent the minimal characteristics necessary for structural design. Nonetheless, parameters such as: yield stress, limit of proportionality, strain at the rupture and strain at maximum stress are also relevant. The second to last parameter is a local phenomenon and may heavily depend on the shape and dimensions of the test specimen.

4.2.3 Uncertainties in Material Modelling

Material properties vary randomly in space, which means the strength from one geographical point in a structure to another is not the same. Besides spacial variations, the following uncertainties between the measured properties of the specimens and the properties of the real structure should be accounted for:

1. Systematic deviations identified in laboratory testing by relating the observed structural property to the predicted property, suggesting some bias in prediction.

2. Random deviations between the observed and predicted structural property, generally suggesting some lack of completeness in the variables considered in the model.

3. Uncertainties in the relation between the material incorporated in the structural sample and the corresponding material samples.

4. Different qualities of workmanship affecting the properties of (fictitious) material samples, for example when modelling the material supply as a supply of material samples.

5. The effect of different qualities of workmanship when incorporating the material in actual structures, not reflected in corresponding material samples.

6. Uncertainties related to alterations in time, predictable only by laboratory testing, field observations, among others.

4.2.4 Case Study Implementation

Due to the physical and mechanical uncertainties, the FE models were developed assuming, according to the JCSS model code [16], for some key parameters a probabilistic distribution. Those key parameters along with the assumed probabilistic distribution are presented in Table 4.1. The parameters distribution was performed using an automatic MatLab sequence, outputting random values following the desired distribution, means and standard deviation (SD).

Table 4.1: Probabilistic characterization of the key parameters

Key parameter	Distribution	Mean	SD	Units
Concrete's strength (f_c)	Lognormal	19.4	1.3	MPa
Concrete's mass density (ρ_c)	Normal	24	0.96	kN/m^3
Steel's yield strength (f_y)	Normal	341.4	12.6	MPa

Concrete's Compressive Strength

The probabilistic distribution for the concrete's compressive strength should follow a lognormal distribution considering the mean value the one applied to the calibrated numerical model and standard deviation defined in 4.1, according to [16]. Since crushing tests were performed on concrete specimens the expression 4.1 became unnecessary and the standard deviation value considered was the one obtained from the crushing tests.

$$\sigma = s' \cdot \sqrt{\frac{n}{n'-1} \cdot \frac{v'}{v'-2}} \tag{4.1}$$

Concrete's Mass Density

The self weight of a structure combines both the weight of structural and non-structural components. The main characteristics of the self weight can be described as follows:

- The probability of occurrence at an arbitrary point-in-time is close to one;
- The variability with time is normally negligible;
- The uncertainties of the magnitude is normally small in comparison with other kinds of loads.

Concerning the uncertainties one can distinguish between:

- Variability within a structural part;
- Variability between different structural parts of the same structure;
- Variability between various structures.

The variabilities within a structural part are normally small and can be often neglected. However, for the concrete's mass density a normal distribution was assumed with a 25 kN/m^3 mean value and a variation coefficient of 0.03, according to [16].

Steel's Yield Strength

Reinforcing steel is generally classified and produced according to grades related with a specified yield stress limit, for example S300, S400 and S500. However, the structure's rebars employ a not graded steel. Therefore, and according to [16], a normal distribution was assumed with a 341,4MPa mean value and SD of 12,6MPa resulting from performed pull tests. The parameters distribution is presented in Figure 4.6.

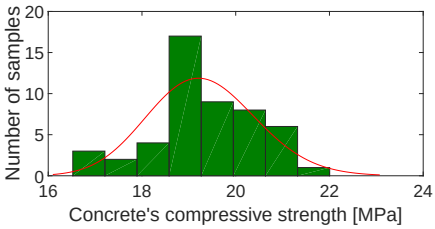

(a) Concrete compression strength

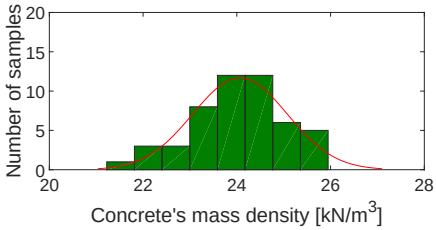

(b) Concrete density

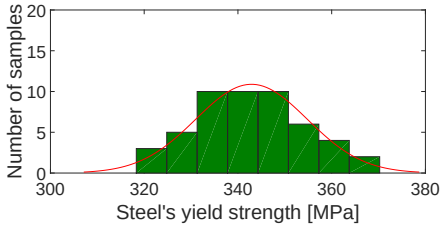

(c) Steel rebars yield strength

Figure 4.6: Parameters probabilistic distributions

Sample Space

One parameter that is key in a statistical analysis is the dimension of the sample space. The number of samples is important to know the beneficial process time to reliability of results ratio. Bigger sample spaces leads to more reliable results but to higher processing/analysis time. On the other hand smaller sample spaces demand less analysis work but lead to lower confidence in results.

In order to know if a 50 sample space was suitable to produce statistically reliable results, a study of the relative error evolution of the standard deviation was conducted throughout the sample space. In Figure 4.7 and 4.8 one can observe that the SD stabilized in values close to the ones initially defined as the sample space increased, and that the relative error dropped below 1 % when the 50 samples mark was reached, which deems the sample space fitting and the results as statistically reliable.

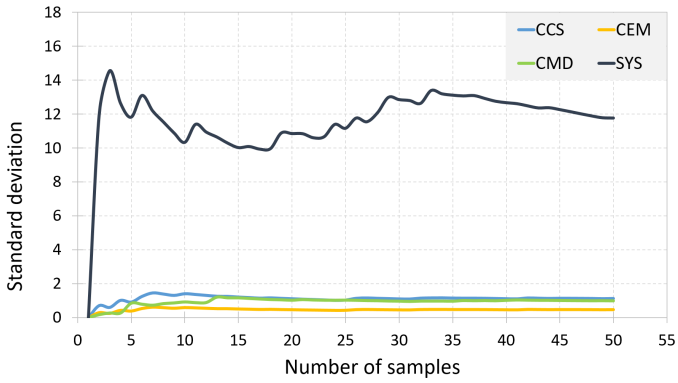

Figure 4.7: Standard deviation's evolution throughout the sample space

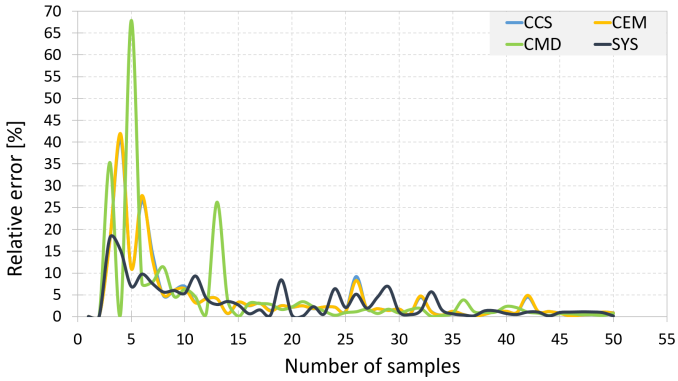

Figure 4.8: Relative error of the standard deviation's evolution throughout the sample space

Therefore, 50 samples of the RC frame were developed for each retrofitting scheme (simple frame, BRB frame and CBF frame), following the variation of the generated parameters. Considering the seismic scenarios described before, the accelerograms were associated to each of the 50 FE model samples and incremental dynamic analyses were performed in order to build the associated fragility curves and assess the seismic vulnerability of the samples.

4.3 Incremental Dynamic Analysis

The Incremental Dynamic Analysis (IDA) is a parametric analysis method that allows to estimate thoroughly structural performance under seismic loads [87]. Basically, in a IDA analysis the structure is subjected to a series of ground motion nonlinear time-history analysis of increasing intensity. The maximum values of top displacement are then plotted against their base shear counterparts, for each of the dynamic runs, yielding the so called dynamic pushover or IDA envelope curves.

This type of analysis served as a baseline for the development of the present work, allowing to develop the fragility curves.

4.3.1 Basic Principles and Scope

The IDA has been increasingly gaining more importance, being considered as a thorough methodology for the structural performance of buildings under seismic actions [86]. The IDA is a parametric analysis method that allows to estimate thoroughly structural performance under seismic loads [87]. To preform an IDA, a ground motion acceleration record, representative of the magnitude and source characteristics that dominate the hazard at the desired exceedance probability is selected. The ground motion is then scaled to various levels of intensity, sufficiently low such that the structure's response is linear, and incrementally increasing until either structural instability is achieved or the predicted drift demand is very large [88]. In 2000 the IDA was established as the state-of-the art method to determine the global collapse capacity by the U.S. Federal Emergency Management Agency (FEMA) guidelines. The use of the IDA is now a widely applicable method and some of its objectives include [87]:

- extensive understanding of the relations between the range of response or demands and the range of potential levels of a ground motion record;
- further understanding of the structural impact of higher intensity and least common ground motions;
- better understanding of the structural response variations as the ground motion intensity increases;
- allow to estimate the global structural system's dynamic capacity;
- study the variation of the previous items from one ground motion to record to another, understanding how stable, or unstable, they are.

4.3.2 Concepts and Fundamentals

To understand the methodology behind the IDA it is important to plainly define some fundamental concepts.

A Scale Factor (SF) in the IDA context is the non-negative scalar, $\lambda \in [0, +\infty[$, that originates a_λ when multiplied to the original acceleration time-history a_1. The SF

is basically a one-to-one mapping from the original accelerogram to all its scaled images. It is then obvious that if $\lambda < 1$ the original accelerogram is scaled-down, if $\lambda > 1$ it is scaled-up and for a value of $\lambda = 1$ the original accelerogram remains the same. Even though the SF is a simple way to characterize the scaled images of an acceleration time-history, it conveys no information regarding the intensity of the scaled accelerogram and its effect on a given structure. So there is the need to define a effective way to measure the "'intensity"' of an accelerogram.

Some of the quantities used to characterize a ground motion record's intensity, such as the Modified Mercalli Intensity Scale, the Moment Magnitude Scale and even the duration; are difficult to scale and are deemed as non-scalable. Therefore, the most common examples of scalable Intensity Measures (IM) used are the Peak Ground Acceleration (PGA), Peak Ground Velocity, the $\zeta = 5\%$ damped Spectral Acceleration at the structure's first period ($S_a(T_1, 5\%)$), and the normalized factor R = λ/λ_{yield} (whith λ_{yield} being the lowest scaling needed to cause yielding for a given record and structural model). After defining the intensity measure, a way to monitor the structure's "'state"' and seismic response is needed.

The Damage Measure (DM) is an observable quantity deductible from the output of the corresponding non-linear dynamic analysis. Its suitable selection depends on the application and the structure itself. Some suitable choices could be maximum base shear, peak roof drift, peak storey ductilities, node rotations, floor peak interstorey drift angles and various proposed damage indices, for example the global cumulative hysteretic energy. Once the IDA is performed the output is presented in the form of dynamic pushover curves. It is not possible to retrieve a thorough assessment of the structural response from the outputted curves, but extremely useful information can be extracted, such as the transition from linear to non-linear states, structural response degradation and the structure's collapse. Therefore, to properly assess the structure's performance it is important to preform some adequate processing of the data through the IDA curves. As such performance levels or limit-states are important pieces in performance-based earthquake engineering, and the key to assess them is present in the IDA curve. However, it is needed to define them in a objectively manner that makes sense in the IDA curve context, i.e. by establishing rules or statements that when reached or satisfied, signals reaching a limit-state. According to Vamvatsikos and Cornell [87] there are two basic rules to define a limit-state: A DM-based rule and a IM-based rule. The underlying concept of the first is that the DM is a damage indicator, therefore, when it surpasses a certain value the structural model is assumed to be in the limit-state. The limit-state values can be obtained through past experiments, engineering experience or theory. The concept is to identify when the defined limit-states are surpassed starting from the least severe all the way to the most severe. The IM-based rule consists of having a single point on the IDA curve that clearly divides the non-collapse region from the collapse region.

Although the IM-based rule provides a distinct barrier between the collapse and the non-collapse area it is only relevant when exists the need to better assess collapse capacity. Furthermore, there is the obstacle of prescribing a value that

defines collapse consistently for all IDA curves. Consequentially, and due to the its simplicity, ease of implementation and the ability to provide information about the structure across various behaviour phases the DM-based rule was adopted in the present work. In the presence of multiple IDA curves it is of extreme importance an adequate statistical approach in order to allow a proper discussion and evaluation of the results [87].

4.3.3 IDA Procedure and Application

In an Incremental Dynamic Analysis a series of time-history analysis are performed, each one more intense than the previous. In order to preform a single IDA the following steps must be completed:

- Definition of a suitable seismic scenario;
- Selection of a suitable and scalable IM;
- Selection of a suitable DM;
- Definition of a SF to be applied to the IM;
- Execution of the IDAs according to the defined SF;
- Evaluation of the Damage States (DS).

In the present work the numerical models were submitted to a series of accelerograms in which the PGA was incremented in steps of 0.05 g starting from a low elastic response, 0.05g, until either the collapse or numerical instability was reached, always controlling if at least 50% of the FE models collapsed. 150 IDAs were performed (50 for the Simple Frame, 50 for the BRB Frame and 50 for the CBF Frame), corresponding to around 2000 time-history analysis and 300 IDA curves, one for both x and y directions. Afterwards, these IDA curves are used to define the Damage States in order to obtain the structure's fragility curves. In Figure 4.9 an example of an IDA curve and the damage states is presented.

4.4 Damage States

All structures are vulnerable to damage during a ground motion solicitation. The quantification of that damage is of utmost importance and damage indices are used to predict possible damage occurrence. Firstly, DS were used to assess the seismic intensity of a defined area after a seismic event, however, the use has extended to post earthquake damage assessment, structural vulnerability assessment, loss estimation and rehabilitation/retrofitting of structures. DS allow for the assessment of a building's damage and provides a categorization of structural damage from an undamaged state through to a complete damaged or collapse state, providing understanding of de building's condition post-earthquake [89].

4.4.1 Procedure and Application to the Case Study

Five damage states were considered in the present work, according to previous works [90, 91]: DS_0 - None, DS_1 - Slight, DS_2 - Moderate, DS_3 - Extensive and DS_4 - Complete/Collapse.

Their definition was conducted according to Vargas [17], by means of a simplified bilinear representation of the IDA curves, relying on the yield displacement (D_y) and ultimate displacement (D_u). In Table 4.2 the damage states definition is presented.

Table 4.2: Damage states definition

Damage states
$DS_1 = 0.7 \cdot D_y$
$DS_2 = D_y$
$DS_3 = D_y + 0.25 \cdot (D_u - D_y)$
$DS_4 = D_u$

The simplified bilinear representation of the IDA curve is obtained by ensuring that the areas below and above the curve remain equal and the ultimate displacement is considered when there is a drop of 20% from the maximum base shear [17], as pictured in Figure 4.9.

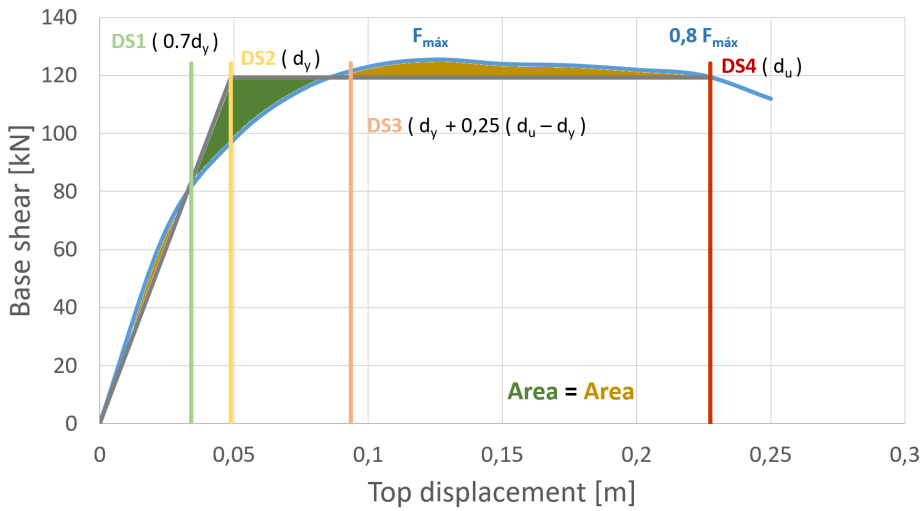

Figure 4.9: Bilinear representation of the IDA curve and associated damage states

The damage state's displacement threshold values along with the bilinearized yield force for each IDA curve are presented in Figure 4.10 for the Simple, BRB and CBF Frame. It can be observed that, as the damage states get heavier, the more dispersed are the points, revealing that uncertainties increase with the non linearity of the structural behaviour.

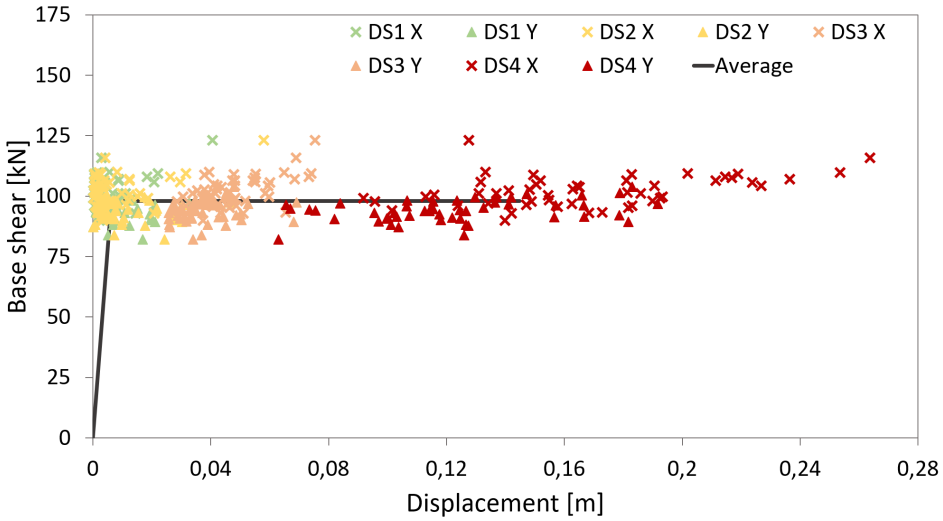

(a) Simple Frame

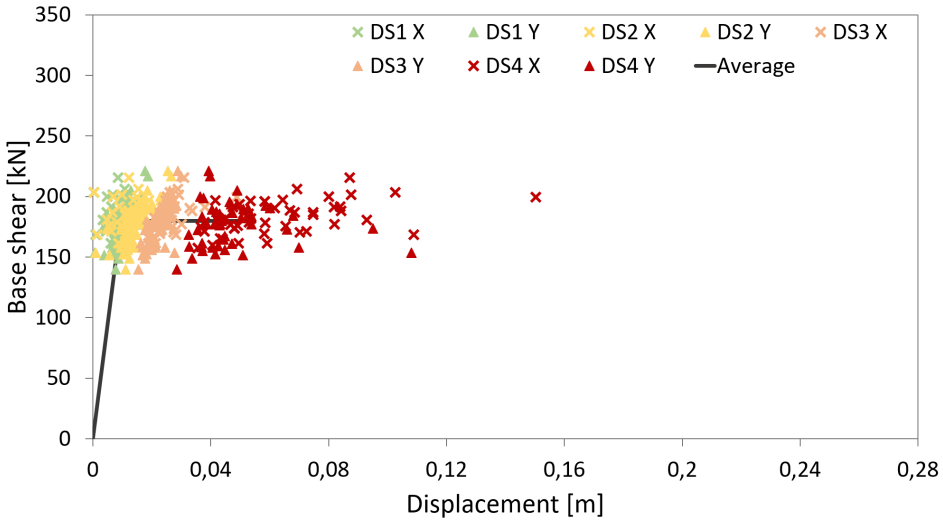

(b) BRB Frame

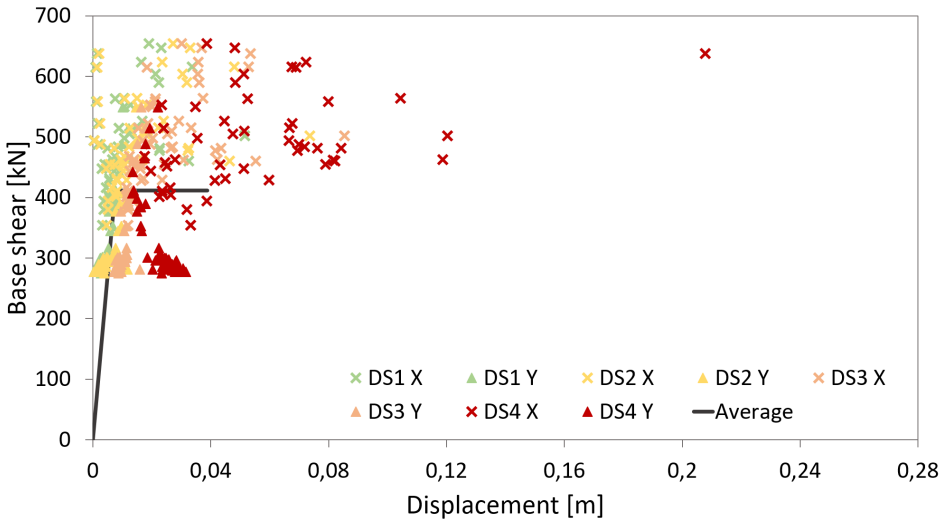

(c) CBF Frame

Figure 4.10: Damage state's threshold values obtained from the bilinearization of the IDA curves

4.5 Fragility Curves

4.5.1 Introduction and Background

For the proper development of a seismic risk analysis of a structural system it is imperative to identify the seismic vulnerability of component structures associated with various states of damage. The vulnerability assessment by means fo fragility curves is a widely practised approach when the information is to be developed accounting for a multiple of uncertain sources involved, for example, in seismic hazard estimation, structural characteristics, soil-structure interaction, and site conditions [92]. The vulnerability of a given structure can be described using vulnerability functions and/or fragility functions. Vulnerability functions express the probability of losses for a given ground motion level, such as social losses or economical losses, whereas fragility functions describe the probability of exceeding different limit states for a given ground motion level, such as damage or injury levels. A vulnerability function relates the level of ground motion with the mean damage ratio, a fragility function relates the level of ground motion with the probability of exceeding the limit states [93]. Figure 4.11 displays examples of both functions. Vulnerability function can be obtained from fragility ones by applying consequence functions, which describe the probability of loss, conditional on the damage state.

Fragility curves relate the seismic intensity to the probability of reaching or exceeding a damage level for each element at risk, which makes them a key component in seismic risk assessment. The ground motion level can be quantified using different earthquake intensity parameters, such as PGA, peak ground velocity (PGV), peak ground displacement (PGD), spectral acceleration, spectral velocity or spectral displacement. Fragility curves are often described by a lognormal probability distribution function as in Equation 4.2 [93].

$$P_f(ds \geq ds_i \mid IM) = \Phi\left[\frac{1}{\beta_{tot}} \cdot ln\left(\frac{IM}{IM_{mi}}\right)\right] \tag{4.2}$$

where $P_f()$ is the probability of being present or exceeding a particular DS, for a given seismic intensity level defined by the earthquake IM, Φ is the standard cumulative probability function, IM_{mi} is the median threshold value of the earthquake IM required to cause the i_{th} DS and β_{tot} is the total standard deviation. Therefore, the use of equation 4.2 to develop fragility curves requires the definition of both the IM_{mi} and β_{tot} parameters.

4.5.2 Fragility Curves Development

In order to develop fragility curves one can resort to several approaches, usually grouped under: empirical, judgemental, analytical and hybrid. The empirical ones are based on past earthquake surveys and, as such, are specific of a particular geographic location, as they are derived from actual seismo-tectonic and geotechnical conditions, as well as the properties of the damaged structure. Judgemental fragility curves are build through expert's opinion and experience and

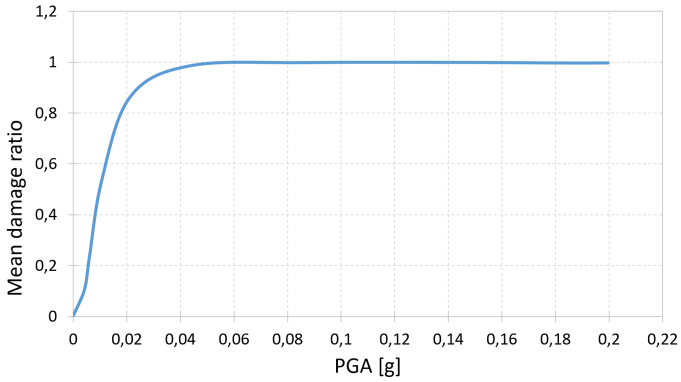

(a) Vulnerability function

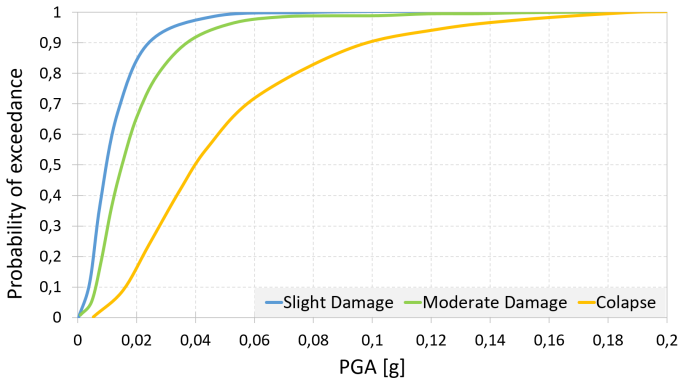

(b) Fragility function

Figure 4.11: Examples of vulnerability and fragility functions

are versatile and relatively swift to derive. However, since they depend on the level of experience of the experts consulted, their reliability is questionable [93]. In the analytical fragility curves the adopted damage distributions, simulated from the analysis of the structural models under increasing ground motions loads, serve as their statistical basis. Therefore, they result in a reduced bias and augmented reliability in the vulnerability estimation for different structures when compared to a judgemental approach. Due to computation evolution analytical approaches to vulnerability curves generation are becoming ever more attractive in terms of ease and efficiency by which data can be generated [94].

4.5.3 Typology

Apart from the inherent uncertainties the principal assumption in the vulnerability assessment of structures is that structures having similar structural characteristics, being in similar geotechnical conditions, are expected to preform in the same way for a given seismic loading. Therefore, the damage is directly related to structural properties of the risk exposed elements. Typology is thus a fundamental descriptor of a system , derived from the inventory of each element. Among some typical typology descriptors/parameters are geometry, material properties, morphological

features, age, seismic design level, anchorage of equipment, soil conditions and foundations details [95].

One of the main challenges when preforming a seismic risk assessment is the knowledge of the inventory of a specific structure in a region and the ability to create classes of structural types, for example with respect to material, geometry and seismic design level. Therefore, the first step should be the creation of a reasonable taxonomy that is able to classify the different kinds of structures in the system [93].

4.5.4 Intensity Measures

A careful and discerning selection of a IM that characterizes the ground motion and best correlates with the element's response if of extreme importance in the derivation of fragility curves. Different characteristics of the motion may be described by different IMs, ones being more unfavourable to the structure or system under analysis. Therefore, in seismic risk analysis, the use of a specific IM should be guided by the extent to which the measure corresponds to damage to local elements of a system or the global system itself.

Intensity measures can be grouped in two main classes: empirical intensity measures and instrumental intensity measures [93]. The former, resorts to macroseismic scales to identify the observed effects of ground motion over a limited area. The latter, relies on an analytical value measured by an instrument or computed by analysis of recorded accelerograms, to express the severity of a ground motion.

The approach followed for the derivation of the fragility curves and the typology of the element at risk also influences the selection of the intensity parameter. For example, for the derivation of empirical fragility curves, a good IM would be PGA, PGV or spectral acceleration, since empirical curves use actual records of seismic ground motions to describe the seismic intensity [96]. On the other hand, when ground failure is key to assess a element's vulnerability (soil liquefaction, fault rupture, landslides) permanent ground deformation is the most appropriate IM [93].

4.5.5 Uncertainties Consideration

It is necessary to consider some uncertainties in the fragility curves parameters, as well as in the relationship between the physical damage state and the performance of the element at risk. These uncertainties can be categorized as aleatory or epistemic. Aleatory uncertainties are related to the intrinsic randomness of a phenomenon. The epistemic uncertainty is caused by lack of knowledge or scarce data. This distinction is needed, within an engineering analysis model, solely because the lack-of-knowledge part of the uncertainty can be represented in the model by auxiliary non-physical variables, allowing to capture information obtained from more data gathering and more advanced scientific principles [97].

Generally, the fragility parameter's uncertainty is estimated through the standard deviation, β_{tot}, which describes the total variability for each fragility curve [93]. According to [98], three sources of uncertainties are usually considered: the damage state's definition (β_{DS}), the response and resistance capacity of the element (β_C) and the earthquake input motion (β_D). Assuming these three contributors are stochastically independent and lognormally distributed random variables, the total variability can by modelled by their combination, as shown in 4.3.

$$\beta_{tot} = \sqrt{\beta_{DS}^2 + \beta_C^2 + \beta_D^2} \tag{4.3}$$

4.5.6 Fragility Curves Deriving Methods

Introduction

The development of fragility curves/functions in the field of seismic engineering can be done based in different methods, classified in four generic groups [93]:

- Empirical curves;
- Expert-opinion-based curves;
- Analytical curves;
- Hybrid curves.

A brief overview of these four groups is provided in the following sections, along with an assessment of their advantages and disadvantages.

Empirical Methods

The study of field surveys of actual damage in buildings after a seismic event and the study of the seismic events themselves allows to compile extensive statistics on the damage states of different typology under ground motion loading, serving as base for the empirical curves and functions [93]. With data from 50.000 Italian buildings, Sabetta et al. [99] developed empirical fragility curves where, converted from the observed macroseismic intensity, the PGA and spectral response parameters are used to express the probability of exceeding a damage state. Rossetto and Elnashai [94] developed empirical functions for various typologies of RC buildings based on data from 340.000 buildings exposed to 19 earthquakes.

The main advantage of empirical methods is the fact that their based in real observational data, as such all detail of the exposed stock are taken into account as well as soil-structure interaction effects, topography, lithological site effects and the variability in the structural capacity of a group of buildings. However, their advantages limit their application potential. Even though the observational data renders a more realistic approach it remains specific of a given area with particular conditions, earthquake parameters and structural capacity of the building's stock. Another drawback is the low frequency of large magnitude earthquakes events

near densely populated areas and, as a result, the observational data used to curve generation tend to be scarce and highly clustered in the low ground motion intensity range. The rapid execution of the post-earthquake surveys and the use of poorly defined damage scales from engineers also introduce some uncertainties in the statistics[93, 94].

Analytical Methods

Analytical methods adopt damage distribution estimations obtained through numerical simulation of the structure's response to seismic action. Two methods can be employed depending on the considered representation of the seismic input: Static methods, with the seismic input represented by a response spectrum, and dynamic methods, where an acceleration time-history represents the seismic input [93].

A proper representation of the non-linear behaviour and stiffness of the structure is of paramount importance, although a balanced compromise between the model's representation accuracy and cost-efficiency must be considered. So the choice of the proper representation becomes somewhat important: plastic hinge modelling (concentrated plasticity) vs. fibre element modelling (distributed plasticity) and 2D representation vs. 3D representation.

Another distinction can be made between direct methods, in which the fragility curve are functions of ground motion intensity measure types (PGA, PGV and $S_a(T)$) and indirect ones, that estimate the damage probability with respect to structural response parameters [93].

Dynamic Analysis

As implied, this method relies in numerous non-linear dynamic analyses of a numerical structural models with a series of acceleration time-histories. The fragility curves are then developed considering various statistical procedures, which make them directly applicable to a seismic scenario. Rossetto and Elnashai [100] developed fragility curves for RC building with 3 storeys and infill walls, by introducing uncertainties in the mechanical properties of the concrete, steel and masonry. More recently, Perdigão [86] developed fragility curves for a pre-cast, three span concrete footbridge with uncertainties introduced in the mechanical properties of the concrete, steel, structure's age and structural behaviour of the beam-column connection's steel dowels.

Contrary to what happens with specific buildings, when fragility curves are developed for a typology or a class of buildings it is necessary to account for a large variability in the structural response. Therefore, uncertainties should be considered in [93]:

- the mechanical properties: by introducing these uncertainties the variability in the construction techniques and material quality is taken into account, for

example the amount of reinforcement in RC frames, concrete type, among others;

- morphological and geometrical properties: for a proper representation of a given building typology a whole range o possibilities must be taken into account, as such one must model several models that cover the whole typology in terms of, for example, plan dimensions, number of storeys, wall openings, irregularities, and so forth.

As it could be expected, in order to cover a given typology correctly, the number of models to analyse can grow dramatically, leading to a significant amount of dynamic analyses.

For some road elements, like tunnels and bridges, dynamic analysis are often used to derive fragility functions, since static procedures, such as pushover approaches, are less adapted to these type of components [93].

Another key issue in this approach lies in the choice of the ground motion records. The fragility parameters, both standard deviation and median, are greatly influenced by the quality and distribution of intensity measures in the record samples. Usually, the studied typology is restricted to a given geographical area and, based on specific intervals of magnitude, source-to-site distance, and other scenario characteristics, such as focal depth and mechanism, it is possible to select adequate time-histories [93].

Although the fragility curves derived by using dynamic analysis involve relatively large efforts, they are able to reproduce the seismic response of elements more accurately. Furthermore, the use of complete time-histories, instead of its spectral representations, can lead to the development of fragility models based on a wider range of ground motion parameters and vector-valued parameters [101].

Capacity Spectrum Method

The vulnerability assessment of an element using mechanical models and capacity curves is fully described both in the HAZUS methodology [98] and the Risk-UE Level 2 approach [102], where each typology is defined by a bilinear representation of the capacity curve obtained through a static pushover analysis [93].

The resulting capacity curves, expressed in the spectral acceleration and spectral displacement space domain, are used to get the performance point of the structural element and deduce the spectral displacement, which corresponds to a given damage level. With the associated uncertainties, the spectral displacement, S_d, that defines the threshold of a given damage state, DS, is assumed to be distributed by:

$$S_d = \overline{S_d}_{,DS} \cdot \varepsilon_{DS} \tag{4.4}$$

where:

- $\overline{S_d}_{,DS}$ is the median value of S_d of damage state, DS;
- and ε_{DS} is a lognormally distributed variable with standard deviation β_{DS}.

The probability of reaching or exceeding a damage state d_s, of a building of a given typology, can be expressed as a cumulative lognormal function with respect to the spectral displacement at the performance point [93]:

$$P\left[DS|S_d\right] = \Phi\left[\frac{1}{\beta_{DS}} \cdot ln\left(\frac{S_d}{\overline{S_d}_{,DS}}\right)\right] \tag{4.5}$$

and the probability values for each damage state are given by:

$$P(D_0) = 1 - P\left[d_{s_1}|S_d\right] \tag{4.6}$$

$$P(D_k) = P\left[d_{s_k}|S_d\right] - P\left[d_{s_{k+1}}|S_d\right] \tag{4.7}$$

$$P(D_4) = P\left[d_{s_4}|S_d\right] \tag{4.8}$$

with k = 1, 2 and 3.

In the HAZUS methodology 36 building typologies are contemplated, identified with the structural type and height class. Each of the contemplated typologies are associated with various tabulated characteristics, such as the true elastic fundamental-mode period of the building, T_e, the typical roof height, h, among others.

Inter-story drift ratios are used to define the damage states, relying in four threshold values, Δ_{DS}, for the slight, moderate, extensive and complete damage states. The median S_d value corresponding to the damage state DS can be obtained from the drift threshold value, through the equation 4.9 [93].

$$\overline{S_d}_{,DS} = \Delta_{DS} \cdot \alpha_2 \cdot h \tag{4.9}$$

The variability of a fragility curve is represented by the standard deviation, β_{DS}, which is obtained by the convolution between the standard deviation accounting for the variability of the capacity curve, β_C, and the standard deviation describing the variability of the seismic demand, β_D, combined with the uncertainty on the definition of the damage state threshold, $\beta_{M(DS)}$:

$$\beta_{DS} = \sqrt{(CONV\left[\beta_C, \beta_D\right])^2 + (\beta_{M(DS)})^2} \tag{4.10}$$

The same main steps applied to the HAZUS procedure are applied to the Risk-UE Level 2 approach [93]:

- typological classification of elements;
- development of capacity curves;
- determination of the performance point based on the seismic level;

- assessment of the probabilities to reach or exceed the different damage states.

In the Risk-UE method the inter-story drift ratios are identified based on the capacity curve, which makes them structures specific, as opposed to the HAZUS method where fixed values are recommended for each typology. Table 4.3 presents the threshold values for each damage state, as a function of yielding and ultimate capacity points.

Table 4.3: Threshold values of the damage states according to the Risk-UE approach (adapted from [102])

Damage Grade	Damage Definition	Drift Limit	Spectral Displacement Limit
$DS0$	No damage	$\Delta < 0.7\Delta_y$	$D < 0.7D_y$
$DS1$	Sight	$0.7\Delta_y < \Delta < 0.7\Delta_y + 0.05\Delta_{uy}$	$0.7D_y < D < D_y$
$DS2$	Moderate	$0.7\Delta_y + 0.05\Delta_{uy} < \Delta < 0.7\Delta_y + 0.2\Delta_{uy}$	$D_y < D < D_y + D_{uy}$
$DS3$	Extensive	$0.7\Delta_y + 0.2\Delta_{uy} < \Delta < 0.7\Delta_y + 0.5\Delta_{uy}$	$D_y + D_{uy} \leq D_u$
$DS4$	Very heavy	$0.7\Delta_y + 0.5\Delta_{uy} < \Delta < 0.7\Delta_y + 1.0\Delta_{uy}$	$D_u \leq D$
With: $\Delta_{uy} = 0.9\Delta_u - 0.7\Delta_y$ and $D_{uy} = 0.25(D_u - D_y)$			

Nonlinear static analysis can also be used to generate fragility curves that do not necessarily rely on the structural response parameter, by using the response spectrum to associate each estimated performance point with the equivalent intensity measure of the seismic records that are used [98]. This means that the damage probability can be directly estimated through the fragility curves, without going through the capacity curve.

Expert Judgement

In this procedure the estimation of the mean loss or the probability of damage of a given element under different levels of seismic loading is obtained by the judgement of field experts [93].

The main advantage of this technique is the fact that it is not affected by the lack of extensive damage data or the reliability of the structural model used in the analytical procedures. However, the result's quality is directly proportional to the experience revealed by the consulted experts. As such, by consulting a large number of experts and assigning some weigth to their contributions based on their expertise level, the potential bias of the curves can be reduced [103].

Hybrid Methods

As the name implies, hybrid fragility curves result from the combination of two or more of the previous methods, for example using both analytical and observational data, or complemented by expert judgement. The main advantage is the ability to compensate both the subjectivity of expert opinion and the lack of observational

data for the structural model's deficiencies. With this approach analytical fragility curves can be updated and improved by integrating post.seismic observations. This allows to calibrate the analytical results or to compensate some scarce data at high seismic levels [104].

4.6 Results and Comparison

The fragility curves presented in this section are the result of 150 incremental dynamic analysis, resulting in more than 1000 hours of numerical simulation developed in the FE package SeismoStruct, and the analysis of 300 IDA curves and respective damage states. The IDA results were addressed in both directions of the RC structure for the three numerical models. As such, three sets of fragility curves were developed per numerical model, in the X direction, in the Y direction and a combination of both directions, all expressed in regards to PGA. As mentioned before, the X and Y directions are defined and illustrated in Figure 3.4.

Starting with the simple frame, in Figure 4.12 the fragility curves in both directions is presented.

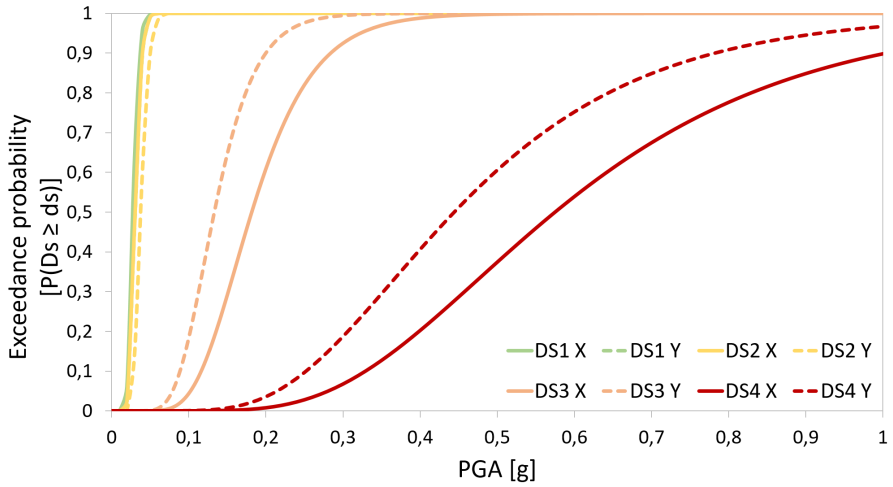

Figure 4.12: Simple frame fragility curves in both directions, X and Y

Crossing both damage states form each orthogonal direction and choosing the worst case scenario the global fragility curves were yielded. The global fragility curves of the simple frame, regardless of the direction, are pictured in Figure 4.13. The 0.3 PGA level is highlighted in Figure4.13, this level is the project PGA level, assuming the test structure to be located in Faro region for where the seismic action was generated, according to EC8 [18] and for which the exceedance probability was calculated. The probability values were obtained from the expressions presented earlier and are illustrated in Figure 4.14.
It can be concluded that for a PGA level of 0.3g, the Simple Frame has a 100% probability of suffering damage, with 81% probability of suffering extensive damage (DS3) and 18% of suffering complete damage or collapse. It is now evident that

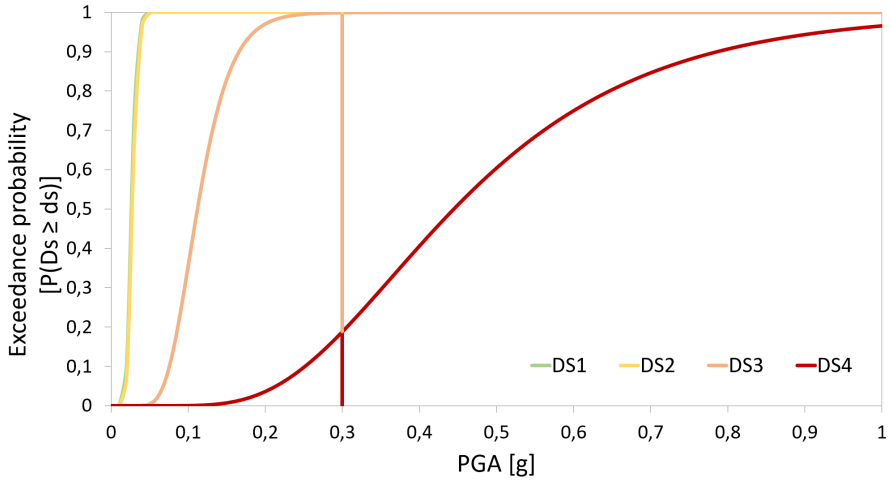

Figure 4.13: Simple frame global fragility curves

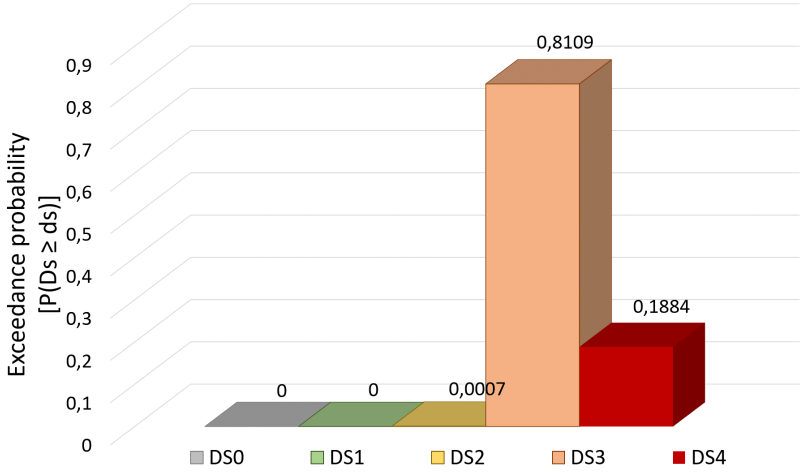

Figure 4.14: Simple frame's exceedance probability values of each damage state for a PGA level of 0.3g

the RC frame does not preform well under ground motion solicitations, which was expected, since no horizontal loading and seismic details were considered in its design. Therefore, the need for a seismic retrofitting was highlighted by these results.

The same study was conducted for the BRB Frame. Represented in Figure 4.15 the fragility curves for the BRB Frame in both directions can be observed. With the exception of the collapse damage state (DS4) all other three curves for the Y direction show slightly more inclined curves and, therefore, lower probabilities of exceedance.

After crossing the results for both directions and choosing the worst case scenario the global fragility curves were yielded, and are illustrated in Figure 4.16. The

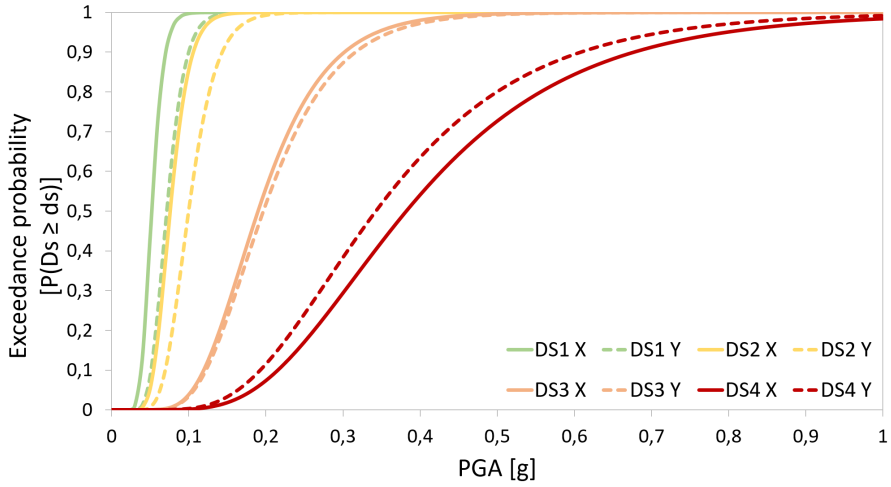

Figure 4.15: BRB frame fragility curves in both directions, X and Y

probability values for each damage state for a PGA level of 0.3g are pictured in Figure 4.17.

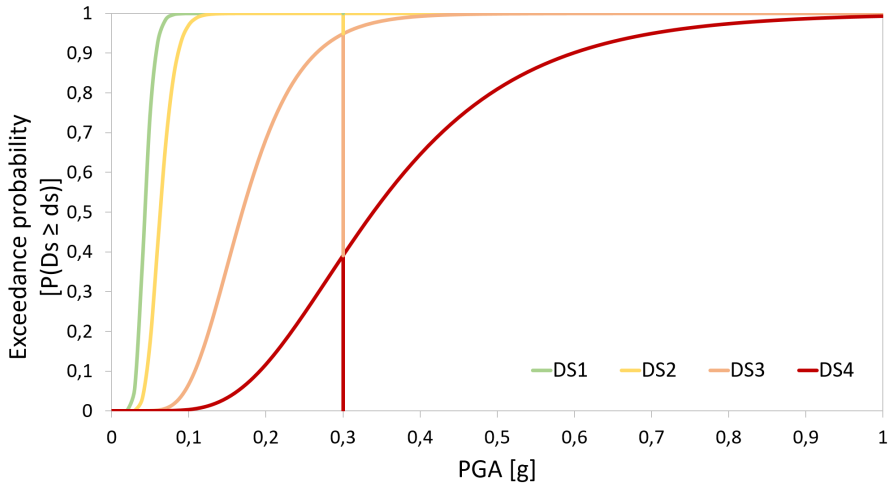

Figure 4.16: BRB frame global fragility curves

Analysing Figure 4.17 it can be observed that the probability of the structure suffering damage remains 100%, and that, although there was a reduction on DS3 and slight growth in DS2, no major improvement of the structure was obtained with the application of BRBs, with DS4 even increasing from 19% to 39%. These results were unforeseen, as it would be expected to observe both a significant increase in the DS2 damage state value and a decrease in the DS4 damage state value. These odd results may be a result of the bi-linearisation process of the IDA curve. In this process the collapse is considered when there is a drop of 20% in the maximum base shear value. For the Simple Frame there is no problem with that assumption, since when the columns loose lateral stiffness there is no other element to support

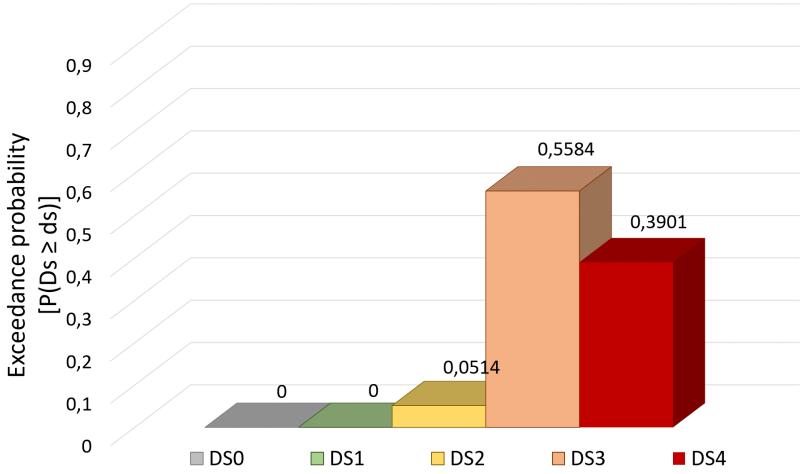

Figure 4.17: BRB frame's exceedance probability values of each damage state for a PGA level of 0.3g

those forces. Although, for the BRB and CBF Frame this assumption my not be correct, since the 20% base shear drop could be the result of the brace's yielding and, therefore, not representing the structure's collapse. This false assumption could lead to the wrong definition of the structure's collapse and cause minimal to no improvement to the fragility curves, and not represent the actual contribution of the braces.

In order to eliminate the possible error of the bi-linearisation assumption, a different approach was carried out in the numerical analysis results. Until now, all IDA curves were developed considering the total base shear and the RC frame's top displacement, as an alternative, and to have a better understanding of the collapse point, IDA curves of the most stressed column were developed for the Simple Frame. Therefore, it was possible to obtain the column's threshold top displacement values for each damage state. Thus for both the BRB Frame and CBF Frame the damage states were defined based on these threshold values and not on the bi-linearisation of the IDA curve.

After the development of the new 100 IDAs for the Simple Frame's columns, 50 in each direction, and crossing the results from both directions the global fragility curves were yielded. In Figure 4.18 a comparison between the previous fragility curves, named Top, and the column fragility curves for the Simple Frame is presented.

In the same way, a comparison was also carried out between both the Top and Column probability values of each damage state for a PGA level of 0.3, and is illustrated in Figure 4.19. It can be observed that the results remained similar, despite a the increase in the DS2 and DS4 damage states, and a decrease in the DS3 damage state. This confirms that for the Simple Frame the bi-linearisation of the IDA process was acceptably accurate.

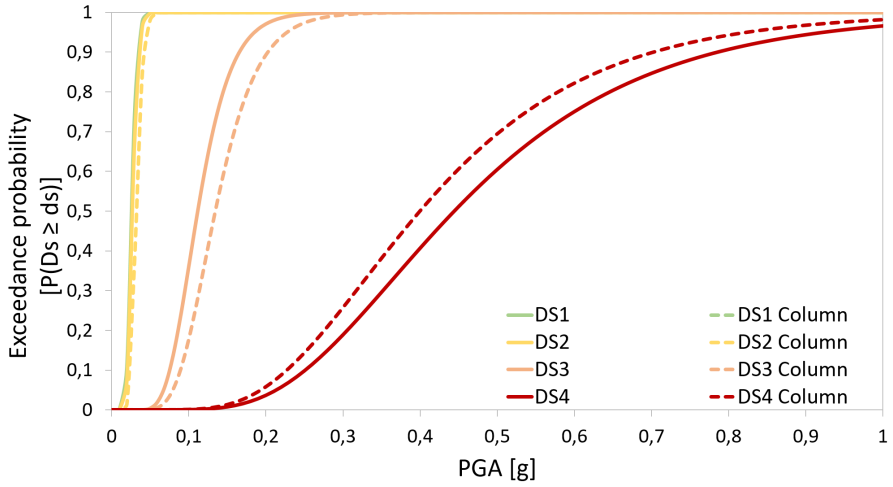

Figure 4.18: Comparison between the Top and Column fragility curves of the Simple Frame

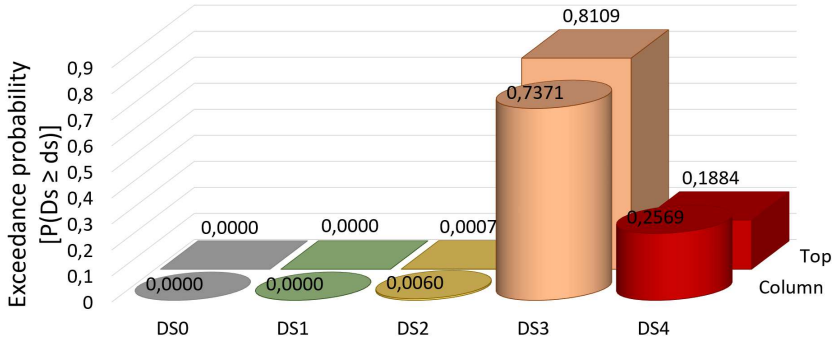

Figure 4.19: Comparison between the Top and Column probability values for each damage state

With the new analysis of the Simple Frame's results through the bilinear form of IDA, the benchmark displacement values for each damage state were set, for each of the 50 numerical model samples. These values will be used to assess the damage states for the BRB Frame. For example, if the IDA bi-linearisation for a given model sample defined the displacement values of 0.001 m, 0.003 m, 0.030 m and 0.100 m for the DS1, DS2, DS3 and DS4 respectively, the points of the same sample BRB Frame model's IDA curve will be compared to these benchmark values and awarded the respective damage state. An illustration of this process is presented in Table 4.4.

With the benchmark displacement values setted for each model sample and for each orthogonal direction, the BRB Frame's IDA curves can now be examined and

Table 4.4: Example of the damage state definition of the BRB Frame

Table 4.5: Damage state's benchmark values from the Simple Frame IDA curve's bi-linearization

Damage state [-]	Drift [m]
DS1 - Slight	0.00189
DS2 - Moderate	0.00269
DS3 - Extensive	0.03063
DS4 - Collapse	0.11447

Table 4.6: BRB Frame IDA curve points

PGA [g]	Drift [m]	Base shear [kN]
0.05	0.0089	10.222
0.10	0.0136	11.821
0.15	0.0171	12.319
0.20	0.0423	16.748
0.25	0.0393	16.094
0.30	0.0681	16.155
0.35	0.1469	13.176
0.40	0.1957	10.415

the damage states defined. The fragility curves for both de X and Y direction are illustrated in Figure 4.20. Combining both directions damage states and choosing the worst case scenario the BRB global fragility curves were yielded and are represented in Figure 4.21.

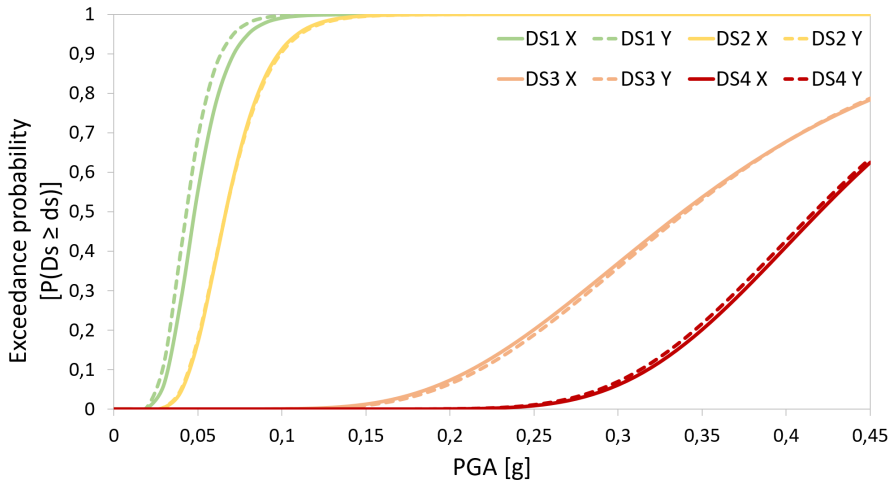

Figure 4.20: New BRB Frame fragility curves in both directions, X and Y

The probability of exceedance values of each damage state for a PGA level of 0,3g are illustrated in Figure 4.22. It can be observed that although the BRB Frame remains with 100% chance of suffering damage most of it is moderate, with 55%. This represents an increase of ≈90% in the DS2 damage state compared to the previous BRB Frame analysis. Also, a reduction was evident for both the DS3 and DS4, with a decrease of ≈50% and ≈56% respectively.

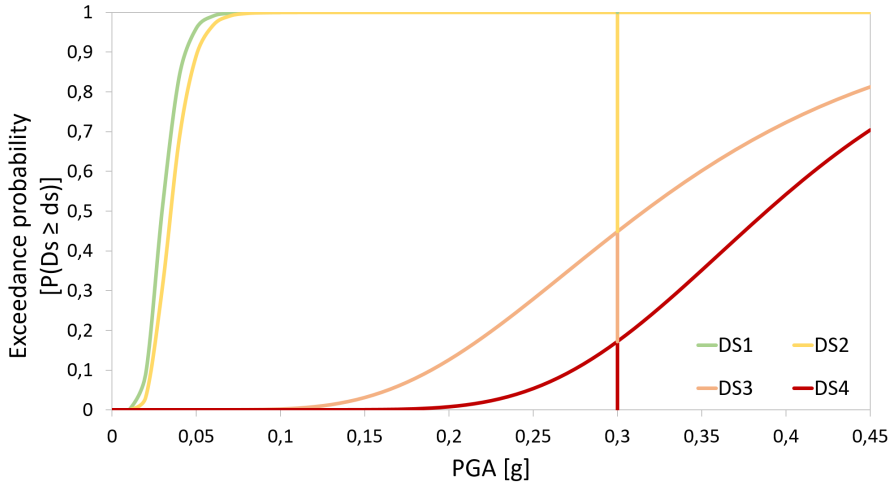

Figure 4.21: New BRB Frame global fragility curves

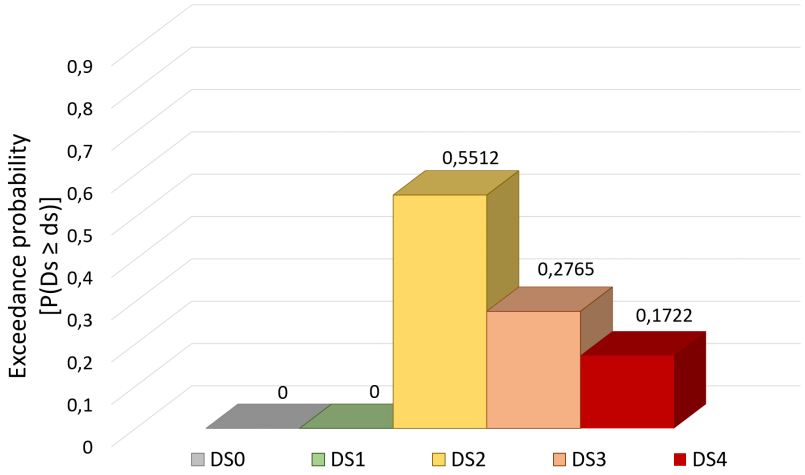

Figure 4.22: New BRB Frame's exceedance probability values of each damage state for a PGA level of 0.3g

These results were more in compliance with what was expected from the BRB devices. The devices were expected to reduce damage on the structure, knowing it would be difficult to completely mitigate it since the structure exhibits severe lacks of seismic detailing in its design.

With the application of the BRBs a significant improvement was observed in the BRB Frame's fragility curves compared with the Simple Frame's ones. Although the probability of the structure suffering damage remained at 100%, a redistribution of the probability values was observed with an increase in the values of the lower damage states at a cost of a reduction in the higher ones. A reduction of ≈33% and ≈62% was verified for DS4 and DS3, respectively. DS2 expressed the best improvement increasing in ≈9086%, from 0.0060 to 0.5512. Therefore, the BRB Frame showed ≈55% chance of suffering moderate damage during a high intensity

earthquake instead of the 0.6% exhibited by the Simple Frame, and ≈17% chance of collapsing opposing the ≈26% from the Simple Frame.

It can be observed that the standard deviation, in all fragility curves, reveals a tendency to increase throughout the damage states progression. This indicates an increase in the uncertainties associated with the seismic vulnerability of the structures and it is made evident with the decrease of incline in the curves as the damage states the structure is subjected to progress. This results from the increase of the non-linear behaviour of the structure as the seismic event's intensity rises.

In structural engineering collapse probability values are normally very low, with very low tolerance. According to the English regulation [19] and Henriques [20], the maximum admissible probability value of reaching the ultimate limit states, p'_{fu}, for different structural typologies, can be determined through equation 4.11:

$$p'_{fu} = K_s \cdot \frac{10^{-4} \cdot T_r}{n_p} \tag{4.11}$$

Were:

- K_s Coefficient responsible of translating society's aversion to accept structural rupture occurrence, it depends on the structure's social function and use type;
- T_r Lifetime period of structures to consider in the design;
- n_p Average number of people victimized in case of structure rupture/ security threshold.

According to [19] for the domestic, office, commerce and industry use the K_s coefficient value is 0.05. The lifetime period of the structure is determined according to the structure's class and for Class 3, common building structures, the defined period is 50 years. For the security threshold, n_p, three values were considered: a reduced one, a normal one and a reinforced one, with values of 0.1, 1 and 10, respectively. Applying these values to Equation 4.11 the maximum admissible probability values of reaching the ultimate limit states present in Table 4.7 are obtained.

Table 4.7: Maximum admissible probability values, p'_{fu}, for K_s = 0.05

Security threshold, n_p	**Structure's lifetime period, T_r 50 years**
Reduced (0.1)	2.5×10^{-3}
Normal (1.0)	2.5×10^{-4}
Reinforced (10)	2.5×10^{-5}

Considering the previous values obtained for the Simple and BRB Frames:

$$P_{fu;Simple} = 2.57 \times 10^{-1}$$
$$P_{fu;BRB} = 1.72 \times 10^{-1}$$

A simple check can now be made in a simple matter:

- If $p'_{fu} \geq P_{fu;Simple;BRB}$ Checked
- If $p'_{fu} \leq P_{fu;Simple;BRB}$ **Unchecked**

In Tables 4.8 and 4.9 the proper checks are highlighted for the Simple Frame and BRB Frame.

Table 4.8: Simple Frame verification

Security threshold, n_p	**Structure's lifetime period,** T_r **50 years**
Reduced (0.1)	**2.5×10^{-3}**
Normal (1.0)	**2.5×10^{-4}**
Reinforced (10)	**2.5×10^{-5}**

Table 4.9: BRB Frame verification

Security threshold, n_p	**Structure's lifetime period,** T_r **50 years**
Reduced (0.1)	**2.5×10^{-3}**
Normal (1.0)	**2.5×10^{-4}**
Reinforced (10)	**2.5×10^{-5}**

A simple glimpse of the previous tables is sufficient to conclude that none of the RC frames is in compliance with the code's maximum admissible probability values of reaching the ultimate limit states. This means that the BRBs failed to elevate the structure's performance to a code compliant level, although they demonstrated good damage reduction capacity.

Chapter 5

Conclusions and Future Work

In the present section the conclusions of the research are highlighted as well as the future work relevant for further research on the subject.

5.1 Conclusions

The efficiency assessment of a seismic retrofitting using buckling restrained braces in a two storey two span RC Framed structure was conducted successfully in the present dissertation.

Firstly, a broad research and understanding of the seismic devices was conducted in order to understand how these devices operate and their purpose. From the information gathered it was possible to have a predictable outcome of the research results. It was expected that the BRB would manage to reduce significantly the structural damage caused by a strong ground motion.

Secondly, following the research of Di Sarno and Manfredi [10], the numerical model development and validation was conducted successfully both in the modal and pushover analysis. The numerical model was then deemed calibrated and was ready to serve as base for the research.

A probabilistic approach was adopted, allowing to account for the seismic action, material properties and structural behaviour's variabilities and uncertainties, together with IDA curves to define the damage states, DS, and lastly generate the fragility curves.

From the fragility curves analysis we can conclude that for the design PGA level of 0.3g, according to the regulation for the Faro region, the Simple Frame has significant probability of suffering extensive damage and even to collapse. It was also evident, and expected, that the Simple Frame is not code compliant in terms of maximum admissible probability values of reaching the ultimate limit states. These results confirm the need for structures with such characteristics to be retrofitted to withstand seismic loads.

After the installation of the BRBs the structure remained with 100% chance of

suffering damage. Although there was a reduction of the more heavy damage states and an increase in the lighter ones, the RC frame wasn't still code compliant in terms of ultimate limit states.

In conclusion the vulnerability assessment and fragility study of the RC Framed structure, Simple and BRB reinforced, was conducted successfully revealing the systems capacity of damage mitigation in severe ground motions solicitations.

5.2 Future Work

Although the objectives of the present dissertation were, in a general way, achieved, some future research suggestions on the subject are presented below:

- Study the needed BRB retrofitting scheme to bring the structures to respect the ruling code demands in terms of ultimate limit states;
- Conduct a similar study considering a retrofitting additional steel frame. This would give a better load carrying capacity to the columns, mitigating the serious seismic details lacking;
- Conduct a similar study giving more attention to the BRB's design. Applying all the recent code demands and obligations;
- Conduct a comparative study between the use of BRBs and traditional concentric braces;
- In order to reach a wider span of buildings study different building's configuration, both in geometry and in retfrofitting schemes.

References

[1] Qiang Xie. State of the art of buckling-restrained braces in asia. *Journal of constructional steel research*, 61(6):727–748, 2005.

[2] Adam S Christopulos. *Improved seismic performance of buckling restrained braced frames*. PhD thesis, University of Washington, 2005.

[3] Keh-Chyuan Tsai, Jiun-Wei Lai, Yean-Chih Hwang, Shen-Ling Lin, and Chong-Hsing Weng. Research and application of double-core buckling restrained braces in taiwan. In *Proceeding of the 13th World Conference on Earthquake Engineering, Paper*, 2004.

[4] SL Lin, AC Wu, PC Lin, KC Tsai, and GA MacRae. Development and implementation of buckling restrained braces in taiwan. In *The New Zealand Society for Earthquake Engineering Conference*, 2012.

[5] André Almeida, Ricardo Ferreira, Jorge M Proença, and António S Gago. Seismic retrofit of rc building structures with buckling restrained braces. *Engineering Structures*, 130:14–22, 2017.

[6] NTC'08. *Norme Techniche per le Costruzioni technical standards for construction*. Gazzeta Ufficiale della Republica Italiana, 2008.

[7] CEN. *EN15129 - anti-seismic devices.* Brussels: ComitÃ© EuropÃ©en de Normalisation, 2009.

[8] WADA Akira. Fatigue properties of practical-scale unbonded braces. *Nippon steel technical report*, 82(0), 2000.

[9] Gaetano Della Corte, Mario D'Aniello, Raffaele Landolfo, and Federico M Mazzolani. Review of steel buckling-restrained braces. *Steel Construction*, 4(2):85–93, 2011.

[10] L Di Sarno and G Manfredi. Experimental tests on full-scale rc unretrofitted frame and retrofitted with buckling-restrained braces. *Earthquake Engineering & Structural Dynamics*, 41(2):315–333, 2012.

[11] Regio Decreto (R.D.) 16/11/39 n.2229. Norme per l'esecuzione delle opere in conglomerato cementizio semplicemente armato. G.U. n.92 del 18/04/1940 (in Italian).

[12] MJM Priestley, GM Calvi, and MJ Kowalsky. Displacement-based seismic design of structures. IUSS Press: Pavia, Italy, 2007.

[13] MARCO MENEGOTTO. Method of analysis for cyclically loaded rc plane frames including changes in geometry and non-elastic behavior of elements under combined normal force and bending. In *Proc. of IABSE symposium on resistance and ultimate deformability of structures acted on by well defined repeated loads*, pages 15–22, 1973.

[14] Filip C Filippou, Egor P Popov, and Vitelmo V Bertero. Filippou, filip c and popov, egor p and bertero, vitelmo v. Technical report, Earthquake Engineering Research Center, University of California, 1983.

[15] Alexandra Carvalho, A Campos Costa, and Carlos Sousa Oliveira. A stochastic finite–fault modelling for the 1755 lisbon earthquake. In *13th World Conference on Earthquake Engineering Vancouver, BC, Canada*, 2004.

[16] JCSS Probabilistic Model Code. Joint committee on structural safety. *URL: www.jcss.ethz.ch*, 2001.

[17] Y.F. Vargas Alzate. *Análisis estructural estático y dinámico probabilista de edificios de hormigón armado. Aspectos metodológicos y aplicaciones a la evaluación del daño.* PhD thesis, Universidad Politécnica de Cataluña, 2013.

[18] European Committee for Standardization (CEN). *EN1998-1: Eurocode 8: Design of structures for earthquake resistance - Part 1: General rules, seismic actions and rules for buildings*, 2004.

[19] Construction Industry Research and Information Association. *Rationalisation of safety and serviceability factors in structural codes*, volume 63. Construction Industry Research and Information Association, 1977.

[20] António AR Henriques. Aplicação de novos conceitos de segurança no dimensionamento do betão estrutural. *Porto: Faculdade de Engenharia da Universidade do Porto*, 1998.

[21] J. Ricles, D. Lignos, J. Love, M. Midorikawa, and T. Okazaki. Effects of the 2011 tohoku japan earthquake on steel structures, August 2011. available in http://www.eqclearinghouse.org/2011-03-11-sendai/2011/08/03/eeri-steel-structures-reconnaissance-group/.

[22] T Yoshino and Y Karino. Experimental study on shear wall with braces: Part 2. In *Summaries of technical papers of annuals meeting*, volume 11, pages 403–4, 1971.

[23] M Wakabayashi, T Nakamura, A Katagihara, H Yogoyama, and T Morisono. Experimental study on the elastoplastic behavior of braces enclosed by precast concrete panels under horizontal cyclic loading (parts 1 &2). In *Summaries of technical papers of annual meeting*, volume 10, pages 1041–4. Architectural Institute of Japan, 1973.

[24] M Wakabayashi, T Nakamura, A Katagihara, H Yogoyama, and T Morisono. Experimental study on the elastoplastic behavior of braces enclosed by precast concrete panels under horizontal cyclic loading (parts 1 &2). In

Summaries of technical papers of annual meeting, volume 6, pages 121–8. Architectural Institute of Japan, 1973.

[25] K Kimura, K Yoshioka, T Takeda, Z Fukuya, and K Takemoto. Tests on braces encased by mortar in-filled steel tubes. In *Summaries of Technical Papers of Annual Meeting, Architectural Institute of Japan*, pages 1041–2, 1976.

[26] T Takeda and K Kimura. Experimental study on precast concrete shear walls-part 6. In *Summaries of technical papers of annual meeting*, pages 1677–8. Architectural Institute of Japan, 1979.

[27] S Mochizuki, Y Murata, and S Takahashi. Experimental study onbuckling of unbonded braces under axial forces: Part 1 and 2. In *Summaries of technical papers of annual meeting*, pages 1623–6. Architectural Institute of Japan, 1979.

[28] M Fujimoto, A Wada, E Saeki, A Watanabe, and Y Hitomi. A study on the unbonded brace encased in buckling-restraining concrete and steel tube. *Journal of Structural and Construction Engineering, AIJ*, 34:249–258, 1988.

[29] Atsushi Watanabe, Yasuyoshi Hitomi, Eiichiro Saeki, Akira Wada, and Morihisa Fujimoto. Properties of brace encased in buckling-restraining concrete and steel tube. In *Proceedings of Ninth World Conference on Earthquake Engineering*, volume 4, pages 719–724, 1988.

[30] Mario D'Aniello. *Steel dissipative bracing systems for seismic retrofitting of existing structures: theory and testing*. PhD thesis, Università degli Studi di Napoli Federico II, 2007.

[31] Cameron Black, Ian D Aiken, and Nicos Makris. *Component Testing, Stability Analysis, and Characterization of Buckling-restrained Unbonded Braces (TM)*. Pacific Earthquake Engineering Research Center, 2002.

[32] T Nagao, K Mikuriya, Y Matsumoto, and S Takahashi. An experimental study on the elasto-plastic behavior of unbonded composite bracing (part 1-4). In *Summaries of technical papers of annual meeting*, volume 2, pages 1329–36. Architectural Institute of Japan, Structural Engineering Section, 1988.

[33] T Nagao, K Mikuriya, S Takahashi, and S Yuki. An experimental study on the elasto-plastic behavior of unbonded composite bracing (part 5-7). In *Summaries of technical papers of annual meeting*, volume 2, pages 1501–6. Architectural Institute of Japan, Structural Engineering Section, 1989.

[34] T Nagao and S Takahashi. A study on the elasto-plastic behavior of unbonded composite bracing (part 1: experiments on isolated members under cyclic loading). *Journal of Structural and Construction Engineering*, 415:105–15, 1990.

[35] T Nagao and S Takahashi. A study on the elasto-plastic behavior of unbonded composite bracing (part 2: analytical studies). *Journal of Structural and Construction Engineering*, pages 45–56, 1991.

[36] T Nagao, S Sera, S Nakamura, H Ouchi, K Otani, and K Fukutajima. A study on the rc encased h-section steel brace (part 1: General description, part 2: Results and discussion). In *Summaries of Technical Papers of Annual Meeting of the Architectural Institute of Japan. Structural Engineering Section ?, Tokyo, Japan: AIJ*, pages 1773–1776, 1992.

[37] S Kuwahara, M Tada, T Yoneyama, and K Imai. A study on stiffening capacity of double-tube members. *Journal of Structural and Construction Engineering*, 445(3):151–158, 1993.

[38] M Tada, S Kuwahara, T Yoneyama, and K Imai. Horizontally loading test of the steel frame braced with double-tube members. *Annual technical papers of steel structures*, 1:203–208, 1993.

[39] T Usami and H Kaneko. Strength of h-shaped brace constrained flexural buckling having unconstrained area at both ends. both ends simply supported. *Journal of Structural and Construction Engineering*, pages 171–177, 2001.

[40] T Usami, H Kaneko, and T Ono. Strength of h-shaped brace constrained flexural buckling having unconstrained area at both ends. both ends fixed. *Journal of Structural and Construction Engineering*, pages 211–218, 2002.

[41] K Isoda, S Mase, T Terada, and N Satake. Development of unbonded brace damper restrained by channel section steel. In *Summaries of technical papers of annual meeting*, volume 3, pages 663–8. Architectural Institute of Japan, Structural Engineering Section, 2001.

[42] KC Tsai and YC Huang. Experimental responses of large scale brb frames. *Center for Earthquake Engineering Research*, 2002.

[43] KC Tsai and CH Weng. Experimental responses of double-tube unbonded brace elements and connections. *Center for Earthquake Engineering Research of National Taiwan University*, 2002.

[44] KC Tsai, CH Loh, YC Hwang, and CS Weng. Seismic retrofit of building structures with dampers in taiwan. In *Symposium of Seismic Retrofit of Buildings and Bridges with Base Isolation and Dampers*, 2003.

[45] An-Chien Wu, Pao-Chun Lin, and Keh-Chyuan Tsai. High-mode buckling responses of buckling-restrained brace core plates. *Earthquake Engineering & Structural Dynamics*, 43(3):375–393, 2014.

[46] Kazuo Inoue and S Sawaisumi. Bracing design criterion of the reinforced concrete panel including unbonded steel diagonal braces. *Journal of Structural and Construction Engineering*, 432(3):41–49, 1992.

[47] Eiichiro Saeki, Yasushi Maeda, Hideji Nakamura, Mitsumasa Midorikawa, and Akira Wada. Experimental study on practical-scale unbonded braces. *Journal of Structural and Constructional Engineering, Architectural Institute of Japan*, 476:149–158, 1995.

[48] E Saeki, K Iwamatu, and A Wada. Analytical study by finite element method and comparison with experiment results concerning buckling-restrained unbonded braces. *Journal of Structural and Construction Engineering*, 484:111–120, 1996.

[49] P. Uriz and S. Mahin. *Toward Earthquake-Resistant Design of Concentrically Braced Steel-Frame Structures*. Pacific Earthquake Engineering Research Center, November 2008.

[50] Keh-Chyuan Tsai, Yean-Chih Hwang, Chung-Shing Weng, T Shirai, and H Nakamura. Experimental tests of large scale buckling restrained braces and frames. In *Proceedings, Passive Control Symposium*. Tokyo Institute of Thechnology, Tokyo, 2002.

[51] Jiun-Wei Lai and Keh-Chyuan Tsai. A study of buckling restrained brace frames. Technical report, Report No. CEER/R90-07, Center for, 2001.

[52] YC Huang and KC Tsai. Experimental responses of large scale buckling restrained brace frames. *Rep. No. CEER/R91-03, Center for Earthquake Engineering Research, National Taiwan Univ., Taiwan (in Chinese)*, 2002.

[53] KC Tsai and CH Weng. Experimental responses of double-tube unbonded brace elements and connections. *Center for Earthquake Engineering Research of National Taiwan University*, 2002.

[54] SL Lin and KC Tsai. A study of all metallic and detachable buckling braces. *Center for Earthquake Engineering Research, National Taiwan University*, 2003.

[55] Larry A Fahnestock, James M Ricles, and Richard Sause. Experimental evaluation of a large-scale buckling-restrained braced frame. *Journal of structural engineering*, 133(9):1205–1214, 2007.

[56] Jeffrey W Berman and Michel Bruneau. Cyclic testing of a buckling restrained braced frame with unconstrained gusset connections. *Journal of structural engineering*, 135(12):1499–1510, 2009.

[57] AISC ANSI. Aisc 341-05. seismic provisions for structural steel buildings. american institute of steel construction. *Inc.: Chicago, IL*, 2005.

[58] K Kasai. Current status of japanese passive control scheme for mitigating seismic damage to buildings and equipments. *Structural Engineering Research Center, Tokyo Institute of Technology, Japan*, 2008.

[59] BSSC Building Seismic Safety Council. Nehrp recommended provisions for seismic regulations for new buildings and other structures. *Report FEMA-450 (Provisions), Federal Emergency Management Agency (FEMA), Washington*, 2003.

[60] American Institute of Steel Construction. *Seismic provisions for structural steel buildings*. American Institute of Steel Construction, 2002.

[61] AV Bergami and C Nuti. A design procedure of dissipative braces for seismic upgrading structures. *Earthquakes and Structures*, 4(1):85–108, 2013.

[62] A Filiatrault and S Cherry. A simplified seismic design procedure for friction damped structures. *Procedings of Fourth U.S. National Conference on Earthquake Engineering, 3, Palm Springs, U.S.A.*, 1988.

[63] A Filiatrault and S Cherry. Seismic design spectra for friction-damped structures. *Journal of Structural Engineering*, 116(5):1334–1355, 1990.

[64] V Ciampi. Use of energy dissipation devices, based on yielding of steel, for earthquake protection of structures. In *Proc., Int. Meeting on Earthquake Protection of Build*, volume 14, 1991.

[65] V Ciampi, M De Angelis, and F Paolacci. Design of yielding or friction-based dissipative bracings for seismic protection of buildings. *Engineering Structures*, 17(5):381–391, 1995.

[66] A Vulcano and F Mazza. A simplified procedure for the aseismic design of framed buildings with dissipative braces. In *Atti della 12th European Conference on Earthquake Engineering, London*, 2002.

[67] Jinkoo Kim and Hyunhoon Choi. Behavior and design of structures with buckling-restrained braces. *Engineering Structures*, 26(6):693–706, 2004.

[68] F.C. Ponzo, M. Dolce, G. Vigoriti, G. Arleo, and A. Di Cesare. Progettazione di controventi dissipativi a comportamento dipendente dagli spostamenti. In *Proceedings of XIII Convegno ANIDIS L'ingegneria Sismica in Italia*, Bologna, Italy, 2009.

[69] Peter Fajfar et al. Capacity spectrum method based on inelastic demand spectra. *Earthquake engineering and structural dynamics*, 28(9):979–994, 1999.

[70] Peter Fajfar and Peter Gašperšič. The n2 method for the seismic damage analysis of rc buildings. *Earthquake Engineering & Structural Dynamics*, 25(1):23–67, 2000.

[71] Steve Merritt, Chia-Ming Uang, and Gianmario Benzoni. Subassemblage testing of corebrace buckling-restrained braces. *Final report to CoreBrace, LLC, Department of Structural Engineering, University of California, San Diego*, 2003.

[72] S Merritt, CM Uang, and G Benzoni. Subassemblage testing of star seismic buckling-restrained braces. *Rep. No. TR-2003*, 4, 2003.

[73] S Merritt, CM Uang, and G Benzoni. Uniaxial testing of associated bracing buckling restrained braces. *Department of Structural Engineering, Structural Systems Project, Report No. TR-2003/05, University of California, San Diego, CA*, 2003.

[74] SEAOC-AISC. *Recommended Provisions for Buckling-Restrained Braced Frames*. Structural Engineers Association of California and American Institute of Steel Construction, 2001.

[75] AISC. *Seismic Provisions for Structural Steel Buildings*. American Institute of Steel Construction, Chicago, IL, 1997.

[76] R Antonucci, F Balducci, MG Castellano, and F Donà. Pre-casted rc buildings with buckling restrained braces: the example of the new building of the faculty of engineering in ancona. In *Proceedings of the 2nd International Fib Congress*, 2006.

[77] European Committee for Standardization (CEN). *EN 1992-1-1 Eurocode 2: Design of concrete structures*, 2005.

[78] L Di Sarno and G Manfredi. Seismic retrofitting with buckling restrained braces: application to an existing non-ductile rc framed building. *Soil Dynamics and Earthquake Engineering*, 30(11):1279–1297, 2010.

[79] L Di Sarno and G Manfredi. Experimental tests on full-scale rc unretrofitted frame and retrofitted with buckling-restrained braces, August 2009. Presentation in Behaviour of Steel Structures in Seismic Areas, STESSA.

[80] Seismosoft. *SeismoStruct 2016 - A computer program for static and dynamic nonlinear analysis of framed structures*, 2016. available from http://www.seismosoft.com.

[81] Panagiotis J Madas. *Advanced modelling of composite frames subject to earthquake loading*. PhD thesis, Imperial College London (University of London), 1993.

[82] John B Mander, Michael JN Priestley, and R Park. Theoretical stress-strain model for confined concrete. *Journal of structural engineering*, 114(8):1804–1826, 1988.

[83] J Enrique Martínez-Rueda and AS Elnashai. Confined concrete model under cyclic load. *Materials and Structures*, 30(3):139–147, 1997.

[84] Andrea Prota, Fiorenzo De Cicco, and Edoardo Cosenza. Cyclic behavior of smooth steel reinforcing bars: experimental analysis and modeling issues. *Journal of Earthquake Engineering*, 13(4):500–519, 2009.

[85] Murat Serdar Kircil and Zekeriya Polat. Fragility analysis of mid-rise r/c frame buildings. *Engineering Structures*, 28(9):1335–1345, 2006.

[86] Rui Alexandre da Silva Perdigão. Análise da vulnerabilidade sísmica de um passadiço pré-fabricado em betão armado. Master's thesis, Faculdade de Ciências e Tecnologia da Universidade Nova de Lisboa, 2016.

[87] Dimitrios Vamvatsikos and C Allin Cornell. Incremental dynamic analysis. *Earthquake Engineering & Structural Dynamics*, 31(3):491–514, 2002.

[88] Ronald O Hamburger, Douglas A Foutch, and CA Cornell. Performance basis of guidelines for evaluation, upgrade and design of moment-resisting steel frames. In *Proc., 12th World Conf. on Earthquake Engineering*, 2000.

[89] R Sinha and SR Shiradhonkar. Seismic damage index for classification of structural damage-closing the loop. In *The 15th world conference on earthquake engineering*, 2012.

[90] P Mouroux and B Le Brun. Risk-ue project: an advanced approach to earthquake risk scenarios with application to different european towns. In *Assessing and Managing Earthquake Risk*, pages 479–508. Springer, 2008.

[91] HM MRl. Multi-hazard loss estimation methodology: Earthquake model. *Department of Homeland Security, FEMA, Washington, DC*, 2003.

[92] Masanobu Shinozuka, Maria Q Feng, Jongheon Lee, and Toshihiko Naganuma. Statistical analysis of fragility curves. *Journal of engineering mechanics*, 126(12):1224–1231, 2000.

[93] Amir M Kaynia, Fabio Taucer, and Ufuk Hancilar. *Guidelines for deriving seismic fragility functions of elements at risk: Buildings, lifelines, transportation networks and critical facilities*. Publications Office, 2013.

[94] T Rossetto and A Elnashai. Derivation of vulnerability functions for european-type rc structures based on observational data. *Engineering structures*, 25(10):1241–1263, 2003.

[95] K Pitilakis, M Alexoudi, S Argyroudis, O Monge, and C Martin. Vulnerability and risk assessment of lifelines. In *Assessing and Managing Earthquake Risk*, pages 185–211. Springer, 2008.

[96] Simona Esposito and Iunio Iervolino. Pga and pgv spatial correlation models based on european multievent datasets. *Bulletin of the Seismological Society of America*, 101(5):2532–2541, 2011.

[97] Armen Der Kiureghian and Ove Ditlevsen. Aleatory or epistemic? does it matter? *Structural Safety*, 31(2):105–112, 2009.

[98] National Institute of Building Sciences (NIBS). Hazus-mh: User's manual and technical manuals, 2004.

[99] F Sabetta, A Goretti, and A Lucantoni. Empirical fragility curves from damage surveys and estimated strong ground motion. In *11th European Conference on Earthquake Engineering*, 1998.

[100] Tiziana Rossetto and Amr Elnashai. A new analytical procedure for the derivation of displacement-based vulnerability curves for populations of rc structures. *Engineering structures*, 27(3):397–409, 2005.

[101] Darius Seyedi, Pierre Gehl, John Douglas, L Davenne, N Mezher, and S Ghavamian. Development of seismic fragility surfaces for reinforced concrete buildings by means of nonlinear time-history analysis. *Earthquake Engineering and Structural Dynamics*, 39(1):91–108, 2010.

[102] Zoran V Milutinovic and Goran S Trendafiloski. Risk-ue an advanced approach to earthquake risk scenarios with applications to different european towns. *Contract: EVK4-CT-2000-00014, WP4: Vulnerability of Current Buildings*, 2003.

[103] Keith Porter, Robert Kennedy, and Robert Bachman. Creating fragility functions for performance-based earthquake engineering. *Earthquake Spectra*, 23(2):471–489, 2007.

[104] G Michele Calvi, Rui Pinho, Guido Magenes, Julian J Bommer, L Fernando Restrepo-Vélez, and Helen Crowley. Development of seismic vulnerability assessment methodologies over the past 30 years. *ISET journal of Earthquake Technology*, 43(3):75–104, 2006.